

Structural and functional studies  
of the iron storage protein ferritin  
from *Pyrococcus furiosus*



**Structural and functional studies of the  
iron storage protein ferritin from  
*Pyrococcus furiosus***

PROEFSCHRIFT

Ter verkrijging van de graad van doctor  
aan de Technische Universiteit Delft,  
op gezag van de Rector Magnificus prof. dr. ir. J.T. Fokkema,  
voorzitter van het College voor Promoties,  
in het openbaar te verdedigen op dinsdag 6 november 2007 om 15.00 uur

door

Jana TATUR

Scheikundig Ingenieur  
geboren te Kramatorsk, Oekraïne

Dit proefschrift is goedgekeurd door de promotor:

Prof. dr. W.R. Hagen

Samenstelling promotiecomissie:

Rector Magnificus	voorzitter
Prof. dr. W.R. Hagen	Technische Universiteit Delft, promotor
Dr. ir. P.M. Matias	Instituto de Tecnologia Quimica e Biologica, Oeiras, Portugal
Prof. dr. R.R. Crichton	Université Catholique de Louvain, Louvain la Neuve, Belgium
Prof. dr. G.W. Canters	Leiden University, Leiden
Prof. dr. S. de Vries	Technische Universiteit Delft
Prof. dr. I.W.C.E. Arends	Technische Universiteit Delft
Dr. ir. J.A. Jongejan	Technische Universiteit Delft

The studies in this thesis were performed at the Section Enzymology, Department of Biotechnology, Delft University of Technology. This research has been financially supported by Council for Chemical Sciences of the Netherlands Organisation for Scientific Research (CW-NWO) under project number 700.51.301.

Copyright © 2007 by Jana Tatur

All rights reserved. No part of the material protected by this copyright notice may be reproduced or utilized in any form by any means, electronic or mechanical including photocopying, recording or by any information storage and retrieval system, without written permission from the author.

ISBN 978-90-9022432-9



## Summary

This research focuses on the iron storage protein ferritin. Ferritin is a protein involved in iron homeostasis by storing Fe(II) excess in the form of an Fe(III) mineral core in the presence of oxygen and by releasing iron during iron deficiency. Ferritins are vital for human health. Their malfunction may lead among other diseases to anemia, iron overload, Parkinson or Alzheimer. In addition to its medical significance, there are industrial applications of ferritin such as in nanotechnology, catalysis and environmental cleaning.

Ferritins from archaeal organisms are especially interesting for research because little is known about them compared to those from bacteria, fungi, plants, insects or vertebrates. Moreover, the role and the action mechanism of ferritins in anaerobic organisms is not understood, because the oxygen that is required for iron uptake is not available. Particular aspects about ferritins that still need to be resolved are the role of ferritins in anaerobic organisms, the identification of physiological reductants and, in case of anaerobes, oxidants, the iron incorporation mechanism and the three-dimensional structure of archaeal ferritins.

The research of this study focused on ferritin from the archaeon, hyperthermophile and anaerobe *Pyrococcus furiosus*. Research involved both the fundamental biochemistry of ferritin and ferritin's possible industrial application. The obtained results partially answer some of the questions described above.

The three-dimensional structure of recombinant *P. furiosus* ferritin (PfFtn) overproduced in *E. coli*, has been solved to 2.75 Å. The data have been collected from crystals of ferritin as-isolated and soaked in Fe or Zn prior to data collection. PfFtn differs from the first archaeal ferritin structure from *Archaeoglobus fulgidus* solved recently, but is similar to the structures of ferritins from non-archaeal organisms, namely a sphere of 24 subunits arranged in 432 symmetry. A high number of intrasubunit hydrogen bonds is present which are not observed in ferritins from mesophilic organisms and are probably the cause of the protein's hyperthermostability.

EPR monitored redox titrations of *P. furiosus* ferritin suggest that the ferritin's diiron catalytic center is a stable prosthetic group and not a transient center – a controversial issue in literature. The determination of rather high values of the diiron center's redox potentials is a new important contribution towards understanding the mechanism of ferritins' iron uptake/release reaction and determining physiological redox partners of ferritins. Overproduction of the protein in *E. coli* afforded a quarter of the total cell free extract to be *P. furiosus* ferritin, and complete purification was achieved by one heat step. Such high yield, together with the ease of purification and extreme hyperthermostability (half-life of 48 h at 100°C) of the protein make it an attractive model for development of industrial applications.

Analysis of the *P. furiosus* genome revealed three more genes that encode for ferritin-like family proteins. One of these closely resembles BFR-A ferritin and is highly similar to genes from species related to *P. furiosus*, i.e. *P. abyssi* and *P. horikoshii*. It is likely that besides its metal storage function ferritin also plays a role in DNA protection of these species, which allows them to survive at high temperatures.

Ferritin has been used before for production of carbon nanotubes. However, the yield of nanotubes was poor and not satisfactory for industrial applications. In this thesis, a dramatic nanotubes yield was achieved. The applied method and the cause of previously obtained low yields are discussed.

The thesis begins with a description of the evolution of iron dependant proteins and the illustration of the chemical properties of iron. This is because iron is the main substrate of ferritin and ferritin plays an important role in iron homeostasis. Next, an overview of ferritins and their medical significance is provided. The thesis proceeds with a description of the organism *Pyrococcus furiosus* and the characterization of its ferritin. Here, the reader is taken along to the purification and basic biochemical characterization of the ferritin, elucidation of the ferritin three-dimensional atomic structure, an EPR study of the redox properties of its catalytic center, genome analysis and identification of other

catalytic center, genome analysis and identification of other ferritin-like proteins in *P. furiosus*, and, finally, the application study to improve the yield of carbon nanotubes produced from ferritin. The thesis ends with a number of conclusions.



## Samenvatting

Dit promotieonderzoek richt zich op het ijzeropslageiwit ferritine. Ferritine is een eiwit dat betrokken is bij ijzerhomeostase door opslag van overmatig Fe(II) in de vorm van een minerale kern van Fe(III) in aanwezigheid van zuurstof en door de afgifte van ijzer gedurende ijzergebrek. Ferritinen zijn essentieel voor de menselijke gezondheid. Gebrekkig functioneren ervan kan onder andere leiden tot ziekten zoals bloedarmoede, ijzeroverschot, Parkinson of Alzheimer. Bovendien bestaan er industriële toepassingen zoals in nanotechnologie, katalyse en herstel van milieuverontreinigingen.

Ferritinen van archaea zijn met name interessant voor onderzoek omdat er weinig over bekend is in vergelijking met bacteriën, schimmels, planten, insecten en gewervelden. De rol en het mechanisme van ferritinen in anaërobe organismen is nog onbekend, omdat de zuurstof die nodig is voor ijzeropname niet beschikbaar is. De belangrijkste aspecten die nog opgehelderd dienen te worden zijn de rol van ferritinen in anaërobe organismen, de identificatie van fysiologisch reductanten en, in geval van anaërobe organismen de oxidanten, het ijzerinbouwmechanisme en de driedimensionale structuur van archaeaal ferritine.

Het onderzoek dat ten grondslag ligt aan dit proefschrift focusteert op ferritine van de archaeon, hyperthermofiel en anaeroob *Pyrococcus furiosus*. Het onderzoek omvatte zowel de fundamentele biochemie van ferritine als de mogelijke industriële toepassing ervan. De verkregen resultaten beantwoorden gedeeltelijk enkele van de hierboven beschreven vragen.

De driedimensionale structuur van recombinant *P. furiosus* ferritine (PFFtn) overgeproduceerd in *E. coli*, is bepaald tot een resolutie van 2.75 Å. De gegevens zijn verzameld van kristallen van onbehandeld ferritine en van ferritine dat eerst is geweekt in Fe en Zn ionen. PFFtn verschilt van de onlangs als eerste beschreven archaeale ferritine-structuur van *Archaeoglobus fulgidus*, maar is vergelijkbaar met de structuur van ferritinen van niet-archaeale organismen, te weten een bol

van 24 subunits gerangschikt in een symmetrie van 432. Een groot aantal aan intrasubunitwaterstofbindingen is aanwezig, die niet worden gevonden in ferritinen van mesofiele organismen en die waarschijnlijk de oorzaak zijn van de hyperthermostabiliteit van dit eiwit.

Met EPR gevolgde redoxtitraties van *P. furiosus* ferritine suggereren dat het ferritine di-ijzer katalytische centrum een stabiele prosthetische groep is en geen transiente groep – een controversieel onderwerp in de literatuur. De bepaling van tamelijk hoge redoxpotentialen van het di-ijzer centrum vormt een belangrijke nieuwe bijdrage aan het begrijpen van het mechanisme van ijzeropname/-afgave door de ferritine en voor het vaststellen van de fysiologische redoxpartners van ferritinen. Overproductie van het eiwit in *E. coli* resulteerde in *P. furiosus* ferritine met een opbrengst ter grootte van een kwart van het totale cel-vrije extract, en complete zuivering werd in één stap bereikt met een hittebehandeling. Zo'n hoge opbrengst, eenvoudige zuivering en extreme hyperthermostabiliteit (halfwaardetijd van 48 uur bij 100 °C) van het eiwit maken het een aantrekkelijk model voor ontwikkeling van industriële toepassingen.

Analyse van het genoom van *P. furiosus* onthulde nog drie genen die mogelijk voor een familie van ferritine-achtige eiwitten coderen. Een ervan lijkt erg op bacterieel ferritine-A en vertoont erg veel overeenkomst met genen van soorten die gerelateerd zijn aan *P. furiosus*, te weten *P. abyssi* en *P. horikoshii*. Het is aannemelijk dat ferritine, naast zijn rol bij de opslag van metaal, ook een rol speelt bij de DNA-bescherming van deze soorten, wat ze in staat stelt hoge temperaturen te overleven.

Ferritine is eerder toegepast voor de productie van koolstof nanobuisjes. De opbrengst was echter laag en niet voldoende voor industriële toepassingen. In het heur beschreven onderzoek is een extreem hoge opbrengst aan nanobuisjes bereikt. Dit proefschrift behandelt de toegepaste methode en de reden waarom voorheen lagere opbrengsten werden bereikt.

Het proefschrift begint met een beschrijving van de evolutie van ijzerafhankelijke eiwitten en een verduidelijking van de chemische eigenschappen van ijzer, omdat ijzer het belangrijkste substraat is van ferritine en ferritine een belangrijke rol speelt in ijzerhomeostase.

Vervolgens wordt een overzicht gegeven van ferritinen en hun medische toepassingen. Het proefschrift vervolgt met een beschrijving van *Pyrococcus furiosus* en de karakterisering van zijn ferritine. Hierbij wordt de lezer meegenomen langs de zuivering en basale biochemische karakterisering van de ferritine, elucidatie van de driedimensionale atoomstructuur van de ferritine, EPR-studie van de redox-eigenschappen van zijn katalytische centrum, genomanalyse en identificatie van andere ferritine-achtige eiwitten in *P. furiosus*, en ten slotte, de toepassingsstudie naar het verhogen van de opbrengst van koolstof nanobuisjes gemaakt van ferritine. Het proefschrift eindigt met een aantal conclusies.



# CONTENTS

Summary		<i>i</i>
Samenvatting		<i>iv</i>
<b>CHAPTER I</b>	Introduction: iron, ferritins, <i>Pyrococcus furiosus</i> , and scope of the thesis	<i>3</i>
<b>CHAPTER II</b>	A highly thermostable ferritin from the hyperthermophilic archaeal anaerobe <i>Pyrococcus furiosus</i>	<i>33</i>
<b>CHAPTER III</b>	Crystallization and preliminary X-ray characterization of a ferritin from the hyperthermophilic archaeon and anaerobe <i>Pyrococcus furiosus</i>	<i>59</i>
<b>CHAPTER IV</b>	Crystal structure of the ferritin from the hyperthermophilic archaeal anaerobe <i>Pyrococcus furiosus</i>	<i>73</i>
<b>CHAPTER V</b>	The dinuclear iron-oxo ferroxidase center of <i>Pyrococcus furiosus</i> ferritin is a stable prosthetic group with unexpectedly high reduction potentials	<i>111</i>
<b>CHAPTER VI</b>	Ferritin-like proteins of <i>Pyrococcus furiosus</i>	<i>125</i>
<b>CHAPTER VII</b>	Production of nanotubes in technologically substantial amounts using ferritin	<i>137</i>
<b>CHAPTER VIII</b>	Conclusions and recommendations	<i>149</i>
Abbreviations		<i>155</i>
Curriculum vitae		<i>156</i>
Acknowledgements		<i>157</i>



# CHAPTER I. Introduction: iron, ferritins, *Pyrococcus furiosus* and scope of the thesis



*Iron containing and iron deficient ferritin*

## IRON

### Evolution

Iron is the most abundant element on Earth. In the Earth's core iron constitutes 86% of all elements and in the Earth's crust it is the second most abundant metal after aluminium, and it is followed by Ca, Na, K, Mg<sup>1,2</sup>. In the Earth's crust iron exists mostly in the form of iron oxides/hydroxides but also occurs as sulfides or carbonates and is part of such minerals as ferrihydrite, magnetite, hematite, goethite, pyrite, and siderite. The abundance of iron has been known for a long time. In the 18<sup>th</sup> century, the scientist Georges-Louis Leclerc, Comte de Buffon, tried to estimate the age of the Earth by measuring the cooling time of small iron balls and extrapolating the result to Earth's size. However, this calculation resulted in the age of the Earth to be 74832 years old<sup>3</sup>.

Iron can be toxic to living matter when exposed to oxygen. Yet, cells learned how to overcome iron toxicity. Moreover, iron is a most common element of catalytic centers in enzymes. In humans, iron is an essential trace element<sup>4</sup>. Iron deficiency or iron overload in organisms leads to severe health disorders. The manner in which nature employed iron can be seen in the course of evolution.

Earth soon after its formation approximately 4.5 billion years ago is believed to have had a high pressure and a reducing acidic

environment with an atmosphere consisting of H<sub>2</sub>, H<sub>2</sub>S, He, N<sub>2</sub>, CO<sub>2</sub>, CO, SO<sub>2</sub>, NH<sub>3</sub>, CH<sub>4</sub>, N<sub>2</sub>, S<sub>2</sub>, Cl<sub>2</sub>, and H<sub>2</sub>O, and oceans with dissolved gases and ions, particularly Fe(II)<sup>1,2,5</sup>. The first organisms that appeared were presumably extremophilic anaerobic archaea, such as, or similar to the organism discussed in this thesis, *Pyrococcus furiosus*.

As photosynthetic organisms started to emerge the oxygen atmosphere began to form<sup>6-8</sup>. Bioavailable ferrous iron dissolved in water at approximately 10<sup>-3</sup> M was oxidized into barely soluble 10<sup>-18</sup> M ferric iron<sup>5</sup>, most of which sank to the ocean floor and formed layers of iron oxides/hydroxides<sup>1,9</sup> also known as Banded Iron Formations (BIF). BIFs can now be seen, for example, in the layers of the rocks of Hamersley Province of Western Australia and in the Grand Canyon in the USA.

Time frame, bya	Evolutionary step	Comment
~0.42	Oxygen level reached 21%	Animals and plants
~2.5-2	Eukaryotic thermophiles	
~3-2.5	Photosynthetic bacteria	Accumulation of oxygen
~4-3.5	Hyperthermophilic archaea	
~4.4-4.3	Ocean period	
~4.5	Earth formed	

bya - billion years ago

When all ferrous iron was used up, oxygen accumulated and the present atmosphere was formed. Life had to learn how to protect itself from the oxidizing effect of oxygen. Enzymes such as superoxide dismutase, peroxidase and catalase evolved that could scavenge poisonous oxygen species, such as superoxide, hydrogen peroxide, and hydroxyl radicals<sup>4,10</sup>.

### **Iron and reactive oxygen species**

Iron constitutes a part of the active center of enzymes that remove oxidative oxygen species, e.g. superoxide dismutase removes superoxide anion and catalase removes hydrogen peroxide. Paradoxically, iron is also a substrate in reactions that lead to the formation of these species.



$\text{FeII} + \text{H}_2\text{O}_2 \rightarrow \text{FeIII} + \text{OH}^- + \text{HO}\cdot$	hydroxyl radical	(1)
$\text{FeII} + \text{O}_2 \rightarrow \text{FeIII} + \text{O}_2^{\cdot-}$	superoxide anion radical	(2)
$\text{FeII} + \text{O}_2^{\cdot-} + 2\text{H}^+ \rightarrow \text{FeIII} + \text{H}_2\text{O}_2$	hydrogen peroxide	(3)
$\text{FeII} + \text{HO}\cdot \rightarrow \text{FeIII} + \text{OH}^-$	hydroxyl anion	(4)
$\text{H}_2\text{O}_2 + \text{HO}\cdot \rightarrow \text{H}_2\text{O} + \text{O}_2^{\cdot-} + \text{H}^+$		(5)
$\text{H}_2\text{O}_2 + \text{O}_2^{\cdot-} + \text{H}^+ \rightarrow \text{O}_2 + \text{HO}\cdot + \text{H}_2\text{O}$		(6)
$\text{FeII} + \text{HO}\cdot + \text{H}^+ \rightarrow \text{FeIII} + \text{H}_2\text{O}$		(7)

Reaction 1 is often called the Fenton reaction, named after H.J.J. Fenton who discovered the oxidative properties of a mixture consisting of an aqueous solution of ferrous salt and hydrogen peroxide in 1876<sup>6,11</sup>. The complete set of reactions (1-7) is known as the Haber-Weiss reactions<sup>12</sup> named after the scientists who contributed to establishing the precise reaction forms.

Despite the risks associated with reactive oxygen radicals in living matter, these species also play a defensive role in organisms. These radicals are produced during normal metabolism in neutrophils, macrophages, and act as bactericides. They have also been implicated in playing a role in a cellular signaling leading to an increased cell replication.

Yet, if not properly controlled, oxygen radicals are destructive to cells. The hydroxyl radical from equation (1) has a very high redox potential of 2.33 V and is the most aggressive oxidative species of all oxygen intermediates. It is the main agent in peroxidation of lipids and destruction of proteins and nucleic acids among reactive oxygen species.

Therefore, the free iron and/or free oxygen radicals need to be stored, captured, or catalytically converted. Natural evolution has led to enzymes that perform these functions. Besides the already mentioned superoxide dismutase and catalase, there are also peroxidase and glutathione peroxidase that act on hydrogen peroxide. The iron storage protein, ferritin, which is the topic of this study, also plays an important role here. It captures free Fe(II), prevents the Fenton reaction and, in doing so, has an antioxidative function.

## FERRITINS

### General introduction

Ferritin is a hollow globular protein that can bind and store iron in its cavity in the form of a Fe(III)-oxide-hydroxide mineral. Theoretically up to 4500 Fe can be stored by ferritin<sup>13</sup>, however, in practice not more than 3000 Fe are found. Upon iron capture ferritin changes color from slightly yellowish when it is almost free of iron to bright coral-red when it is fully loaded (Fig. 1.1).



**Figure 1.1.** Solutions of *P. furiosus* iron loaded (left) and apo (right) ferritin

A ferritin molecule consists of 24 identical or homologous subunits. The structural motif of each subunit is a four  $\alpha$ -helix bundle (helices A, B, C and D) with a short fifth  $\alpha$ -helix (helix E) tilted towards the bundle axis and masking one end of the cylindrical assembly (Fig. 1.2). There are four loops between the five ferritin helices.

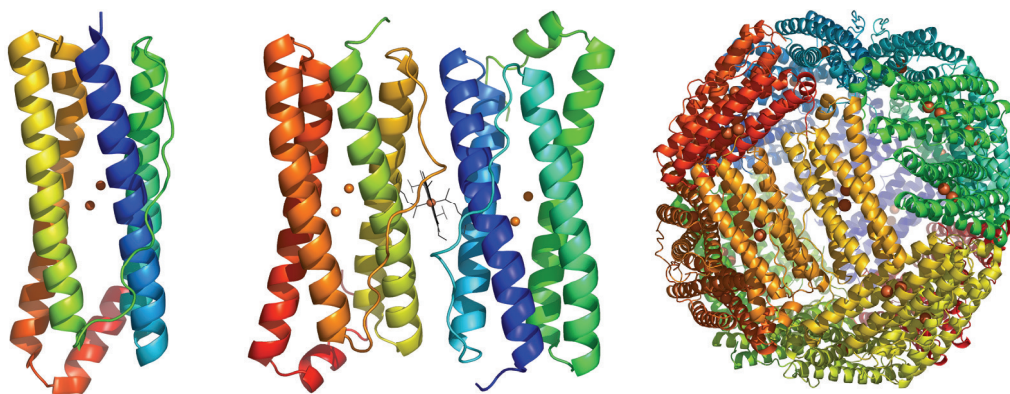


**Figure 1.2.** Ferritin structure. Left panel – single subunit (H-type AfFtn, pdb code 1S3Q); middle panel – dimer with heme group as in BFR-ferritins (EcBFR, pdb code 1BFR); right panel – ferritin oligomer composed of 24 subunits (EcBFR). Red spheres represent iron sites A and B from the ferroxidase centers

The loops AB, CD and DE are short, one-to-three amino acids in lengths, and the BC loop is long, approximately 16-19 amino acids in

length in different ferritins. The 24 subunits of *circa* 20 kDa result in a ferritin spherical structure of *circa* 500 kDa with an outer and inner diameter of *circa* 12 and 8 nm, respectively (Fig. 1.2).

Although the ferritin 24-meric spherical structure is conserved among different organisms, the variations on the primary amino acid sequence level lead to various mechanisms in iron uptake/release. In this chapter the distribution, functions, iron reaction mechanisms, and medical applications of ferritins are described.

### **Distribution and structure**

Ferritins occur in a broad variety of organisms from prokaryotes to mammals in both anaerobic and aerobic life forms. Ferritins are divided into two main groups - non-heme and heme containing ferritins. The latter are also called bacterioferritins (BFR) for reason of their first discovery in bacteria <sup>14</sup>. The heme ferritins can bind up to 12 heme groups located between every two ferritin subunits <sup>15</sup> (Fig. 1.2). A possible function of heme in BFR is an electron transfer between ferroxidase centers of two subunits.

Ferritin subunits assemble in 432 symmetry. The only exception to this rule is ferritin from *A. fulgidus* that crystallized in 23 symmetry <sup>16</sup>. Chapter IV, Crystal Structure of the Ferritin from the Hyperthermophilic Archaeal Anaerobe *Pyrococcus furiosus*, provides further information on symmetry and structural specialties of ferritins.

### **Ferritin subunits**

The 24-meric ferritin shell can be a homo or a heteropolymer composed of H and/or L subunits or homopolymer of M subunits. The names “H” and “L” were initially chosen for two types of ferritin samples, which exhibited different migration mobility in denaturing gels. The two samples originated from (H)eart and (L)iver tissues. Later, more ferritins from the same organ and even from the same cell were discovered that demonstrated different migration on SDS gel. As a result, the terminology has been changed to H(eavy) and L(ight),

sometimes also called (H)igh and (L)ow, referring to molecular mass and mobility in gel electrophoresis<sup>17,18</sup>. H ferritins are larger (Mr≈21 kDa) than L ferritins (Mr≈19 kDa), more acidic and have a lower iron content. The ratio of H and L subunits varies in ferritins from different organs in the human body. H-subunit rich ferritins, responsible for fast iron turnover, originate from heart, brain and thymus and L rich ferritins, known for their higher iron storage capacity, derive from liver and spleen<sup>10</sup>.

An important distinction between H ferritin and L ferritin is the presence of a so-called Ferroxidase Center (FC), consisting of two iron atoms. FC is present in each subunit of H type ferritin and is the cause of fast iron incorporation kinetics in comparison to L ferritin.

Another type of ferritin that was discovered later on the basis of different mRNA encoding protein<sup>19</sup> is M ferritin, where M stands for middle. M ferritins are homo-multimers<sup>20,21</sup>. M ferritin is similar to H type ferritin in possessing the FC center ligands, although it differs from H and L ferritins in molecular mass and amino acid sequence.

Besides the discussed H, L and M ferritins, other ferritins exist that differ from commonly known types by one or another characteristic. For example, some species of gram-negative and cyanobacteria, i.e. *Pseudomonas aeruginosa*, *Pseudomonas putida*, *Magnetospirillum magnetotacticum*, *Synechocystis*<sup>22-25</sup> and *Idiomarina loihiensis* contain two types of BFR. These BFRs lack characteristic amino acids involved in either heme or FC center ligation, and they seem to work cooperatively in iron catalysis and iron storage. A similar cooperativity in function was proposed for H and L chain ferritins. Although H ferritin can oxidize and store iron, the L-chain ferritin, which lacks the FC center responsible for fast oxidation, is able to generate mineral cores with higher degree of crystallinity. Figure 1.3 shows the alignment of H, L, M and BFRs ferritins.

	10	20	30	40	50	60	70	80	90	100																																																																			
H_Pfur	-----MLSERMLKALNDQLNRE	LYSAYLYFAMAAYFE	--DLGLEGFANW	KQAQAE	EE	IG	ALRFFNYI	YDRNGRVELDEI	PKPPK	-EWESPLKAF	EAA 90																																																																		
H_Ec	-----MLKPEMIEKINEQMN	ELYSLLLYQMSAWCS	--YHFFGAAAF	LRRAHQEEM	FMQRLFDY	LTDTGNL	PRINTVES	PFA	EYSSLDL	ELFQET 90																																																																			
L_Horse	MSSQIRQNYSTEVEAAVNRL	VNLVLRASYTYLSLGFY	FDRDDVALE	GVCHFFRE	LAAEKKRE	GAF	ERLLKM	QNRGGRAL	FQDLQK	PSQDEWGT	ILDAMKAA 100																																																																		
L_Rabbit	MTSQIRQNYSPVEAAVNRL	VNLVLRASYTYLSLGFY	FDRDDVALE	GVSHFFRE	LAAEKKRE	EA	ERLLKM	QNRGGRAL	FQDVQK	PSQDEWGT	ILNAMEAA 100																																																																		
M_Frog	MVSQVRQNYHSDCEAAVNRL	NLELYASYTYSSMYAF	FRDDVALH	NVAEFFKE	SHHEERE	FAEK	FMKYQNK	RGRVVLQD	IKKPER	DEWNGNT	LEAMQAA 100																																																																		
M_Ssalar	MESQIRQNYHHDCEARAINR	MINMEMFASYTYTSM	AFYSRDDVAL	PGFAHFFK	ENSEEERE	FAD	KLLSFQNK	RGRILLQD	IKKPER	DEWNGLE	AMQCA 100																																																																		
Bfr_Ddes	-MAGNREDRKAKVIEVLN	KARAMELHAIHQYMNQ	HYSLD	--DMDYGEL	AANMKLIA	DEMR	FAENFA	ERIKEL	GGEP	TQKEGK	--VVTGQAVP	VIYESD 95																																																																	
Bfr_Ec	-----MKGDTKVINYLK	LGNELVAINQYFL	HARMFK	--NWGLKRL	NDVEY	HE	SIDEMK	ADRYIER	ILFLE	GLPNLQ	DLGK--LNIGED	VEEMLRSD 90																																																																	
	110	120	130	140	150	160	170	180																																																																					
H_Pfur	YEHKFI	SKSIYELAA	EAEEKDY	STRAFL	E	WFINE	QVEE	EA	SVK	IKLDK	LKFAK	DSQIL	FMLDK	EL	SARAP	KL	PGL	LMQ	GE-- 174																																																										
H_Ec	YKHQ	LITQKIN	ELAAH	AMTNDY	PTNF	LQ	WYVSE	QHEE	EKL	FKS	IIDK	LSL	AGK	SGE	GLY	FID	KEL	STL	D	TQ	N-- 165																																																								
L_Horse	IVLE	KSINQ	ALLDL	HAL	GSQA	ADPH	LCDF	LESH	FD	EEV	KLIK	KMG	DL	TNI	QRL	V	GSQ	AG	L	GE	YL	FER	L	TL	KHD-- 175																																																				
L_Rabbit	LAL	EKNL	QALLDL	HAL	GS	AHTD	PHL	CD	FLEN	H	FD	EEV	KLIK	KMG	DL	TNI	R	RL	S	GP	AS	L	GE	YL	FER	L	TL	KHD-- 175																																																	
M_Frog	LQL	EKT	VN	QALLDL	H	KLAT	D	KV	D	PHL	CD	F	L	E	S	E	L	E	E	Q	V	K	D	I	K	R	I	G	D	F	I	N	L	K	R	L	G	L	P	E	N	G	E	Y	L	F	D	K	H	S	V	K	E	S	-- 176																						
M_Ssalar	LQL	EKN	VN	QALLDL	H	KIAS	D	KV	D	PHL	CD	F	L	E	T	H	L	N	E	Q	V	E	A	I	K	L	G	D	H	I	T	N	L	T	K	M	D	A	V	K	N	M	A	E	Y	L	F	D	K	H	T	L	G	G	Q	-- 176																					
Bfr_Ddes	ADQ	E	A	T	E	A	Y	S	Q	F	L	K	V	C	K	E	Q	D	I	V	T	A	R	L	F	E	R	I	E	E	-	E	Q	A	H	L	T	Y	E	N	I	G	S	H	I	K	N	L	G	--	D	T	Y	L	A	K	I	A	G	T	P	S	T	G	T	A	S	K	G	F	V	T	A	T	P	A	E 179
Bfr_Ec	LAL	E	D	G	A	K	N	L	R	E	A	I	G	Y	A	D	S	V	H	D	V	S	R	D	M	T	E	I	L	R	D	-	E	E	G	H	I	D	W	L	E	T	E	L	D	L	I	Q	K	M	-----	G	L	Q	N	Y	L	Q	A	I	R	E	E	G	-- 158												

**Figure 1.3.** Alignment of amino acid sequences of H, L, M and BFR ferritins from *P. furiosus*, *E. coli*, *horse*, *rabbit*, *Ra. catesbeiana*, *S. salar*, and *D. desulfuricans*. Protein accession numbers at Swiss-Prot <sup>26,27</sup> are, respectively, Q8U2T8, P0A998, P02791, P09451, P07798, P49947, Q93PP9 and P0ABD3. The figure was prepared with ClustalW <sup>28</sup>. Red color highlights the catalytic metal center ligands. Modifications in binding ligands in BFR proteins are highlighted in turquoise: the last binding motif of the catalytic metal center is modified to ExxH and Met57 coordinates a heme group. Yellow color highlights amino acids responsible for iron uptake in L ferritins

The percentage identity between amino acid sequences of H, L, M and BFR ferritins is illustrated here:

Human	H – L	52.5 %
Frog	H – L	64.2 %
	H – M	83.5 %
	L – M	60.8 %
Human H – <i>E. coli</i> BFR		19.4 %
PfFtn H – <i>E. coli</i> BFR		16.7 %
BFR-A <i>P. aerogenosa</i> – <i>E. coli</i> BFR		44 %
BFR-B <i>P. aerogenosa</i> – <i>E. coli</i> BFR		69.6 %
BFR-A – BFR-B <i>P. aerogenosa</i>		46 %

### **Ferritin-like proteins: DPS, DPSL, and Frataxin**

#### **DPS**

The DPS, DNA protecting Protein during Starvation (such as oxidative stress or nutritional starvation<sup>29</sup>), is a protein similar to ferritin in terms of structure and function. DPS is a spherical protein consisting of 12 subunits<sup>30-32</sup> (Fig. 1.4). The assembled dodecameric DPS protein stores up to 500 iron and has an outer and inner diameter of approximately 9 and 4.5 nm, respectively. DPS subunits arrange in 23 symmetry. Similar to ferritin, the DPS subunit is a bundle of four helices, but it lacks the C-terminal helix and possesses a short helix in its BC loop, that does not occur in ferritin (Fig. 1.4). The interaction of DPS with DNA is thought to occur via localisation of DPS layers near and around the DNA<sup>30,33-37</sup>. Interaction of DPS with long-chain molecules such as DNA is an attribute that extends to ferritins. Ferritins have been shown to protect DNA against oxidative damage. Binding of ferritin to microtubulin has been demonstrated by electron microscopy and by increased levels of ferritin in serum upon microtubulin destruction<sup>38-40</sup>.

Like ferritins, DPS proteins contain iron sites that are involved in an iron oxidation reaction. However, in DPS these sites occur at the

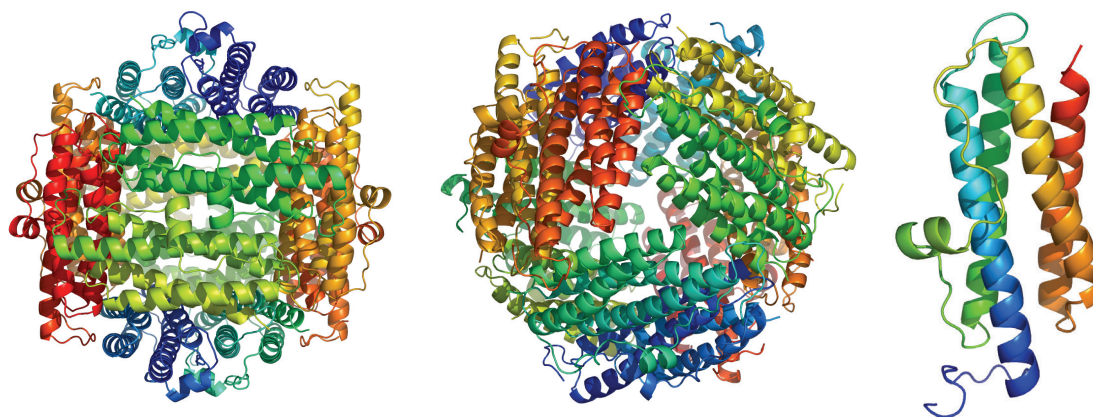


**Figure 1.4.** DPS protein. Left and middle panels – *E. coli* DPS oligomer demonstrating 2 and 3 fold symmetry, respectively. Right panel shows single DPS subunit (*E. coli*, pdb code 1DPS). Images were prepared with PyMOL <sup>41</sup>

interface of two subunits, which are related by twofold symmetry, rather than within the four-helical bundle as in ferritin. There are two (in the majority of DPS <sup>31,36,37,42</sup>) or four (*Bacillus brevis* <sup>33</sup>) iron ions per subunit pair in DPS (Fig. 1.5). The amino acid sequence identity between *E. coli* cytoplasmic ferritin FtnA and *E. coli* DPS is 19.4 %.

### DPSL

The *S. solfataricus* DPSL protein and its homologs from other organisms (often annotated as bacterioferritins-like subfamily) are

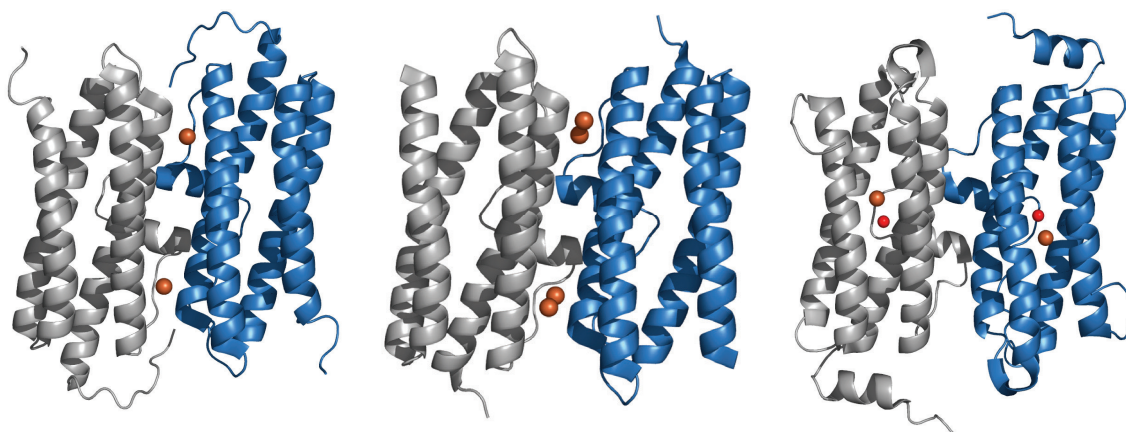


**Figure 1.5.** Metal centers in DPS from *E. coli* (left, pdb code 1DPS), DPS from *B. brevis* (middle, pdb code 1N1Q) and DPS-like protein from *S. solfataricus* (right, pdb code 2CLB). Orange spheres are iron atoms and red spheres in *S. solfataricus* are zinc atoms. Images were prepared with PyMOL <sup>41</sup>

intermediate in terms of their structure between ferritin and DPS and

represent a separate ferritin-like protein group, DPSL<sup>43-45</sup>. Contrary to the DPS iron center at the subunit interface, the SsolFDPSL possesses a ferritin-like metal center that is buried within a four-helical bundle (Fig. 1.5). The *S. solfataricus* DPSL protein is similar to DPS in its 23 symmetrical dodecameric structure and the presence of a short  $\alpha$ -helix in the BC loop; on the other hand, like ferritins it possesses ferroxidase center ligands with a di-metal center inside of the subunit and short C-terminal helix. A typical feature of DPSL proteins is a set of conserved cysteine residues that in *S. solfataricus* DPSL crystal structure (Cys 101 and 126) have been shown to be adjacent to the di-metal center and proposed to play a redox active role in iron uptake reaction<sup>45</sup>.

### Frataxin

Frataxin is a mitochondrial iron chaperon participating in iron metabolism and elimination of reactive oxygen species<sup>46-49</sup>. Frataxin is involved in Fe-S cluster assembly<sup>50,51</sup> and is required for aconitase Fe-S cluster maintenance<sup>52</sup>. It is proposed to function in heme biosynthesis<sup>53</sup>, iron storage<sup>54-56</sup>, and oxidative phosphorylation<sup>57</sup>. Frataxin malfunction in humans leads to Friedreich's ataxia, a degenerative disease affecting the nervous and cardiovascular systems<sup>58</sup>.

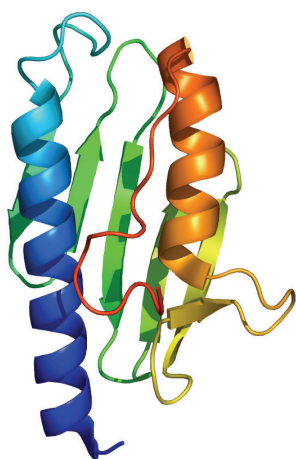


**Figure 1.6.** The frataxin monomer (mature human frataxin, pdb code 1EKG). The image was prepared with PyMOL<sup>41</sup>

Frataxin is a 2-helices-6-beta-sheets protein (Fig. 1.6.) of approximately Mr 14 kDa. Yeast frataxin polymerizes stepwise from a



single subunit  $\alpha$  to  $\alpha 3$ ,  $\alpha 6$ ,  $\alpha 12$ ,  $\alpha 24$  into a total of 48 subunits,  $\alpha 48$ , with a total Mr 840 kDa<sup>59-61</sup>. Contrary to ferritins and DPS the oligomerisation of frataxin monomers does not occur spontaneously, but in the presence of FeII and O<sub>2</sub>. The assembled 48-mer frataxin binds approximately 50 Fe per monomer, or 2400 Fe per 48-mer<sup>55</sup>.

### **Ferroxidase center and catalytic metal sites**

H-type ferritins possess iron centers within every subunit (Fig. 1.2). Initially two iron atom binding sites, named A and B, were identified. The two iron sites are located approximately 3 Å from each other and together are called a ferroxidase center (FC). The name comes from the ferroxidase reaction, i.e. the oxidation of ferrous iron Fe(II) to ferric Fe(III). Later a third iron site, site C, was identified in bacterial H-type ferritins from *E. coli* (EcFtnA), *A. fulgidus* (AfFtn), and *P. furiosus* (PfFtn)<sup>16,62,63</sup> (see chapter IV). This site is located near the ferroxidase center; approximately 6-7 Å away from sites A and B. Table 1.1 shows patterns of the characteristic amino acids involved in the coordination of the ferroxidase centers and, if applicable, sites C in PfFtn, EcFtnA, AfFtn, Human H chain ferritin (HuHF), *E. coli* BFR (EcBFR) and *S. solfataricus* DPSL (SsolFDPSL). Amino acids that coordinate site C in PfFtn, AfFtn and EcFTNA are shown in bold.

DPS proteins do not possess intersubunit ferroxidase centers but have one iron site per each monomer located at the exterior of the 4-helical bundle in the interface of two subunits that are related by two-fold symmetry. The exception is *Bacillus brevis* DPS protein that has two iron sites per monomer in this interface.

DPSL (DPS-like) protein from *Sulfolobus solfataricus* possesses a metal center that is similar to the ferroxidase center of classical ferritins<sup>45</sup> and is located within the helical bundle (Fig. 1.5). Moreover, it has a typical pattern of the amino acids as those that coordinate the site C in PfFtn, AfFtn and EcFTNA (Fig. 1.7). The location of these amino acids on the inner side of *S. solfataricus* DPSL shell is very similar to PfFtn, AfFtn and EcFTNA and suggests the

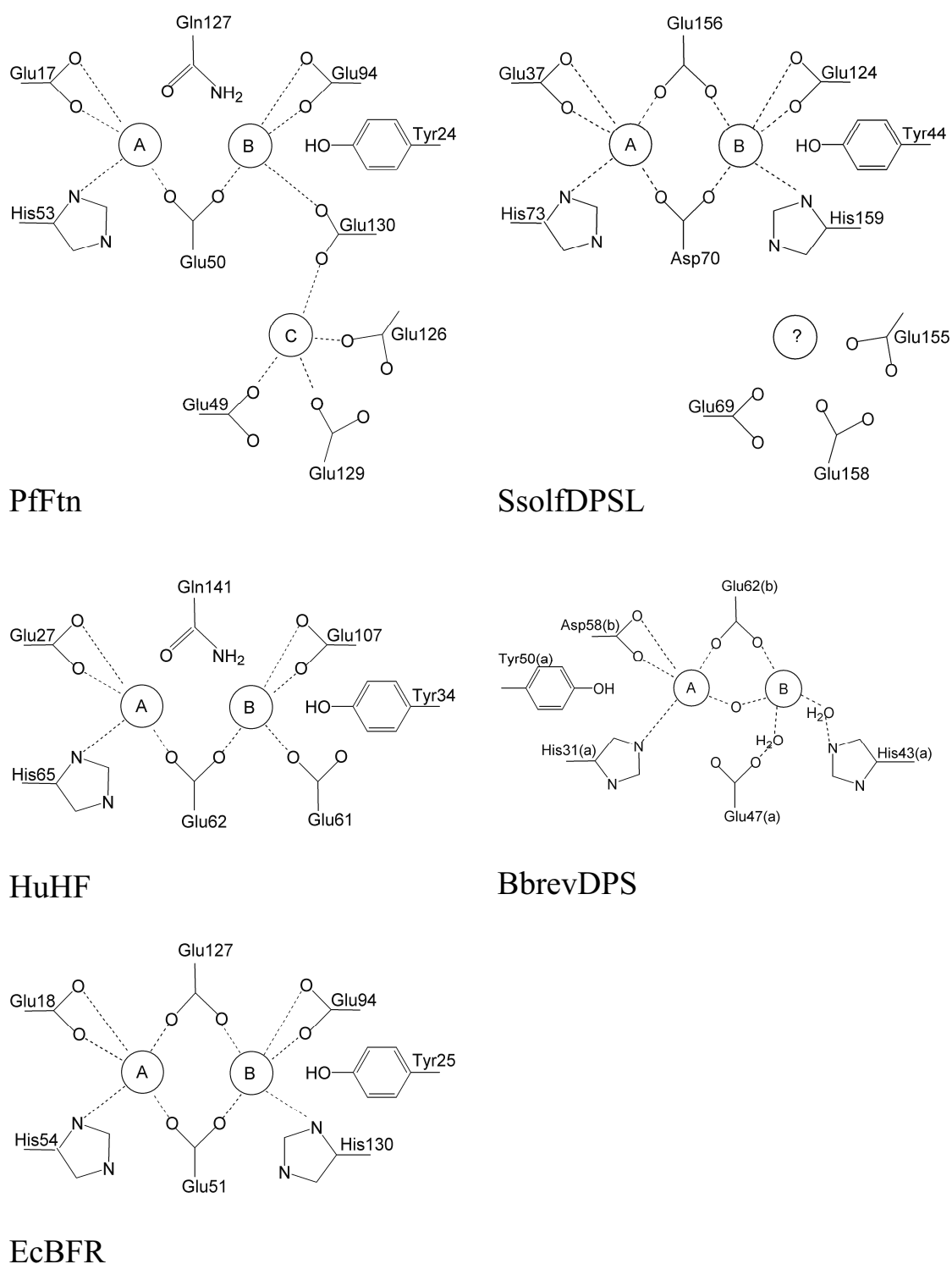


**Figure 1.7.** The coordination schemes of the ferroxidase centers and the catalytic metal sites of *P. furiosus* Ftn (PfFtn), *E. coli* FtnA (EcFTNA), Human H chain ferritin (HuHF), *E.coli* BFR (EcBFR), *S. solfataricus* DPSL (SsolfDPSL), and *B. brevis* DPS (BbrevDPS)

possibility that SsolfdPSL protein possesses a metal in the site C that has not been observed yet (table 1.1, fig. 1.7).

**Table 1.1.** A pattern of the characteristic amino acids coordinating the catalytic metal centers in *P. furiosus* Ftn (PfFtn), *E. coli* FtnA (EcFTNA), *A. fulgidus* (AfFtn), Human H chain ferritin (HuHF), *E. coli* BFR (EcBFR), and *S. solfataricus* DPSL (SsolfdPSL).

	<i>Helix A</i>	<i>Helix B</i>	<i>Helix C</i>	<i>Helix D</i>
<i>PfFtn</i>	E <sub>17</sub>	<b>E<sub>49</sub>E<sub>50</sub>XXH<sub>53</sub></b>	E <sub>94</sub>	<b>E<sub>126</sub>Q<sub>127</sub>XE<sub>129</sub>E<sub>130</sub></b>
<i>EcFTNA</i>	E <sub>17</sub>	<b>E<sub>49</sub>E<sub>50</sub>XXH<sub>53</sub></b>	E <sub>94</sub>	<b>E<sub>126</sub>Q<sub>127</sub>XE<sub>129</sub>E<sub>130</sub></b>
<i>AfFtn</i>	E <sub>19</sub>	<b>E<sub>51</sub>E<sub>52</sub>XXH<sub>55</sub></b>	E <sub>96</sub>	<b>E<sub>128</sub>Q<sub>129</sub>XE<sub>131</sub>E<sub>132</sub></b>
<i>HuHF</i>	E <sub>27</sub>	E <sub>61</sub> E <sub>62</sub> XXH <sub>65</sub>	E <sub>107</sub>	Q <sub>141</sub>
<i>EcBFR</i>	E <sub>18</sub>	E <sub>51</sub> XXH <sub>54</sub>	E <sub>94</sub>	E <sub>127</sub> X X H <sub>130</sub>
<i>SsolfdPSL</i>	E <sub>37</sub>	<b>E<sub>69</sub>D<sub>70</sub>XXH<sub>73</sub></b>	E <sub>124</sub>	<b>E<sub>155</sub>E<sub>156</sub>XE<sub>158</sub>H<sub>159</sub></b>

### **Mechanisms of iron incorporation into ferritin**

Iron incorporation in ferritins proceeds in three main steps: binding of Fe(II), oxidation to Fe(III), and mineralization in the cavity as an iron oxide-hydroxide mineral. However, different mechanisms of iron uptake/release in different types of ferritins are observed. In H-chain ferritins the ferroxidase center is the major unit responsible for iron oxidation. It has been proposed to function as a stable di-iron prosthetic group or as a transient center in different H chain ferritins <sup>64-67</sup>.

### **Mammalian H-chain ferritins**

In mammalian H-chain ferritins the iron uptake reaction proceeds via binding of Fe(II) to the ferroxidase center, oxidation by O<sub>2</sub> or H<sub>2</sub>O<sub>2</sub> and formation of  $\mu$ -1,2-peroxo-diferric intermediates, subsequent transformation of peroxo- into oxo-diferric intermediates and translocation of the oxo-diferric intermediates to the nucleation centers on internal cavity for mineral formation. At high amount of Fe(II) the oxidation of iron also occurs via an autocatalytic reaction on the growing mineral core.

### Bacterial H-chain ferritins

The mechanism in bacterial H-chain ferritins is similar to that in mammalian H ferritins, however, the stoichiometry of Fe to O<sub>2</sub> is higher in bacterial ferritins. This might be due to the presence of site C near the ferroxidase center that is involved in catalysis.

### L-chain ferritins

In L-chain ferritins the ferroxidase center is not present. Therefore, iron oxidation occurs only by means of an autocatalytic reaction on the mineral core. The Fe/O<sub>2</sub> ratio in this reaction is lower than in case of mammalian H-chain ferritins.

### BFR

The mechanism of the ferroxidase reaction in heme containing ferritins is suggested to proceed via a joint action of two ferroxidase centers. In this process, one of the FC centers reacts with O<sub>2</sub> and produces H<sub>2</sub>O<sub>2</sub> that subsequently reacts with the second FC. The stoichiometry of Fe to O<sub>2</sub> in BFR is similar to that for bacterial H-chain ferritins.

The time of iron uptake reactions in ferritins varies from milliseconds for iron binding and oxidation<sup>64,68,69</sup> up to 24 h for mineral core formation<sup>70</sup>.

### Iron mineral core of ferritin

Oxidized iron is stored in the ferritin cavity as an Fe(III) oxide/hydroxide mineral with some amount of phosphate (P<sub>i</sub>). The ratio Fe/P<sub>i</sub> varies from approximately 10-20 in mammalian ferritins to 1-2 in bacterial ferritins and BFRs.

The structure of the mineral core has been studied with X-ray, electron diffraction, electron microscopy, EXAFS, XANES, and Mössbauer spectroscopy. These studies revealed that the main structure of the ferritin mineral core is highly similar to the ferrihydrite mineral 5Fe<sub>2</sub><sup>III</sup>O<sub>3</sub> · 9(H<sub>2</sub>O)<sup>71</sup>. More recently, other techniques have been

employed such as NMR relaxometry<sup>70,72</sup>, electron nanodiffraction, and high resolution electron microscopy. These studies showed that the ferritin mineral core can also contain minor amounts of hematite  $\alpha$ - $\text{Fe}^{\text{III}}_2\text{O}_3$ , some cubic magnetite  $\text{Fe}^{\text{II}}\text{Fe}^{\text{III}}_2\text{O}_4$ /maghemite  $\gamma$ - $\text{Fe}^{\text{III}}_2\text{O}_3$  phases or wüstite  $\text{Fe}^{\text{II}}\text{O}$ <sup>73</sup>. In case of human ferritin the mineral core structure is different in samples of brain ferritin from healthy individuals and those with iron associated degenerative disorders such as hemochromatosis, Alzheimer's disease and Progressive Supranuclear Palsy (or the Steele-Richardson-Olszewski syndrome). In case of iron related diseases, the hematite is not observed, the ferrihydrite is almost absent and instead the mineral core structure is similar to wüstite (also found in hemosiderin), and magnetite-like mineral<sup>74</sup>.

### **Ferritin's role in the organism and medical implication**

Ferritin is a protein involved in iron homeostasis of an organism. Consequently, it plays a role in iron related diseases, which are caused by or result in iron overload, iron deficiency or oxidative damage. Examples of such diseases are hereditary sutural cataract<sup>75</sup> and neuroferritinopathy, also known as dominant adult-onset basal ganglia disease<sup>76,77</sup>, which are illnesses associated with mutations in the L ferritin gene, neurodegenerative diseases (Parkinson's, Alzheimer's and Batten's diseases, sclerosis), sickle cell anemia, thalassemia, cardiovascular disorders (coronary artery disease, ischaemic heart disease, myocardial infarction), rheumatoid arthritis, hemochromatosis, diabetes, cirrhosis, cancer and more. Ferritin can localize near DNA and protect DNA against oxidative damage. H ferritin has been shown to play an important role in chemokine receptor signaling and receptor-mediated cell migration<sup>78</sup>. Bacterioferritin from *Brucella melitensis* increases the T-helper-1 type immune response in mice<sup>79,80</sup>. The H-chain ferritin has been shown to be important for embryo development; H ferritin deletion in mice resulted in embryo death<sup>81</sup>. In addition, a related protein, placenta immunomodulatory ferritin (PLIF), that consists of incomplete H-chain ferritin and a C-terminal 48 amino

acids domain, plays a major role in placentation and embryonic development inhibiting the immune response<sup>82</sup>.

Ferritin's application in the area of medicine includes diet design to treat anemia<sup>83-85</sup>, usage of serum ferritin level as a cancer marker<sup>86</sup>, and fabrication of ferritin immunosensors for this purpose<sup>87-89</sup>. Other medical applications of ferritin that are now developing include regulation of ferritin's iron uptake/release by chemically opening or closing ferritin's pores<sup>90</sup>, usage of ferritin as an endogenous MRI reporter for noninvasive MRI imaging<sup>91,92</sup>, development of gene therapy where induction of nuclear H ferritin expression may prevent sickle cell anemia, cancer and other diseases described above, and cancer treatment with anti-ferritin monoclonal antibodies<sup>93-95</sup>.

### ***PYROCOCCUS FURIOSUS* AND SCOPE OF THE THESIS**

The archaeon *Pyrococcus furiosus* is a strict anaerobe that thrives in shallow marine hot springs. It was discovered in sediment off

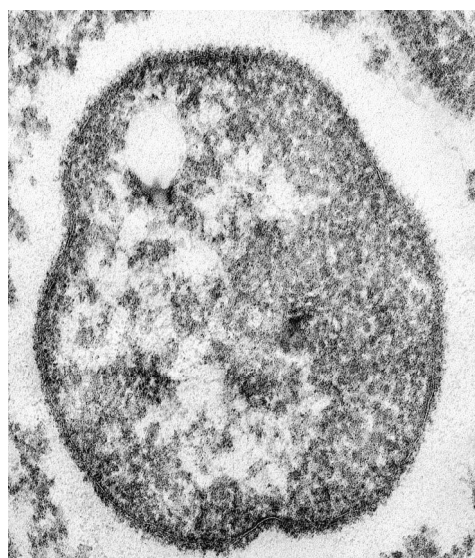


**Figure 1.8.** *Pyrococcus furiosus* cell. Thin section electron microphotograph<sup>i</sup>

---

<sup>i</sup> The sample was prepared by prefixing the cells in 3% v/v glutaraldehyde at pH 7.0 in presence of 0.2 M NaCl, postfixing in 1% w/v OsO<sub>4</sub>/0.2 M NaCl for 3 h at room temperature, washing and staining overnight with 1% w/v uranyl acetate, dehydrating in an ethanol series and embedding in Epon resin. Thin sections were contrasted with 1% w/v lead citrate and examined under a JEOL 100 transmitting electron microscope (Japan). The image was prepared in collaboration with the Institute of Microbiology of the Russian Academy of Sciences, Moscow, Russia

the shore of Porto di Levante, Vulcano, Italy <sup>96</sup>. *P. furiosus* belongs to the kingdom of Euryarchaeota, family of Thermococci. It is a heterotroph, growing on starch, maltose, peptone, or tryptone, plus yeast extract and producing CO<sub>2</sub>, H<sub>2</sub>, H<sub>2</sub>S (if grown on S<sup>0</sup>) and acetate. *P. furiosus* is a hyperthermophile which grows between 70-103 °C and has an optimal growth temperature of 100 °C. The growth pH range is 5-9. Cell wall does not contain murein; cell membrane contains isopranyl ether lipids, which are characteristic for archaea. This archaeon has a spherical body of *circa* 2 μm in diameter and polytrichous flagella (figure not shown). Figure 1.8 shows a thin section electron microphotograph of the *P. furiosus* cell. The cell wall is well visible. As usual for archaea, the periplasmic space is narrow and can hardly be distinguished in this figure. The white area is probably DNA and the white oval on the top could be a polyglucosic inclusion.

This thesis focuses on a ferritin protein of *P. furiosus* (PfFtn). As described in the Summary, there are number of intriguing issues about ferritins from anaerobic organisms. The following chapters address these issues with PfFtn as an example.

Chapter II, “A Highly Thermostable Ferritin from the Hyperthermophilic Archaeal Anaerobe *Pyrococcus furiosus*”, describes the purification and initial biochemical/biophysical characterization of ferritin from *P. furiosus*. This chapter describes structural and kinetic properties of PfFtn. Based on gel electrophoresis the protein appears to be similar to known ferritins: it is a 24-mer with total Mr 480 kDa. PfFtn is able to oxidize Fe(II) and store it in its cavity as Fe(III). The iron storage capacity of PfFtn is high (2700 Fe/24-mer) and is comparable to that of bacterial ferritins. The EPR spectrum of the iron loaded PfFtn represents a characteristic signal for a superparamagnet, which originates from the iron mineral core inside of PfFtn. The kinetics features are discussed and extreme hyperthermostability of the protein is demonstrated.

Chapter III, “Crystallization and preliminary X-ray

characterization of a ferritin from the hyperthermophilic archaeon and anaerobe *Pyrococcus furiosus*”, describes the initial work towards the elucidation of PfFtn three-dimensional structure, namely crystals production and preliminary data collection and structure analysis. Crystals were grown with the hanging drop vapor diffusion method against a 2 M ammonium sulfate solution from as-isolated and from iron loaded protein samples. PfFtn crystals had a pyramidal shape with average size of 100-200  $\mu\text{m}$ . Only crystals from as-isolated protein produced sufficient diffraction quality with a resolution of 3 Å. Crystals from an iron loaded sample diffracted to 6 Å. Improvement of crystallization has been attempted by using different crystallization solutions and conditions as well as by growing the crystals in a high magnetic field (1-1.5 Tesla). This latter procedure has been reported to improve the quality of crystals in several studies, mostly on lysozyme<sup>97-99</sup>. However, no better crystals appeared than those grown against 2 M ammonium sulfate in zero magnetic field. The produced crystals belonged to the orthorhombic space group  $C222_1$ , with unit-cell parameters  $a = 258.1$ ,  $b = 340.1$ ,  $c = 266.5$  Å. A total of 36 monomers were found in the asymmetric unit, corresponding to one and a half 24-mers. The structure determination was carried out via the molecular replacement method using ferritin from *Thermatoga maritima* as the search model.

Chapter IV, “Crystal Structure of the Ferritin from the Hyperthermophilic Archaeal Anaerobe *Pyrococcus furiosus*”, is a follow up of chapter III where three-dimensional structure of PfFtn is reported. While working on this chapter we collected additional data from crystals produced from as-isolated and iron loaded samples and from as-isolated crystals soaked in iron or zinc. Data were collected at and near the metals’ X-ray absorption edges. The best data set could be refined to 2.75 Å. In this chapter the quaternary structure, the occupation of metal sites at the ferritin ferroxidase center, the stability of the ferroxidase center, and the basis of protein thermostability are discussed. The quaternary structure appears to be different from that of



the previously crystallized archaeal ferritin from the hyperthermophile *Archaeoglobus fulgidus*.

There are three metal sites in the subunit interface. However, only one metal site A is observed in the as-crystallized protein. Sites B and C are observed upon crystal soaking in solution of Fe(II) or Zn(II). The stability of the ferroxidase center sites A and B was investigated in an EPR study under crystallization-imitating conditions.

The thermostability analysis was performed by comparison of the PfFtn crystal structure with that of two hyperthermophiles and two mesophiles.

Chapter V, “The dinuclear iron-oxo ferroxidase center of *Pyrococcus fusiosus* ferritin is a stable prosthetic group with unexpectedly high reduction potentials”, discusses the stability of the PfFtn ferroxidase center based on results of EPR studies. EPR spectroscopy on PfFtn showed that the dinuclear ferroxidase center of PfFtn is a stable cofactor with three redox states. However, this could be different in other ferritins. The redox potentials of the ferroxidase center have been determined and appear to be rather high. This has implications for the mechanism of the iron uptake-release reaction, and these are discussed.

Chapter VI, “Ferritin-like proteins of *Pyrococcus furiosus*” describes the genome analysis of *P. furiosus* in a search for more ferritin-like proteins. Indeed, three more genes were identified, that are located close to each other in the genome and next to a putative FUR (ferric uptake regulator) protein gene. One of the identified proteins, namely Pf1195, is similar to BFR-A type ferritins. While PfFtn does not have homologues in *P. abyssi* and *P. horikoshii*, relative species of *P. furiosus*, the Pf1195 is highly similar to PAB0624 and PH1057 from *P. abyssi* and *P. horikoshii*, respectively. This once more supports the ferritin as an essential protein in anaerobes, even in those that thrive at 2 km below sea level in hyperthermal vents. One of the roles of ferritin in hyperthermophilic organisms is apparently DNA protection, a function that allows survival at extreme temperatures.

Chapter VII, “Production of nanotubes in technologically substantial amounts using ferritin” describes the way to increase the yield of nanotubes produced with ferritin. While several methods of nanotubes production exist, the ferritin method presents an advantage because it is easy in performance and results in well-shaped clear nanotubes. In this method the ferritin’s mineral core is used as a metal nanoparticle that serves as a nucleation seed for growing nanotubes. However, the yield of the produced nanotubes was not high until now. In this study a dramatic increase of the nanotubes yield was achieved by thorough emptying of the ferritin core and reloading it with iron. The natural ability of ferritin to store phosphate and other similar oxoanions results in a soft heterogeneous mineral core of as-isolated ferritins. The heterogeneous core can easily be destroyed at the high temperatures of the nanotube growth and cannot serve as a nucleation seed.

## REFERENCES

1. Turner, D. R. & Hunter, K. A. *The biogeochemistry of iron in seawater* (eds. Buffle, J. & Leeuwen van, H. P.) (John Wiley & Sons Lts, West Sussex, 2001).
2. Bashkin, V. N. *Modern biogeochemistry* (Kluwer Academic Publishers, Dordrecht, 2002).
3. Gratzer, W. *Eurekas and euphorias. The Oxford book of scientific anecdotes* (University Press, Oxford, 2002).
4. Jacobs, A. & Worwood, M. *Iron in biochemistry and medicine, II* (Academic Press, London, 1980).
5. Williams, R. J. P. & Fraústo da Silva, J. J. R. *The chemistry of evolution. The development of our ecosystem* (Elsevier B. V., 2006).
6. Symons, M. C. R. & Gutteridge, J. M. C. *Free radicals and iron: chemistry, biology and medicine* (Oxford University Press, Oxford, 1998).
7. Schlegel, H. G. *General microbiology* (Cambridge University Press, Cambridge, UK, 1997).

8. Wiegel, J. & Adams, M. W. W. *Thermophiles: the keys to molecular evolution and the origin of life?* (Taylor & Francis, 1998).
9. Schatz, G. The tragic matter. *FEBS Lett* 536, 1-2 (2003).
10. Crichton, R. R. *Inorganic biochemistry of iron metabolism: from molecular mechanisms to clinical consequences* (John Wiley & Sons, Chichester, 2001).
11. Fenton, H. J. H. On a new reaction of tartaric acid. *Chem. News* 33, 190 (1876).
12. Haber, F. & Weiss, J. The catalytic decomposition of hydrogen peroxide by iron salts. *Proc. Roy. Soc.* 147, 332-351 (1934).
13. Fischbach, F. A. & Anderegg, J. W. An x-ray scattering study of ferritin and apoferritin. *J Mol Biol* 14, 458-473 (1965).
14. Stiefel, E. I. & Watt, G. D. Azotobacter cytochrome b557.5 is a bacterioferritin. *Nature* 279, 81-83 (1979).
15. Dautant, A. et al. Structure of a monoclinic crystal form of cytochrome b1 (Bacterioferritin) from *E. coli*. *Acta Crystallogr D Biol Crystallogr* 54, 16-24 (1998).
16. Johnson, E., Cascio, D., Sawaya, M. R., Gingery, M. & Schröder, I. Crystal structures of a novel tetrahedral open pore ferritin from the hyperthermophilic archaeon *Archaeoglobus fulgidus*. *Structure* 13, 637-648 (2005).
17. Theil, E. C. Ferritin: structure, gene regulation, and cellular function in animals, plants, and microorganisms. *Annu Rev Biochem* 56, 289-315 (1987).
18. Drysdale, J. W. Ferritin phenotypes: structure and metabolism. *Ciba Foundation Symposium* 51, 41-57 (1977).
19. Dickey, L. F., Sreedharan, S., Theil, E. C., Didsbury, J. R., Wang, Y. H. & Kaufman, R. E. Differences in the regulation of messenger RNA for housekeeping and specialized-cell ferritin. A comparison of three distinct ferritin complementary DNAs, the corresponding subunits, and identification of the first processed in amphibia. *J Biol Chem* 262, 7901-7 (1987).
20. Andersen, O., Dehli, A., Standal, H., Giskegjerde, T. A., Karstensen, R. & Rorvik, K. A. Two ferritin subunits of Atlantic salmon (*Salmo salar*): cloning of the liver cDNAs and antibody preparation. *Mol Mar Biol Biotechnol* 4, 164-70 (1995).

21. Mignogna, G., Chiaraluce, R., Consalvi, V., Cavallo, S., Stefanini, S. & Chiancone, E. Ferritin from the spleen of the Antarctic teleost *Trematomus bernacchii* is an M-type homopolymer. *Eur J Biochem* 269, 1600-6 (2002).
22. Moore, G. R., Kadir, F. H., al-Massad, F. K., Le Brun, N. E., Thomson, A. J., Greenwood, C., Keen, J. N. & Findlay, J. B. Structural heterogeneity of *Pseudomonas aeruginosa* bacterioferritin. *Biochem J* 304 (Pt 2), 493-7 (1994).
23. Miller, C. D., Kim, Y. C., Walsh, M. K. & Anderson, A. J. Characterization and expression of the pseudomonas putida bacterioferritin alpha subunit gene. *Gene* 247, 199-207 (2000).
24. Keren, N., Aurora, R. & Pakrasi, H. B. Critical roles of bacterioferritins in iron storage and proliferation of cyanobacteria. *Plant Physiol* 135, 1666-73 (2004).
25. Bertani, L. E., Huang, J. S., Weir, B. A. & Kirschvink, J. L. Evidence for two types of subunits in the bacterioferritin of *Magnetospirillum magnetotacticum*. *Gene* 201, 31-6 (1997).
26. Gasteiger, E., Gattiker, A., Hoogland, C., Ivanyi, I., Appel, R. D. & Bairoch, A. ExpPASy: The proteomics server for in-depth protein knowledge and analysis. *Nucleic Acids Res* 31, 3784-8 (2003).
27. Boeckmann, B., Bairoch, A., Apweiler, R., Blatter, M. C., Estreicher, A., Gasteiger, E., Martin, M. J., Michoud, K., O'Donovan, C., Phan, I., Pilbout, S. & Schneider, M. The SWISS-PROT protein knowledgebase and its supplement TrEMBL in 2003. *Nucleic Acids Res* 31, 365-70 (2003).
28. Combet, C., Blanchet, C., Geourjon, C. & Deleage, G. NPS@: Network Protein Sequence Analysis. *Trends Biochem Sci* 25, 147-150 (2000).
29. Almiron, M., Link, A. J., Furlong, D. & Kolter, R. A novel DNA-binding protein with regulatory and protective roles in starved *Escherichia coli*. *Genes Dev.* 6, 2646-2654 (1992).
30. Grant, R. A., Filman, D. J., Finkel, S. E., Kolter, R. & Hogle, J. M. The crystal structure of Dps, a ferritin homolog that binds and protects DNA. *Nat. Struct. Biol.* 5, 294-303 (1998).
31. Zeth, K., Offermann, S., Essen, L. O. & Oesterhelt, D. Iron-oxo clusters biomineralizing on protein surfaces: structural analysis of *Halobacterium salinarum* DpsA in its low- and high-iron states. *Proc. Natl. Acad. Sci. USA* 101, 13780-13785 (2004).
32. Roy, S., Gupta, S., Das, S., Sekar, K., Chatterji, D. & Vijayan, M. X-ray analysis of *Mycobacterium smegmatis* Dps and a comparative study

- involving other Dps and Dps-like molecules. *J Mol Biol* 339, 1103-13 (2004).
33. Ren, B., Tibbelin, G., Kajino, T., Asami, O. & Ladenstein, R. The multi-layered structure of Dps with a novel di-nuclear ferroxidase center. *J Mol Biol* 329, 467-77 (2003).
  34. Ilari, A., Latella, M. C., Ceci, P., Ribacchi, F., Su, M., Giangiacomo, L., Stefanini, S., Chasteen, N. D. & Chiancone, E. The unusual intersubunit ferroxidase center of *Listeria innocua* Dps is required for hydrogen peroxide detoxification but not for iron uptake. A study with site-specific mutants. *Biochemistry* 44, 5579-87 (2005).
  35. Papinutto, E., Dundon, W. G., Pitulis, N., Battistutta, R., Montecucco, C. & Zanotti, G. Structure of two iron-binding proteins from *Bacillus anthracis*. *J Biol Chem* 277, 15093-8 (2002).
  36. Zanotti, G., Papinutto, E., Dundon, W., Battistutta, R., Seveso, M., Giudice, G., Rappuoli, R. & Montecucco, C. Structure of the neutrophil-activating protein from *Helicobacter pylori*. *J Mol Biol* 323, 125-30 (2002).
  37. Ceci, P., Ilari, A., Falvo, E. & Chiancone, E. The Dps protein of *Agrobacterium tumefaciens* does not bind to DNA but protects it toward oxidative cleavage: x-ray crystal structure, iron binding, and hydroxyl-radical scavenging properties. *J Biol Chem* 278, 20319-20326 (2003).
  38. Hasan, M. R., Morishima, D., Tomita, K., Katsuki, M. & Kotani, S. Identification of a 250 kDa putative microtubule-associated protein as bovine ferritin. Evidence for a ferritin-microtubule interaction. *Febs J* 272, 822-31 (2005).
  39. Hasan, M. R., Koikawa, S., Kotani, S., Miyamoto, S. & Nakagawa, H. Ferritin forms dynamic oligomers to associate with microtubules in vivo: implication for the role of microtubules in iron metabolism. *Exp Cell Res* 312, 1950-60 (2006).
  40. Ramm, G. A., Powell, L. W. & Halliday, J. W. Effect of the microtubular inhibitor vinblastine on ferritin clearance and release in the rat. *J Gastroenterol Hepatol* 11, 1072-8 (1996).
  41. DeLano, W. L. The PyMOL molecular graphics system. (DeLano Scientific, San Carlos, 2002). <http://pymol.sourceforge.net/>
  42. Ilari, A., Stefanini, S., Chiancone, E. & Tsernoglou, D. The dodecameric ferritin from *Listeria innocua* contains a novel intersubunit iron-binding site. *Nat Struct Biol* 7, 38-43 (2000).

43. Ramsay, B., Wiedenheft, B., Allen, M., Gauss, G. H., Lawrence, C. M., Young, M. & Douglas, T. Dps-like protein from the hyperthermophilic archaeon *Pyrococcus furiosus*. *J Inorg Biochem* 100, 1061-8 (2006).
44. Wiedenheft, B., Mosolf, J., Willits, D., Yeager, M., Dryden, K. A., Young, M. & Douglas, T. An archaeal antioxidant: characterization of a Dps-like protein from *Sulfolobus solfataricus*. *Proc Natl Acad Sci U S A* 102, 10551-6 (2005).
45. Gauss, G. H., Benas, P., Wiedenheft, B., Young, M., Douglas, T. & Lawrence, C. M. Structure of the DPS-like protein from *Sulfolobus solfataricus* reveals a bacterioferritin-like dimetal binding site within a DPS-like dodecameric assembly. *Biochemistry* 45, 10815-27 (2006).
46. Pandolfo, M. The molecular basis of Friedreich ataxia. *Neurologia* 15, 325-9 (2000).
47. Bencze, K. Z. et al. The structure and function of frataxin. *Crit Rev Biochem Mol Biol* 41, 269-91 (2006).
48. Yoon, T., Dizin, E. & Cowan, J. A. N-terminal iron-mediated self-cleavage of human frataxin: regulation of iron binding and complex formation with target proteins. *J Biol Inorg Chem* (2007).
49. Cook, J. D., Bencze, K. Z., Jankovic, A. D., Crater, A. K., Busch, C. N., Bradley, P. B., Stemmler, A. J., Spaller, M. R. & Stemmler, T. L. Monomeric yeast frataxin is an iron-binding protein. *Biochemistry* 45, 7767-77 (2006).
50. Foury, F., Pastore, A. & Trincal, M. Acidic residues of yeast frataxin have an essential role in Fe-S cluster assembly. *EMBO Rep* 8, 194-9 (2007).
51. Busi, M. V., Maliandi, M. V., Valdez, H., Clemente, M., Zabaleta, E. J., Araya, A. & Gomez-Casati, D. F. Deficiency of *Arabidopsis thaliana* frataxin alters activity of mitochondrial Fe-S proteins and induces oxidative stress. *Plant J* 48, 873-82 (2006).
52. Bulteau, A. L., O'Neill, H. A., Kennedy, M. C., Ikeda-Saito, M., Isaya, G. & Szweda, L. I. Frataxin acts as an iron chaperone protein to modulate mitochondrial aconitase activity. *Science* 305, 242-5 (2004).
53. Yoon, T. & Cowan, J. A. Frataxin-mediated iron delivery to ferrochelatase in the final step of heme biosynthesis. *J Biol Chem* 279, 25943-6 (2004).
54. O'Neill, H. A., Gakh, O., Park, S., Cui, J., Mooney, S. M., Sampson, M., Ferreira, G. C. & Isaya, G. Assembly of human frataxin is a mechanism for detoxifying redox-active iron. *Biochemistry* 44, 537-45 (2005).

55. Park, S., Gakh, O., O'Neill, H. A., Mangravita, A., Nichol, H., Ferreira, G. C. & Isaya, G. Yeast frataxin sequentially chaperones and stores iron by coupling protein assembly with iron oxidation. *J Biol Chem* 278, 31340-51 (2003).
56. Nichol, H., Gakh, O., O'Neill, H. A., Pickering, I. J., Isaya, G. & George, G. N. Structure of frataxin iron cores: an X-ray absorption spectroscopic study. *Biochemistry* 42, 5971-6 (2003).
57. Ristow, M., Pfister, M. F., Yee, A. J., Schubert, M., Michael, L., Zhang, C. Y., Ueki, K., Michael, M. D., 2<sup>nd</sup>, Lowell, B. B. & Kahn, C. R. Frataxin activates mitochondrial energy conversion and oxidative phosphorylation. *Proc Natl Acad Sci U S A* 97, 12239-43 (2000).
58. Campuzano, V., Montermini, L., Molto, M. D., Pianese, L., Cossee, M., Cavalcanti, F., Monros, E., Rodius, F., Duclos, F., Monticelli, A. et al. Friedreich's ataxia: autosomal recessive disease caused by an intronic GAA triplet repeat expansion. *Science* 271, 1423-7 (1996).
59. Karlberg, T., Schagerlof, U., Gakh, O., Park, S., Ryde, U., Lindahl, M., Leath, K., Garman, E., Isaya, G. & Al-Karadaghi, S. The structures of frataxin oligomers reveal the mechanism for the delivery and detoxification of iron. *Structure* 14, 1535-46 (2006).
60. Park, S., Gakh, O., Mooney, S. M. & Isaya, G. The ferroxidase activity of yeast frataxin. *J Biol Chem* 277, 38589-95 (2002).
61. Gakh, O., Adamec, J., Gacy, A. M., Twesten, R. D., Owen, W. G. & Isaya, G. Physical evidence that yeast frataxin is an iron storage protein. *Biochemistry* 41, 6798-804 (2002).
62. Stillman, T. J., Hempstead, P. D., Artymiuk, P. J., Andrews, S. C., Hudson, A. J., Treffry, A., Guest, J. R. & Harrison, P. M. The high-resolution X-ray crystallographic structure of the ferritin (EcFtnA) of *Escherichia coli*; comparison with human H ferritin (HuHF) and the structures of the Fe(3+) and Zn(2+) derivatives. *J Mol Biol* 307, 587-603 (2001).
63. Tatur, J., Hagen, W. R. & Matias, P. M. Crystal structure of the ferritin from the hyperthermophilic archaeal anaerobe *Pyrococcus furiosus*. *J Biol Inorg Chem* 12, 615-630 (2007).
64. Yang, X., Le Brun, N. E., Thomson, A. J., Moore, G. R. & Chasteen, N. D. The iron oxidation and hydrolysis chemistry of *Escherichia coli* bacterioferritin. *Biochemistry* 39, 4915-23 (2000).
65. Baaghil, S., Lewin, A., Moore, G. R. & Le Brun, N. E. Core formation in *Escherichia coli* bacterioferritin requires a functional ferroxidase center. *Biochemistry* 42, 14047-14056 (2003).

66. Le Brun, N. E., Thomson, A. J. & Moore, G. R. Metal centres of bacterioferritins or non-haem-iron-containing cytochromes b557. *Structure and Bonding* 88, 103-138 (1997).
67. Lewin, A., Moore, G. R. & Le Brun, N. E. Formation of protein-coated iron minerals. *Dalton Trans*, 3597-3610 (2005).
68. Le Brun, N. E., Wilson, M. T., Andrews, S. C., Guest, J. R., Harrison, P. M., Thomson, A. J. & Moore, G. R. Kinetic and structural characterization of an intermediate in the biomineralization of bacterioferritin. *FEBS Lett.* 333, 197-202 (1993).
69. Le Brun, N. E., Andrews, S. C., Guest, J. R., Harrison, P. M., Moore, G. R. & Thomson, A. J. Identification of the ferroxidase centre of Escherichia coli bacterioferritin. *Biochem J* 312 (Pt 2), 385-92 (1995).
70. Herynek, V., Bulte, J. W., Douglas, T. & Brooks, R. A. Dynamic relaxometry: application to iron uptake by ferritin. *J Biol Inorg Chem* 5, 51-6 (2000).
71. Towe, K. M. & Bradley, W. F. Mineralogical constitution of colloidal hydrous ferric oxides. *J Colloid Interf Sci* 24, 384-392 (1967).
72. Gossuin, Y., Hautot, D., Muller, R. N., Pankhurst, Q., Dobson, J., Morris, C., Gillis, P. & Collingwood, J. Looking for biogenic magnetite in brain ferritin using NMR relaxometry. *NMR Biomed* 18, 469-72 (2005).
73. Cowley, J. M., Janney, D. E., Gerkin, R. C. & Buseck, P. R. The structure of ferritin cores determined by electron nanodiffraction. *J Struct Biol* 131, 210-6 (2000).
74. Quintana, C., Cowley, J. M. & Marhic, C. Electron nanodiffraction and high-resolution electron microscopy studies of the structure and composition of physiological and pathological ferritin. *Journal of Structural Biology* 147, 166-178 (2004).
75. Vanita, V., Hejtmancik, J. F., Hennies, H. C., Guleria, K., Nurnberg, P., Singh, D., Sperling, K. & Singh, J. R. Sutural cataract associated with a mutation in the ferritin light chain gene (FTL) in a family of Indian origin. *Molecular Vision* 12, 93-99 (2006).
76. Curtis, A. R. J., Fey, C., Morris, C. M., Bindoff, L. A., Ince, P. G., Chinnery, P. F., Coulthard, A., Jackson, M. J., Jackson, A. P., McHale, D. P. et al. Mutation in the gene encoding ferritin light polypeptide causes dominant adult-onset basal ganglia disease. *Nature genetics* 28, 350-354 (2001).



77. Levi, S. & Cozzi, A. Neuroferritinopathy: a neurodegenerative disorder associated with L-ferritin mutation. *Best Practice & Research Clinical Haematology* 18, 265-276 (2005).
78. Li, R., Luo, C., Mines, M., Zhang, J. & Fan, G. H. Chemokine CXCL12 induces binding of ferritin heavy chain to the chemokine receptor CXCR4, alters CXCR4 signaling, and induces phosphorylation and nuclear translocation of ferritin heavy chain. *J Biol Chem* 281, 37616-27 (2006).
79. Al-Mariri, A., Tibor, A., Mertens, P., De Bolle, X., Michel, P., Godefroid, J., Walravens, K. & Letesson, J. J. Protection of BALB/c mice against *Brucella abortus* 544 challenge by vaccination with bacterioferritin or P39 recombinant proteins with CpG oligodeoxynucleotides as adjuvant. *Infect Immun* 69, 4816-22 (2001).
80. Smith, J. L. The physiological role of ferritin-like compounds in bacteria. *Crit Rev Microbiol* 30, 173-185 (2004).
81. Ferreira, C., Bucchini, D., Martin, M. E., Levi, S., Arosio, P., Grandchamp, B. & Beaumont, C. Early embryonic lethality of H ferritin gene deletion in mice. *J Biol Chem* 275, 3021-4 (2000).
82. Nahum, R., Brenner, O., Zahalka, M. A., Traub, L., Quintana, F. & Moroz, C. Blocking of the placental immune-modulatory ferritin activates Th1 type cytokines and affects placenta development, fetal growth and the pregnancy outcome. *Hum Reprod* 19, 715-22 (2004).
83. Theil, E. C. Iron, ferritin, and nutrition. *Annu Rev Nutr* 24, 327-43 (2004).
84. Lonnerdal, B., Bryant, A., Liu, X. & Theil, E. C. Iron absorption from soybean ferritin in nonanemic women. *Am J Clin Nutr* 83, 103-7 (2006).
85. Liu, X., Hintze, K., Lonnerdal, B. & Theil, E. C. Iron at the center of ferritin, metal/oxygen homeostasis and novel dietary strategies. *Biol Res* 39, 167-71 (2006).
86. Milman, N., Sengelov, H. & Dombernowsky, P. Iron status markers in patients with small cell carcinoma of the lung. Relation to survival. *Br J Cancer* 64, 895-898 (1991).
87. Yoon, H. C., Yang, H. & Byun, S. Y. Ferritin immunosensing on microfabricated electrodes based on the integration of immunoprecipitation and electrochemical signaling reactions. *Analytical Sciences* 20, 1249-1253 (2004).
88. Ko, J. S., Yoon, H. C., Yang, H., Pyo, H.-B., Chung, K. H., Kim, S. J. & Kim, Y. T. A polymer-based microfluidic device for immunosensing biochips. *Lab Chip* 3, 106-113 (2003).

89. Zhang, X., Wang, S., Hu, M. & Xiao, Y. An immunosensor for ferritin based on agarose hydrogel. *Biosensors and Bioelectronics* 21, 2180-2183 (2006).
90. Liu, X., Jin, W. & Theil, E. C. Opening protein pores with chaotropes enhances Fe reduction and chelation of Fe from the ferritin biomineral. *Proc Natl Acad Sci U S A* 100, 3653-8 (2003).
91. Cohen, B., Dafni, H., Meir, G., Harmelin, A. & Neeman, M. Ferritin as an endogenous MRI reporter for noninvasive imaging of gene expression in C6 glioma tumors. *Neoplasia* 7, 109-117 (2005).
92. Genove, G., DeMarco, U., Xu, H., Goins, W. F. & Ahrens, E. T. A new transgene reporter for in vivo magnetic resonance imaging. *Nat Med* 11, 450-4 (2005).
93. Broyles, R. H. & Floyd, R. A. Gene regulation therapy involving ferritin. United States Patent 20020128183 (2001).
94. Kadouche, J. & Levy, R. Use of anti-ferritin monoclonal antibodies in the treatment of some cancers. United States Patent 7153506 (2006).
95. Yuen, A. R., Higgins, J. P., Baker, R., Kamel, O. W., Warnke, R. A., Knox, S. J. Distribution of monoclonal antiferritin antibody in Kaposi's sarcoma, Hodgkin's disease, and hepatocellular carcinoma. *Hum Pathol* 34, 381-4 (2003).
96. Fiala, G. & Stetter, K. O. *Pyrococcus furiosus* sp. nov. represents a novel genus of marine heterotrophic archaeobacteria growing optimally at 100°C. *Arch microbiol* 145, 56-61 (1986).
97. Yin, D. C., Wakayama, N. I., Inatomi, Y., Huang, W. D. & Kuribayashi, K. Strong magnetic field effect on the dissolution process of tetragonal lysozyme crystals. *Adv Space Res* 32, 217-23 (2003).
98. Yin, D. C., Inatomi, Y., Wakayama, N. I., Huang, W. D. & Kuribayashi, K. An investigation of magnetic field effects on the dissolution of lysozyme crystal and related phenomena. *Acta Crystallogr D Biol Crystallogr* 58, 2024-30 (2002).
99. Ataka, M. & Wakayama, N. I. Effects of a magnetic field and magnetization force on protein crystal growth. Why does a magnet improve the quality of some crystals? *Acta Crystallogr D Biol Crystallogr* 58, 1708-10 (2002).





# CHAPTER II<sup>i</sup>. Highly thermostable ferritin from the hyperthermophilic archaeal anaerobe *Pyrococcus furiosus*

## ABSTRACT

A ferritin from the obligate anaerobe and hyperthermophilic archaeon *Pyrococcus furiosus* (optimal growth at 100°C) has been cloned and overproduced in *Escherichia coli* to one-fourth of total cell-free extract protein, and has been purified in one step to homogeneity. The ferritin (PfFtn) is structurally similar to known bacterial and eucaryal ferritins; it is a 24-mer of 20 kDa subunits, which add up to a total Mr 480 kDa. The protein belongs to the non-heme type of ferritins. The 24-mer contains approximately 17 Fe (as isolated), 2700 Fe (fully loaded), or <1 Fe (apoprotein). Fe-loaded protein exhibits an EPR spectrum characteristic for superparamagnetic core formation. At 25°C  $V_{\max} = 25 \mu\text{mole core Fe}^{3+}$  formed per min per mg protein when measured at 315 nm, and the  $K_{0.5} = 5 \text{ mM Fe(II)}$ . At 0.3 mM Fe(II) activity increases 100-fold from 25 to 85°C. The wild-type ferritin is detected in *P. furiosus* grown on starch. PfFtn is extremely thermostable; its activity has a half-life of 48 h at 100°C and 85 minutes at 120°C. No apparent melting temperature was found up to 120°C. The extreme thermostability of PfFtn has potential value for biotechnological applications.

---

<sup>i</sup> This chapter has been published as Tatur J, Hagedoorn P-L, Overeijnder ML, & Hagen WR. A Highly Thermostable Ferritin from the Hyperthermophilic Archaeal Anaerobe *Pyrococcus furiosus*. *Extremophiles*, 10 (2), 139-148 (2006)



## INTRODUCTION

Ferritins are present in a wide variety of organisms: bacteria, archaea, fungi, plants, insects and vertebrates. Their main role is presumably iron storage; excess of  $\text{Fe}^{2+}$  from a cell environment is internalized and then taken up by ferritin, oxidized, and stored as ferrihydride in its cavity until the cell needs it. Upon addition of reducing equivalents, iron is released. This function of ferritins is a key part of the homeostasis machinery of higher organisms that ensures the right balance of iron in the organism. Iron is an essential nutrition element as it is used for the biosynthesis of a myriad of prosthetic groups, such as heme or iron-sulfur clusters. At the same time iron excess in higher organisms leads to oxidative stress, which may result in permanent cell damage.

There are two major classes of ferritin: non-heme ferritin and heme containing ferritin or bacterioferritin. Non-heme ferritin, which is normally designated as ferritin, is present in many different species from prokaryotes to man. Bacterioferritin has been found only in bacteria and fungi. Ferritin and bacterioferritin are globular shells consisting of 24 subunits with approximate subunit size of 20 kDa, and they can theoretically bind up to 4500 Fe(III) ions per 24-mer<sup>1</sup>. A bacterioferritin harbors up to 12 heme groups per 24-mer<sup>2</sup>. An additional or alternative function for both types of ferritins in anaerobic organisms is believed to be a protection from traces of oxygen and its derivatives<sup>3,4</sup>. There is a related group of proteins, which form smaller shells of 12-mers and can incorporate *circa* 500 Fe atoms in a smaller core structure<sup>5</sup>. These proteins are frequently associated with the protection of DNA against oxidative damage, and they are named DNA-binding protein from starved cells, or Dps<sup>6</sup>.

Recent research on ferritins has been directed towards the elucidation of the differences in functions of bacterioferritins and ferritins, the role of ferritins in anaerobic organisms, and understanding the mechanism of iron incorporation. Crystallographic structures are available on ferritins, bacterioferritins, and Dps's from several species

(reviewed in <sup>4</sup>). Archaeal structural data are thus far limited to a ferritin from the sulfate-reducing thermophile *Archaeoglobus fulgidus* <sup>7</sup> and a Dps-like ferritin from the mesophilic halophile *Halobacterium salinarum* <sup>8</sup>. The latter study provides the first detailed description of a possible route from initially bound Fe(II), via oxidation of the ferroxidase site inside each subunit, to the formation of a specific iron-oxo cluster at a nucleation site <sup>8</sup>.

In the present study the putative ferritin gene from the obligate anaerobe and hyperthermophilic archaeon *Pyrococcus furiosus* has been cloned and overproduced in *Escherichia coli*. The protein purified to homogeneity showed to be a functional non-heme ferritin. The protein is the most thermostable ferritin known so far. A preliminary X-ray characterization of this ferritin has been performed <sup>9</sup> and its structure solution is on the way.

## **EXPERIMENTAL PROCEDURES**

### **Protein production**

Wild-type *P. furiosus* DSM 3638 cells were cultivated anaerobically at 92°C on starch as carbon source in the presence of 0.5 M NaCl as previously reported <sup>10</sup>. Cell-free extract was prepared as outlined in <sup>11</sup> by osmotic shock of the *P. furiosus* cells.

The putative structure gene for ferritin from *P. furiosus* (SWISS-Prot primary accession number Q8U2T8) was cloned into pET24a(+) vector (Novagen) and the protein was overproduced in BL21-CodonPlus (DE3)-RIL *E. coli* host cells (Stratagene) using the T7 promoter-lac operator IPTG induced system as earlier described <sup>9</sup>.

The produced recombinant *E. coli* cells were broken with a cell disruptor (Constant Systems) and ferritin was purified in one step by heat treatment at 100°C for 30 minutes. The precipitated proteins were removed by centrifugation.

The supernatant was buffer-exchanged into 50 mM Hepes, pH 7, NaCl 250 mM (working buffer) and concentrated over Amicon, YM-100, to give the final preparation of the protein.



### **Gel electrophoresis**

The SDS, native, and isoelectric focusing electrophoresis was performed on a Phast System (Amersham Biosciences) using 10-15% pre-cast gradient gels and 3-9 pI for IEF. The markers mix (Amersham Biosciences) consisted of thyroglobuline (porcine thyroid, 0.76 mg/ml), ferritin (horse spleen, 0.5 mg/ml), catalase (bovine liver, 0.36 mg/ml), lactate dehydrogenase (bovine heart, 0.48 mg/ml) and albumin (bovine serum, 0.40 mg/ml) for native gels and phosphorylase b (rabbit muscle, 0.67 mg/ml), albumin (bovine serum, 0.83 mg/ml), ovalbumin (chicken egg white, 1.47 mg/ml), carbonic anhydrase (bovine erythrocyte, 0.83 mg/ml), trypsin inhibitor (soybean, 0.80 mg/ml) and  $\alpha$ -lactalbumin (bovine milk, 1.16 mg/ml) for SDS gels. For SDS electrophoresis the sample was boiled for 5 minutes prior to applying to the gel to stimulate dissociation of the subunits. Protein was stained with Coomassie Brilliant Blue (CBB). Iron staining of native gels was done with Prussian blue: freshly made 2.5% potassium ferrocyanide with 2.5% of hydrochloric acid. Staining of the wild type ferritin was performed by running two lanes of the sample on the native gel, cutting the gel in two halves and staining one half with CBB and the other one with Prussian blue.

### **Molecular mass determination**

Molecular mass ( $M_r$ ) of the protein was determined with Superdex 200 HR 10/30 gel filtration chromatography calibrated with blue dextran (6 mg/ml), thyroglobuline (6 mg/ml), horse spleen ferritin (12 mg/ml), catalase (7 mg/ml), aldolase (10 mg/ml) and bovine heart cytochrome *c* (2 mg/ml) as markers. The experiment was performed with 20 mM Tris/HCl buffer pH 8, containing 0.15 M NaCl at a flow rate of 0.5 ml/min. The  $M_r$  was also determined from SDS and native gel electrophoresis.

### **N-terminal sequencing**

The N-terminal amino acid sequencing was performed via Edman

degradation on a sample blotted onto PVDF membrane.

### **Activity assay**

The ferroxidase activity of the recombinant ferritin was measured at 25-85°C by following the increase in absorption at 315 nm after the addition of iron (II) sulfate. The reaction was performed in the working buffer. The iron sulfate solution was freshly prepared in water, containing 0.1% HCl (v/v) for stabilizing the Fe(II) against auto-oxidation<sup>12</sup>, and made anaerobic by flushing with argon. The specific activity was assayed in units per mg of protein where one unit is the number of  $\mu\text{moles}$  of  $\text{Fe}^{2+}$  converted into core  $\text{Fe}^{3+}$  per minute. The extinction coefficient used was  $\epsilon_{315}=2200 \text{ M}^{-1}\text{cm}^{-1}$ <sup>13</sup>.

### **Spectroscopy**

UV-visible spectra were recorded with a Hewlett Packard 8453 photodiode array spectrophotometer; steady-state kinetics was followed on a fiber optics Avantes DM-2000 spectrophotometer. EPR spectra were recorded on a Bruker 200 D EPR spectrometer equipped with a home-built cryogenic flow system and with data collection and peripheral equipment as described in<sup>14</sup>. Spin quantitation was done versus a copper standard i.e., 10.0 mM  $\text{CuSO}_4$ , 10 mM HCl, 2 M  $\text{NaClO}_4$ . Effective  $g$  values of high-spin Fe(III) were estimated with the program RHOMBO<sup>15</sup>.

### **Thermostability**

The thermostability of the ferritin iron incorporation activity was studied by incubating the protein at 100°C in a water bath or autoclaving at 120°C and withdrawal of samples after specific time intervals followed by activity assay at 30°C. Protein was kept in HPLC bottles closed with rubber covers and capped. Samples were withdrawn with a syringe to prevent evaporation and concentration of the protein. In autoclaving experiment the time scale is the actual autoclaving time at 120°C and does not include heating and cooling time of the autoclave.

The data points were fitted (Igor 5.0) to a sigmoidal process.

Differential scanning calorimetry was performed with MicroCal VP-DSC.

### **Analytical determinations**

Protein concentration was determined with bicinchoninic acid using bovine serum albumin as the standard (BCA Kit, Pierce). The possible interference of iron in the iron-loaded samples was controlled by precipitation with trichloroacetic acid (BCA Kit instructions, Pierce). Iron was determined based on <sup>16,17</sup> as follows: to 30  $\mu\text{l}$  of protein of approximately 4  $\mu\text{M}$  concentration (24-mer) 3  $\mu\text{l}$  of HCl was added in order to disrupt the protein. After incubation at room temperature for a few minutes, the sample was centrifuged (13400 rpm, 15 min). The supernatant was collected and 50  $\mu\text{l}$  of 3 M sodium acetate and 5  $\mu\text{l}$  of 1 M ascorbic acid, pH 5-6 were added. After taking a blank spectrum, 5  $\mu\text{l}$  of 3 mM ferrene were added to the mixture. Iron concentration was calculated using the extinction coefficient of the iron-ferrene complex of 35500  $\text{M}^{-1}\text{cm}^{-1}$  at 593 nm.

### **Preparation of apo-ferritin**

The apo-ferritin was prepared based on <sup>18,19</sup> by reducing the protein solution (up to 0.5  $\mu\text{mole}$  ferritin 24-mer) with an anaerobic 50 mM sodium dithionite solution (200 ml) in the working buffer through a YM-100 membrane in a 50 ml Amicon cell.

The resulting concentrate was collected anaerobically into a glass bottle sealed with a butyl-rubber stopper and an equal amount of a fresh sodium dithionite solution was added. After overnight incubation an anaerobic 0.5% 2,2'-bipyridyl solution in ethanol was added to the sample in order to complex the remaining Fe(II). The resulting 10 ml mix was extensively dialysed against the working buffer in 12 ml dialysis Slide-A-Lyser cassettes (Pierce) and concentrated in an Amicon cell over YM-100.

### **Iron incorporation**

In order to determine the maximum iron storage capacity of PfFtn, aliquots of low iron concentrations were added stepwise to low protein concentration in order to avoid precipitation of ferritin<sup>20</sup>. Conditions for iron incorporation were as described under “Activity assay”. To 0.1-0.15 mg/ml apo-ferritin 0.3 mM iron sulfate was added. The iron uptake was conducted at 25°C and monitored spectrophotometrically at 315 nm. Another aliquot of Fe<sup>2+</sup> was added to the mixture when the iron uptake graph reached a plateau value. Additions were repeated until the solution started to become turbid as an indication of ferritin full iron saturation followed by rust formation from surplus iron and protein precipitation. The iron storage capacity was screened on multiple samples in which iron concentration was increased in steps of 50 Fe/24-mer. Iron determination was then performed on the sample with highest iron loading that showed no precipitation after 3 days of incubation on air.

### **Bioinformatics tools**

Amino acid and DNA sequences were explored with the BLAST program<sup>21</sup> at the Institute for Genomic Research database (TIGR, <http://www.tigr.org>). The multiple alignment was performed with Clustal W<sup>22</sup> software at the Network Protein Sequence analysis website<sup>23</sup>. Swiss-Prot database (<http://au.expasy.org/sprot>) was used to obtain the accession numbers of the proteins.

## **RESULTS**

### **Detection of wild-type ferritin**

The present study on recombinant ferritin from *P. furiosus* was motivated by discovery of the wild type ferritin expression. This was observed in native gel electrophoresis of cell free extract from *P. furiosus* after staining for iron. The only protein band developed on the gel upon iron staining was a band of *circa* 440 kDa, next to the horse spleen ferritin band from the marker mix (Fig. 2.1a). Attempts to purify native ferritin did not result in sufficient amount of protein for

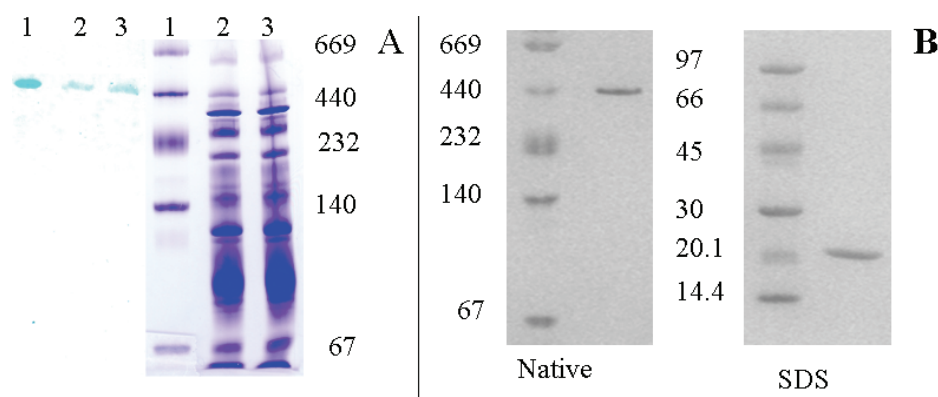


**Figure 2.1.** Wild-type and recombinant ferritin from *P. furiosus*. **A** – wild-type ferritin. Native gel was stained with coomassie brilliant blue for protein (right three lanes) and Prussian blue for iron (left three lanes). 1-Marker mix, 2 and 3 – two different preparations of cell-free extract (CFE). **B** – recombinant ferritin. Native and SDS gel electrophoresis. Molecular masses of markers are in kDa. Protein amounts used were: lane 1, 4  $\mu$ l marker mix (see Experimental procedures for concentrations); lane 2, 144  $\mu$ g CFE; lane 3, 160  $\mu$ g CFE; **B native**, 4  $\mu$ l marker mix and 24  $\mu$ g purified PfFtn; **B SDS**, 2  $\mu$ l marker mix and 18  $\mu$ g purified PfFtn

biochemical/biophysical characterization and therefore the recombinant approach has been chosen.

### **Expression and purification of recombinant ferritin**

The putative ferritin gene from *P. furiosus* was cloned and expressed as a functional protein in *E. coli* cells. The overexpressed ferritin accounted for one-fourth of the total protein in the cell free extract. This was estimated based on 100% purity of the purified ferritin as judged by gel electrophoresis (Fig. 2.1b) and a *circa* fourfold purification factor (table 2.1). A heating step is sometimes used for ferritin purifications<sup>24-27</sup> due to the protein's relatively high thermal stability. In our case the choice to use the heating step was especially motivated by hyperthermostability of *P. furiosus*, growing optimally at 100°C<sup>28</sup>. Initially the protein was purified using a heating step at 80°C, followed by Superdex 200 gel filtration chromatography, but it was subsequently found that the extreme thermostability of PfFtn (see below) allowed isolation in one step via incubation of the protein in a 100°C water bath for 30 minutes. The heating step produced pure protein based on gel electrophoresis.

**Table 2.1.** Purification table. Activities were measured at 25°C

	V	Concentr.	Total protein	Specific act.	Purific.	Yield	Ferritin (%)
	(ml)	(mg/ml)	(mg)	(U/mg)	fold	(%)	of total protein
CFE	153.0	36.0	5508.0	0.51	1.0	100.0	27.5
Heat step	31.0	16.0	496.0	1.84	3.6	32.7	100.0

The identity of the purified recombinant protein with ferritin from *P. furiosus* was checked by SDS gel electrophoresis of extract from *E. coli* cells grown with and without induction, by the ferritin assay of iron incorporation, and by N-terminal amino acid sequence determination of the purified recombinant protein. The SDS gel showed a bright band appearing in extract from induced cells only (not shown). Activity assays were performed on cell-free extracts from two types of *E. coli* cells, with and without the recombinant ferritin construct, cultivated under the same conditions. Both cell-free extracts were subjected to a heating step of 80°C and centrifugation for removal of precipitated proteins. The activity measurement (25°C) resulted in more than 130 times higher specific activity in the recombinant cells (1.502 U/mg) than in construct deficient host cells (0.011 U/mg). The N-terminal sequence of the purified recombinant ferritin was identical to that in the genome database: MLSERMLKALNDQLNRELYS. The N-terminal Met is not removed by *E. coli*.

### **Quaternary structure**

The molecular mass determined from the SDS gel was 20 kDa and from the native gel 440 kDa (Fig. 2.1b). The predicted molecular mass of the translated structural gene was 20309 Da; the molecular mass determined with mass spectrometry is 20397 Da. Analytical gel filtration chromatography gave an estimated molecular mass of 412 kDa for apoferritin and 438 kDa for ferritin fully loaded with iron. Within experimental uncertainty this is consistent with the protein being a 24-mer of *circa* 20 kDa subunits as for other known ferritins. For further calculations we assume a protein molecular mass of 480 kDa with a subunit size of 20 kDa.

### **Iron staining**

A native gel with apoferritin, ferritin as isolated, and ferritin loaded with 1152 Fe<sup>2+</sup>/24-mer was run in parallel and stained for protein and iron (not shown). Protein staining revealed all three samples with the same electrophoretic mobility. Iron staining showed loaded ferritin, a very light band of ferritin as isolated, and a band of the horse spleen ferritin present in the marker mix. Apoferritin could not be detected on the iron-staining gel.

### **Isoelectric focusing**

Isoelectric focusing of apo-ferritin and Fe-loaded ferritin afforded the same value of pI = 4.5, indicating that there is probably no iron binding on the outer side of the protein.

### **Iron incorporation**

The recombinant ferritin as isolated from *E. coli* contains *circa* 17 Fe per 24-mer. After reductive de-metallation with  $\alpha,\alpha'$ -bipyridyl<sup>18</sup> the apo-ferritin contains < 1 Fe per 24-mer. Prolonged loading of the as-isolated protein with Fe<sup>2+</sup> affords a maximal loading of *circa* 2700 Fe per 24-mer. The latter value was obtained for a sample incubated for 3 days at 22°C since the last iron addition. Ferritin samples loaded with higher amounts of iron, although they looked clear on the first day, on the second day would show precipitation. Apoferritin was also loaded with iron but showed lower iron incorporation capacity than as isolated ferritin; it could incorporate approximately 600 iron ions less than as isolated ferritin.

### **Spectroscopy**

The UV-vis spectrum of the apoprotein has absorption maxima at 227, 280 nm and a shoulder at 290 nm (Fig. 2.2). After addition of FeSO<sub>4</sub> the absorption increases (dashed line) by the growing-in of a very broad absorption peak approximately centered at 250 nm and extending all the way up to *circa* 550 nm. This spectrum from the ferrihydride core

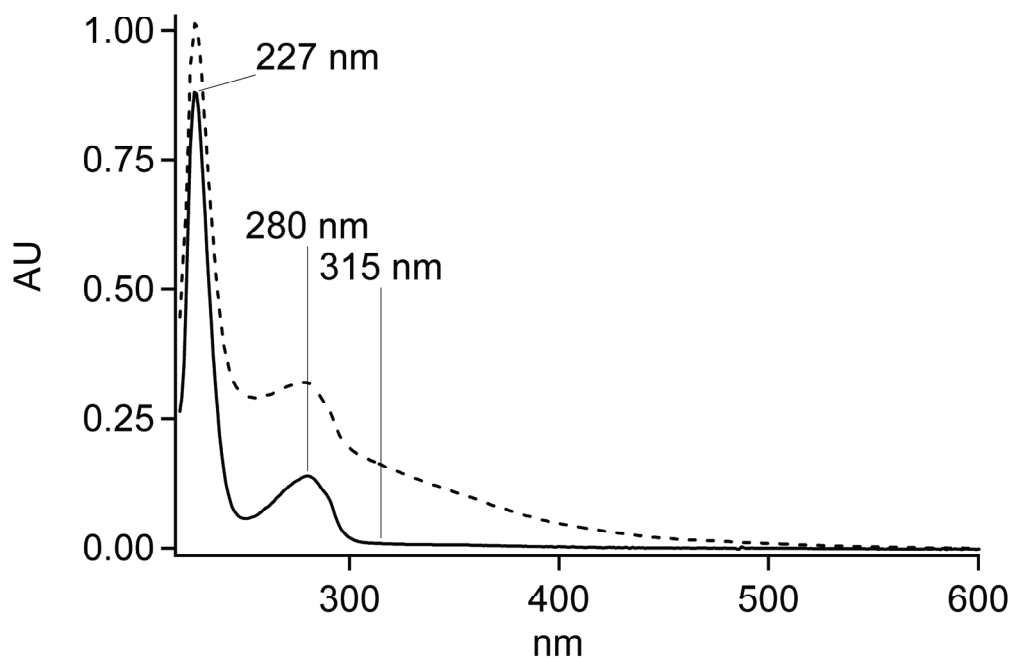


**Figure 2.2.** UV-visible spectra of recombinant *P. furiosus* ferritin. Apoferritin (solid) and Fe-loaded ferritin (dashed). The protein concentration was 0.07  $\mu\text{M}$  and added  $\text{Fe}^{2+}$  was 186  $\mu\text{M}$

is readily quantified at a wavelength of 315 nm<sup>13</sup> where the protein absorption is zero. In figure 2.2 the dashed spectrum corresponds to an intermediate state in iron incorporation. The shape of the iron-core spectrum appears to be invariant over the course of the incorporation (not shown).

Figure 2.3 shows the dependence of the iron incorporation rate, followed at 315 nm, on the substrate concentration. The measurements were performed at 25°C. This experiment could not be done at higher temperatures (up to 85°C) due to fast non-enzymatic  $\text{Fe}^{2+}$  oxidation when  $\text{Fe}^{2+}$  is used in concentrations of the order of 10 mM. The initial part of the graph is distinctly non-Michaelis-Menten, suggestive of cooperativity. A fit to the Hill equation ( $\text{SA} = \text{SA}_{\text{max}} \cdot [\text{S}]^n / ([\text{S}]^n + K_{0.5}^n)$ , where SA is the specific activity (initial rate), S is the concentration of the substrate,  $K_{0.5}$  is the substrate concentration which gives half maximal activity, and  $n$  is the Hill coefficient) gives  $V_{\text{max}} = 25 \text{ U/mg}$ ,  $K_{0.5} = 5 \text{ mM}$ , and  $n = 2$ , where  $n > 1$  is a measure for positive cooperativity. The specific activity at low  $\text{Fe(II)}$  concentration (300  $\mu\text{M}$ ) at 85°C is approximately 100 times higher than at 25°C.



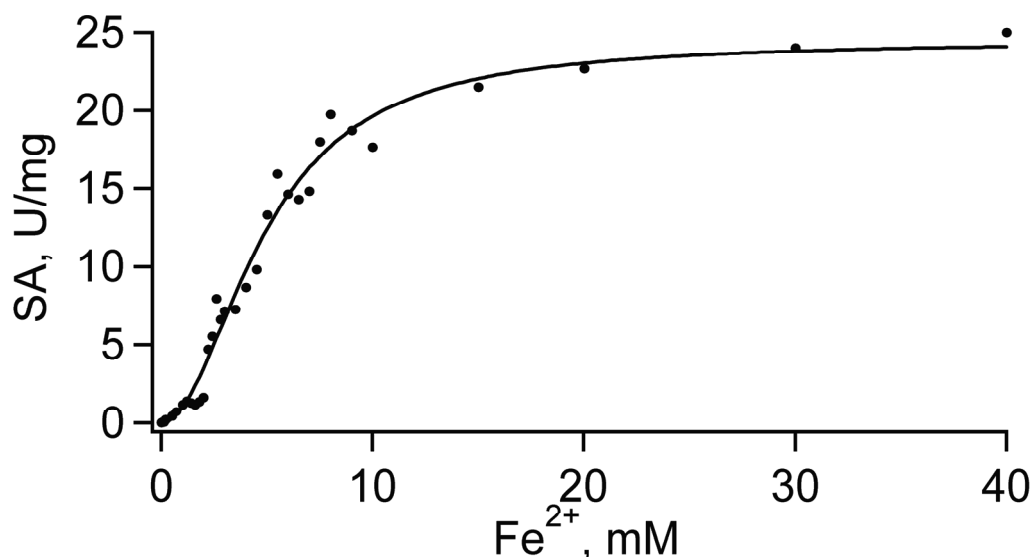


**Figure 2.3.** Steady-state kinetics of *P. furiosus* ferritin. Kinetics was followed at 315 nm, T=25°C. Specific activity (initial rates) is given as a function of substrate concentration. Protein final concentration was 0.3  $\mu$ M

The EPR spectrum of the ferritin, as isolated, is presented in figure 2.4, trace a. In addition to a small peak at  $g = 4.3$  (~1570 Gauss) of insignificant integrated intensity there are two asymmetric peaks at low field with approximate effective  $g$  values of 7.3 and 5.8. Such features are characteristic for high-spin mononuclear Fe(III) at a site of intermediate rhombicity (i.e., with a rhombicity parameter  $0 < E/D < 1/3$ ; see <sup>15</sup>). Theory predicts sets of effective  $g$  values for the transitions within the three Kramers doublets of high-spin Fe(III) <sup>15</sup>, and for rhombicity  $E/D = 0.065$  low-field peaks at  $g = 7.4$  and 5.9 are predicted with comparable peak area from the transitions within the two lowest doublets, while the transition within the highest doublet has insignificant intensity. Remarkably, the signal is quite similar to one previously reported for native wild type bacterioferritin from *E. coli*, where it was putatively assigned to mononuclear Fe(III) located at or near the ferroxidase center <sup>29,30</sup>. The ferroxidase center is a specific binding site for two Fe inside each subunit and is thought to be the site of oxidation of iron by, e.g., molecular oxygen.

When the ferritin is oxidatively loaded with iron (1150 Fe) the spectrum of trace b is obtained. In addition to the mononuclear Fe(III) signal an extremely broad feature is found which is typical for

superparamagnetism in the mineral core of ferritin and bacterioferritin proteins<sup>31-36</sup>. The broad feature is also detectable, with much lower intensity, in the spectrum of as isolated ferritin (trace a), which means that the protein obtained from *E. coli* does not only carry mononuclear Fe(III) but also has a small ferrihydrite core. Superparamagnetic systems are characterized by a blocking temperature below which individual crystalline domains become magnetically ordered either ferromagnetically or antiferromagnetically. The blocking temperature for ferritins has been estimated to be *circa* 25 K<sup>36</sup>. Indeed, when the loaded *P. furiosus* ferritin or the as isolated ferritin are measured at a temperature of 4.2 K, the spectrum of the core has disappeared (not shown) indicating full antiferromagnetic coupling at this temperature.

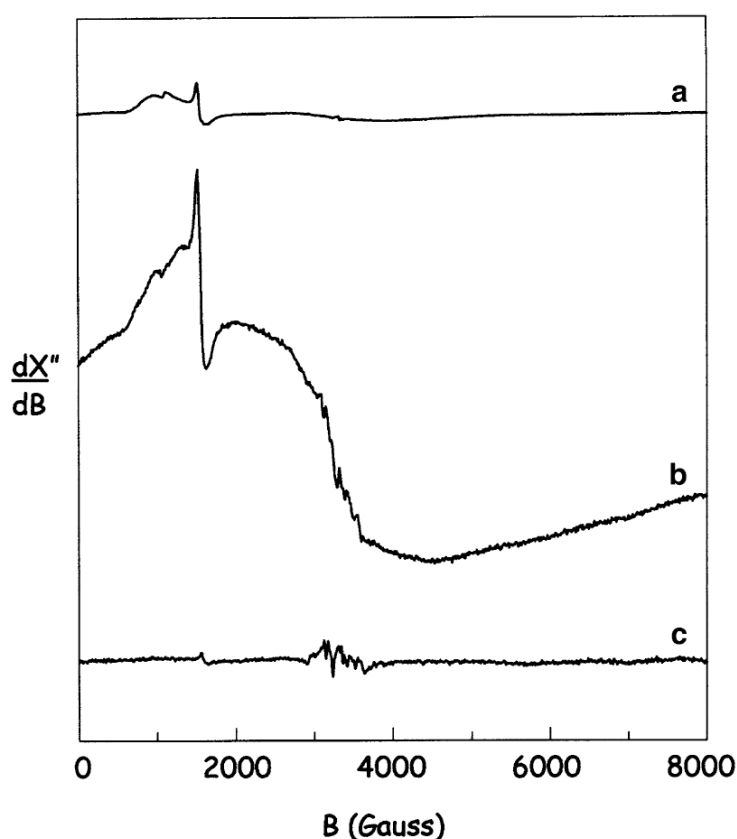


**Figure 2.4.** EPR spectra of *P. furiosus* ferritin expressed in *E. coli*: a - as isolated with ~17 Fe/24-mer; b - after aerobic loading with 1140 FeSO<sub>4</sub>; c - apo-ferritin with < 1 Fe/24-mer obtained after removal of iron from the as isolated protein with bipyridyl under reducing conditions followed by dialysis and re-aeration. The amplitudes of the spectra are normalized with respect to protein concentration (30, 12, 15 mg/ml, respectively). EPR conditions were: microwave frequency, 9.43 GHz; microwave power, 200 mW; modulation frequency, 100 kHz; modulation amplitude, 6.3 Gauss; temperature, 110 K

Treatment of the as isolated ferritin with bipyridyl under reducing conditions followed by dialysis and subsequent exposure to air affords the spectrum of trace c, which is indicative of the complete removal of all iron, and this is consistent with the chemical iron determination of < 1 Fe per 24-mer. The small multiline spectrum around  $g = 2$  (circa 3370 Gauss) is from a trace amount of contaminating Mn(II); it is also found in the Fe-loaded sample.

### **Thermostability**

The recombinant ferritin proved to be highly thermostable. The protein showed no significant drop in its core formation activity during the first 11 h of incubation at 100°C or the first 36 minutes autoclaving at 120°C. The half-life times were 48 h and 85 minutes, respectively (Fig. 2.5, data points were fitted to a sigmoidal curve  $SA = SA_{max} / (1 + \exp((t_{1/2} - t)/k))$ , where  $t_{1/2}$  is the time after which the protein retains 50% of its activity and  $k$  is a denaturation rate). Ferritin did not show a melting temperature when analyzed with differential scanning calorimetry from 20 to 120°C. The protein was also tested for stability against freezing-thawing and showed no drop in activity after 3 cycles.

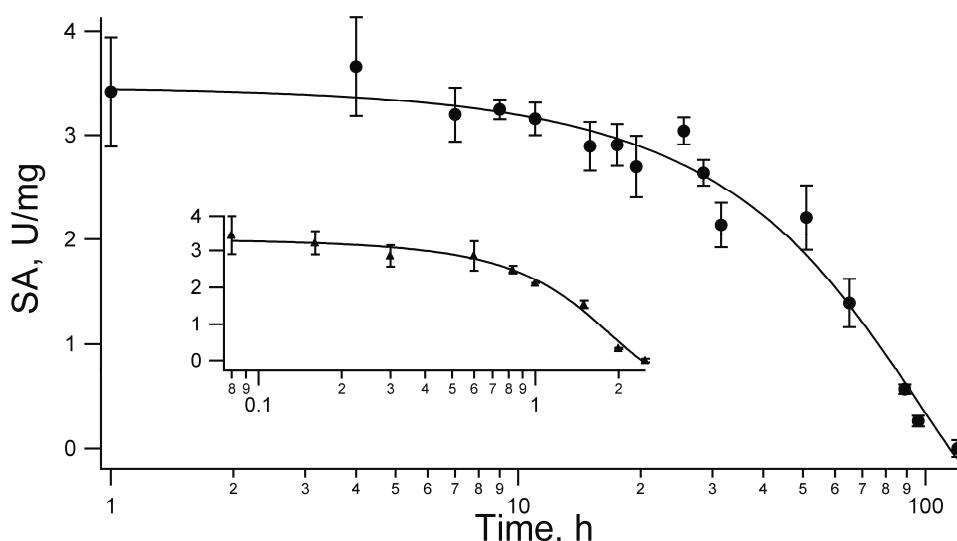


**Figure 2.5.** Thermostability of *P. furiosus* ferritin. The stability was analyzed by incubating the protein at 100°C in a water bath or at 120°C in an autoclave (insert) and withdrawal of samples after specific time intervals followed by measuring the iron incorporation activity (30°C) of the protein in a time course. Protein concentration was 0.3  $\mu$ M and iron (II) was 0.3 mM

### **Sequence alignment**

In figure 2.6 the amino acid sequence of ferritin from *P. furiosus* is aligned with that of *A. fulgidus* ferritin (47% identity, 71% similarity), *E. coli* cytoplasmic ferritin (36 and 56%), human ferritin heavy chain (29 and 47%) and *E. coli* bacterioferritin (17 and 33%). The numbering in figure 2.5 is according to the *P. furiosus* sequence. The typical patterns of ligands to  $\text{Fe}_A^{3+}$ - $\text{Fe}_B^{3+}$  in the ferroxidase center<sup>37</sup> are highlighted in gray. These are E17, Y24, E50 and H53 in the characteristic motif EXXH, E94, and finally Q127 and E130 arranged in the motif QXXE. The latter motif is modified in bacterioferritin, which has Glu<sub>127</sub> and His<sub>130</sub> making it EXXH. The Glu49 in *P. furiosus* and *E. coli* and Glu51 in *A. fulgidus* ferritins and Glu61 in human ferritin are conserved. In the crystal structure of *E. coli* ferritin Glu49 is a ligand to a third iron,  $\text{Fe}_C^{3+}$ , obtained by soaking the crystals in  $\text{Fe}^{2+}$  solution. This position was not occupied when crystals were soaked with  $\text{Zn}^{2+}$ <sup>37,38</sup>. In the case of human ferritin the highlighted residues are putative ligands to the ferroxidase center since no metal ions were yet found in the site<sup>37,39</sup>.

## **DISCUSSION**

### **A ferritin in *P. furiosus***

In the present study it is shown that the strict anaerobic hyperthermophilic archaeon *P. furiosus* produces ferritin and that its gene can be cloned and expressed as a functional ferritin to very high levels in aerobically grown *E. coli* cells. The purified 24-meric protein is competent *in vitro* in binding Fe(II) and converting it to Fe(III) in a superparamagnetic core mineral. The PfFtn iron storage capacity of circa 2700 Fe/holomer is the same as that of *E. coli* bacterioferritin (2700 Fe)<sup>12</sup> and slightly higher than that of *E. coli* ferritin (2000 Fe)<sup>24</sup>. Although theoretically the size of ferritins' inner cavity allows storage of up to 4500 Fe, in practice the capacity is less than 3000<sup>20</sup>.

The paradigmatic function of ferritin in higher eukaryots is storage/release of iron as part of iron homeostasis machinery. The storage requires molecular oxygen; release is dependent on physiological

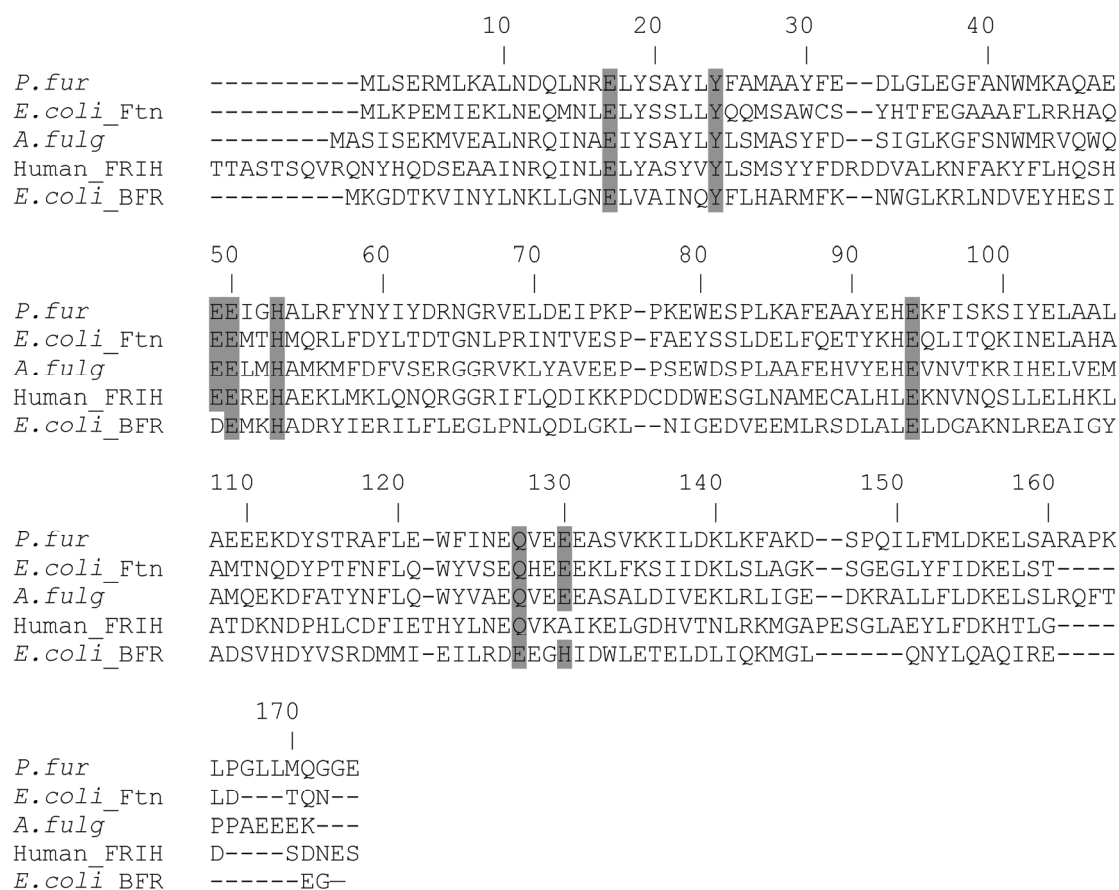


**Figure 2.6.** Amino acid sequence alignment of *P. furiosus* ferritin, *E. coli* cytoplasmic ferritin, *A. fulgidus* ferritin, human ferritin heavy chain, and *E. coli* bacterioferritin. Primary accession numbers are Q8U2T8, P23887, O29424, P02794 and P11056, respectively. The residue numbers are according to the *P. furiosus* sequence. Highlighted is the alignment with the crystallographically identified ligands to the ferroxidase center in *E. coli* cytoplasmic ferritin (reviewed in <sup>37</sup>)

reductant(s) that is yet to be identified.

The superoxide anion radical is a mild reductant *in vitro* <sup>40</sup>. Ferritin or ferritin-like proteins are also ubiquitously found in the prokaryotic world; however, a physiological role is not clearly established especially for anaerobic species. *P. furiosus* is an obligate anaerobe, therefore, a putative iron storage function of its ferritin would require a different oxidant than O<sub>2</sub>. As with other anaerobes, a candidate for this oxidative function is not yet obvious. Ferritin-like proteins have repeatedly been implicated in oxidative-stress protection either as general scavengers of O<sub>2</sub> and derived species or as specific guardians against DNA cleavage <sup>3,27,41</sup>. As an inhabitant of shallow offshore marine niches <sup>28</sup>, *P. furiosus* may well have to occasionally deal with oxidative

stress, as is indicated by the presence of a number of genes encoding proteins with putative functions in protection against oxygen species, e.g., superoxide reductase<sup>42,43</sup> and rubredoxin:O<sub>2</sub> oxidoreductase<sup>44</sup> or rubrerythrin<sup>45</sup>. As a working hypothesis, we may now add ferritin to this list with the caveat that physiological data to support this view are yet to be produced. Also, possible interaction between ferritin and *P. furiosus* DNA has not yet been explored.

### **Structural aspects**

EPR spectroscopy indicates that, when isolated from *E. coli*, the *P. furiosus* ferritin contains *circa* 0.5 Fe per subunit as mononuclear high-spin Fe(III) in a single chemical environment. The significance of this observation is not clear, however, the EPR spectrum is remarkably reminiscent to one reported for wild-type *E. coli* bacterioferritin<sup>29,30</sup>. That signal was assigned to monomeric iron at or near the putative ferroxidase center<sup>29,30</sup>. Assignment to the ferroxidase center would imply preferential loading of that center by a single iron as opposed to cooperative binding of two irons (resulting in magnetic coupling and the absence of an EPR signal). Note, however, the complication that not two but three Fe sites have recently been identified in what appears to be the ferroxidase center of *E. coli* ferritin (EcFtnA)<sup>38</sup>; also three Fe sites have very recently been found in the 12-mer Dps-ferritin of *H. salinarum*<sup>8,46</sup>. Based on the similarity of the EPR spectra, the structure of the mononuclear binding site in *E. coli* bacterioferritin and *P. furiosus* ferritin should be rather similar. The only site that is fully conserved between the two proteins in terms of Fe ligands is what has been labeled ‘A-site’ (ligands: OON) in the structure of *E. coli* ferritin<sup>38</sup> with ligands (in *P. furiosus* and *E. coli* numbering) Glu17, Glu50, His53, and one water.

The EPR spectrum of crystalline and/or amorphous core structures is a characteristic fingerprint for iron-loaded ferritin proteins. The spectrum has been interpreted as reflecting superparamagnetism from nano-sized (anti-)ferromagnetic domains above the blocking temperature

<sup>31-36</sup>. The details of the superparamagnetism will depend on the detailed composition of the nano structures, which in its turn depends on multiple factors, e.g, the extent of iron (and/or other metal ion) loading and the percentage of co-incorporated phosphate (and/or other oxoanion). Indeed, a variety of spectral shapes and positions has been observed <sup>31-36</sup>; however, the combination of an unusually broad EPR spectrum, extending over a field range of *circa* 1 Tesla, with a protein that remains perfectly soluble after loading with a large excess of iron under oxidizing conditions is quite unique for ferritins, and also defines the here described *P. furiosus* protein as a family member.

### **Hyperthermostability**

Ferritins in general are relatively resistant to thermal denaturation. The stability of a protein is a multi-faceted property; however, the retainment of biological activity is the ultimate criterion for overall stability. The ferritin from *P. furiosus* appears to be the most thermostable ferritin known so far; the recombinant 24-mer as isolated from *E. coli* fully retains its activity for the process from Fe(II) binding to ferrihydrite core formation after several hours of incubation in boiling water. The activity even withstands autoclaving at 120°C for some time. The protein is thus potentially an interesting model system for studies on the structural basis of hyperthermostability. From a different perspective, the stability of *P. furiosus* ferritin may well have additional value in biotechnology, where a recent surge in activities is seen in the exploration of (thus far mesophilic) ferritin proteins for the construction of nano-sized structures for biocatalytical <sup>47,48</sup>, environmental cleaning <sup>49</sup> or nanotechnological <sup>50,51</sup> purposes.

**Acknowledgments** We are grateful to prof. Simon de Vries for helpful discussion. We thank prof. Ana Maria Varela Coelho from the ITQB (Oeiras, Portugal) for providing mass spectrometry data. Anton Korteweg from Wageningen University (The Netherlands) is acknowledged for help with differential scanning calorimetry. This research has been financially supported by the Council for Chemical Sciences of the Netherlands Organization for Scientific Research (CW-NWO) under project number 700.51.301.

## REFERENCES

1. Crichton, R. R. *Inorganic biochemistry of iron metabolism: from molecular mechanisms to clinical consequences* (John Wiley & Sons, Chichester, 2001).
2. Frolow, F., Kalb, A. J. & Yariv, J. Structure of a unique twofold symmetric haem-binding site. *Nature Struct. Biol.* **1**, 453-460 (1994).
3. Romão, C. V., Regalla, M., Xavier, A. V., Teixeira, M., Liu, M. Y. & Le Gall, J. A bacterioferritin from the strict anaerobe *Desulfovibrio desulfuricans* ATCC 27774. *Biochemistry* **39**, 6841-6849 (2000).
4. Carrondo, M. A. Ferritins, iron uptake and storage from the bacterioferritin viewpoint. *EMBO J.* **22**, 1959-1968 (2003).
5. Zhao, G., Ceci, P., Ilari, A., Giangiacomo, L., Laue, T. M., Chiancone, E. & Chasteen, N. D. Iron and hydrogen peroxide detoxification properties of DNA-binding protein from starved cells. A ferritin-like DNA-binding protein of *Escherichia coli*. *J. Biol. Chem.* **277**, 27689-27696 (2002).
6. Almiron, M., Link, A. J., Furlong, D. & Kolter, R. A novel DNA-binding protein with regulatory and protective roles in starved *Escherichia coli*. *Genes Dev.* **6**, 2646-2654 (1992).
7. Johnson, E., Cascio, D., Sawaya, M. R., Gingery, M. & Schröder, I. Crystal structures of a novel tetrahedral open pore ferritin from the hyperthermophilic archaeon *Archaeoglobus fulgidus*. *Structure* **13**, 637-648 (2005).
8. Zeth, K., Offermann, S., Essen, L. O. & Oesterhelt, D. Iron-oxo clusters biomineralizing on protein surfaces: structural analysis of *Halobacterium salinarum* DpsA in its low- and high-iron states. *Proc. Natl. Acad. Sci. USA* **101**, 13780-13785 (2004).
9. Matias, P. M., Tatur, J., Carrondo, M. A. & Hagen, W. R. Crystallization and preliminary X-ray characterization of a ferritin from the hyperthermophilic archaeon and anaerobe *Pyrococcus furiosus*. *Acta Crystallogr Sect F* **61**, 503-506 (2005).
10. Arendsen, A. F., Veenhuizen, P. T. & Hagen, W. R. Redox properties of the sulfhydrogenase from *Pyrococcus furiosus*. *FEBS Lett.* **368**, 117-121 (1995).
11. Hagedoorn, P. L., Freije, J. R. & Hagen, W. R. *Pyrococcus furiosus* glyceraldehyde 3-phosphate oxidoreductase has comparable W(6+/5+) and W(5+/4+) reduction potentials and unusual [4Fe-4S] EPR properties. *FEBS Lett.* **462**, 66-70 (1999).



12. Baaghil, S., Lewin, A., Moore, G. R. & Le Brun, N. E. Core formation in *Escherichia coli* bacterioferritin requires a functional ferroxidase center. *Biochemistry* **42**, 14047-14056 (2003).
13. Bonomi, F., Kurtz, D. M. & Cui, X. Ferroxidase activity of recombinant *Desulfovibrio vulgaris* rubrerythrin. *J. Biol. Inorg. Chem.* **1**, 67-72 (1996).
14. Pierik, A. J. & Hagen, W. R. S = 9/2 EPR signals are evidence against coupling between the siroheme and the Fe/S cluster prosthetic groups in *Desulfovibrio vulgaris* (Hildenborough) dissimilatory sulfite reductase. *Eur. J. Biochem.* **195**, 505-516 (1991).
15. Hagen, W. R. EPR spectroscopy of iron-sulfur proteins. *Adv. Inorg. Chem.* **38**, 165-222 (1992).
16. Pierik, A. J., Wolbert, R. B., Mutsaers, P. H., Hagen, W. R. & Veeger, C. Purification and biochemical characterization of a putative [6Fe-6S] prismane-cluster-containing protein from *Desulfovibrio vulgaris* (Hildenborough). *Eur. J. Biochem.* **206**, 697-704 (1992).
17. Hennessy, D. J., Reid, G. R., Smith, F. E. & Thompson, S. L. Ferrene - a new spectrophotometric reagent for iron. *Can. J. Chem.* **62**, 721-724 (1984).
18. Bauminger, E. R., Harrison, P. M., Hechel, D., Nowik, I. & Treffry, A. Mossbauer spectroscopic investigation of structure-function relations in ferritins. *Biochim. Biophys. Acta* **1118**, 48-58 (1991).
19. Dawson, M. C., Elliott, D. C., Elliott, W. H. & Jones, K. M. *Data for biochemical research* (Clarendon Press, Oxford, 1986).
20. Treffry, A. & Harrison, P. M. Incorporation and release of inorganic phosphate in horse spleen ferritin. *Biochem. J.* **171**, 313-320 (1978).
21. Altschul, S. F., Madden, T. L., Schaffer, A. A., Zhang, J., Zhang, Z., Miller, W. & Lipman, D. J. Gapped BLAST and PSI-BLAST: a new generation of protein database search programs. *Nucleic Acids Res.* **25**, 3389-3402 (1997).
22. Thompson, J. D., Higgins, D. G. & T.J., G. CLUSTAL W: Improving the sensitivity of progressive multiple sequence alignment through sequence weighting, position-specific gap penalties and weight matrix choice. *Nucleic Acids Res.* **22**, 4673-4680 (1994).
23. Combet, C., Blanchet, C., Geourjon, C. & Deleage, G. NPS@: Network Protein Sequence Analysis. *Trends Biochem Sci* **25**, 147-150 (2000).
24. Hudson, A. J., Andrews, S. C., Hawkins, C., Williams, J. M., Izuhara, M., Meldrum, F. C., Mann, S., Harrison, P. M. & Guest, J. R. Overproduction,

- purification and characterization of the *Escherichia coli* ferritin. *Eur. J. Biochem.* **218**, 985-995 (1993).
25. Andrews, S. C., Smith, J. M., Hawkins, C., Williams, J. M., Harrison, P. M. & Guest, J. R. Overproduction, purification and characterization of the bacterioferritin of *Escherichia coli* and a C-terminally extended variant. *Eur. J. Biochem.* **213**, 329-338 (1993).
  26. Levi, S., Cesareni, G., Arosio, P., Lorenzetti, R., Soria, M., Sollazzo, M., Albertini, A. & Cortese, R. Characterization of human ferritin H chain synthesized in *Escherichia coli*. *Gene* **51**, 269-274 (1987).
  27. Rocha, E. R., Andrews, S. C., Keen, J. N. & Brock, J. H. Isolation of a ferritin from *Bacteroides fragilis*. *FEMS Microbiol. Lett.* **74**, 207-212 (1992).
  28. Fiala, G. & Stetter, K. O. *Pyrococcus furiosus* sp. nov. represents a novel genus of marine heterotrophic archaeobacteria growing optimally at 100°C. *Arch microbiol* **145**, 56-61 (1986).
  29. Cheesman, M. R., Le Brun, N. E., Kadir, F. H., Thomson, A. J., Moore, G. R., Andrews, S. C., Guest, J. R., Harrison, P. M., Smith, J. M. & Yewdall, S. J. Haem and non-haem iron sites in *Escherichia coli* bacterioferritin: spectroscopic and model building studies. *Biochem. J.* **292**, 47-56 (1993).
  30. Le Brun, N. E., Cheesman, M. R., Thomson, A. J., Moore, G. R., Andrews, S. C., Guest, J. R. & Harrison, P. M. An EPR investigation of non-haem iron sites in *Escherichia coli* bacterioferritin and their interaction with phosphate. A study using nitric oxide as a spin probe. *FEBS Lett.* **323**, 261-266 (1993).
  31. Boas, J. F. & Troup, G. J. Electron spin resonance and Mossbauer effect studies of ferritin. *Biochim. Biophys. Acta* **229**, 68-74 (1971).
  32. Weir, M. P., Peters, T. J. & Gibson, J. F. Electron spin resonance studies of splenic ferritin and haemosiderin. *Biochim. Biophys. Acta* **828**, 298-305 (1985).
  33. Deighton, N., Abu-Raqabah, A., Rowland, I. J., Symons, M. C. R., Peters, T. J. & Ward, R. J. Electron paramagnetic resonance studies of a range of ferritins and haemosiderins. *J. Chem. Soc. Faraday Trans.* **87**, 3193-3197 (1991).
  34. Cheesman, M. R., Kadir, F. H., Al-Basseet, J., Al-Massad, F., Farrar, J., Greenwood, C., Thomson, A. J. & Moore, G. R. E.p.r. and magnetic circular dichroism spectroscopic characterization of bacterioferritin from *Pseudomonas aeruginosa* and *Azotobacter vinelandii*. *Biochem. J.* **286**, 361-367 (1992).

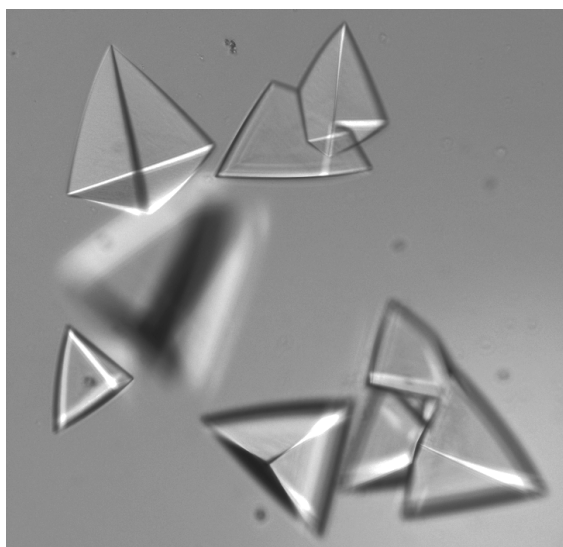
35. Voskoboynik, U. Anomalous field dependence of blocking temperature of natural horse-spleen ferritin. *Acta Phys. Pol. A* **92** (1997).
36. Wajnberg, E., El-Jaick, L. J., Linhares, M. P. & Esquivel, D. M. Ferromagnetic resonance of horse spleen ferritin: core blocking and surface ordering temperatures. *J. Magn. Reson.* **153**, 69-74 (2001).
37. Romão, C. V. (PhD thesis, Universidade Nova de Lisboa, 2003).
38. Stillman, T. J., Hempstead, P. D., Artymiuk, P. J., Andrews, S. C., Hudson, A. J., Treffry, A., Guest, J. R. & Harrison, P. M. The high-resolution X-ray crystallographic structure of the ferritin (EcFtnA) of *Escherichia coli*; comparison with human H ferritin (HuHF) and the structures of the Fe(3+) and Zn(2+) derivatives. *J Mol Biol* **307**, 587-603 (2001).
39. Hempstead, P. D., Yewdall, S. J., Fernie, A. R., Lawson, D. M., Artymiuk, P. J., Rice, D. W., Ford, G. C. & Harrison, P. M. Comparison of the three-dimensional structures of recombinant human H and horse L ferritins at high resolution. *J. Mol. Biol.* **268**, 424-448 (1997).
40. Boyer, R. F. & McCleary, C. J. Superoxide ion as a primary reductant in ascorbate-mediated ferritin iron release. *Free Radic. Biol. Med.* **3**, 389-395 (1987).
41. Smith, J. L. The physiological role of ferritin-like compounds in bacteria. *Crit Rev Microbiol* **30**, 173-185 (2004).
42. Jenney, F. E., Jr., Verhagen, M. F. J. M., Cui, X. & Adams, M. W. W. Anaerobic microbes: oxygen detoxification without superoxide dismutase. *Science* **286**, 306-309 (1999).
43. Adams, M. W. W., Jenney, F. E., Jr., Clay, M. D. & Johnson, M. K. Superoxide reductase: fact or fiction? *J. Biol. Inorg. Chem.* **7**, 647-652 (2002).
44. Ma, K. & Adams, M. W. A hyperactive NAD(P)H:Rubredoxin oxidoreductase from the hyperthermophilic archaeon *Pyrococcus furiosus*. *J Bacteriol* **181**, 5530-3 (1999).
45. Tempel, W., Liu, Z. J., Schubot, F. D., Shah, A., Weinberg, M. V., Jenney, F. E., Jr., Arendall, W. B., III, Adams, M. W. W., Richardson, J. S., Richardson, D. C., Rose, J. P. & Wang, B. C. Structural genomics of *Pyrococcus furiosus*: X-ray crystallography reveals 3D domain swapping in rubrerythrin. *Proteins* **57**, 878-882 (2004).
46. Reindel, S., Anemüller, S., Sawaryn, A. & Matzanke, B. F. The DpsA-homologue of the archaeon *Halobacterium salinarum* is a ferritin. *Biochim. Biophys. Acta* **1598**, 140-146 (2002).

47. Zhang, N., Fengyi, L., Fu, Q. J. & Tsang, S. C. Naturally occurring ferritin as a novel catalyst for selective hydroxylation of phenol. *React. Kinet. Catal. Lett.* **71**, 393-404 (2000).
48. Ueno, T., Suzuki, M., Goto, T., Matsumoto, T., Nagayama, K., Watanabe, Y. Size-selective olefin hydrogenation by a Pd nanocluster provided in an apo-ferritin cage. *Angew Chem Int Ed* **43**, 2527-2530 (2004).
49. Hosein, H. A., Strongin, D. R., Allen, M. & Douglas, T. Iron and cobalt oxide and metallic nanoparticles prepared from ferritin. *Langmuir* **20**, 10283-10287 (2004).
50. Sleytr, U. B., Messner, P., Pum, D. & Sára, M. Crystalline bacterial cell surface layers (S layers): from supramolecular cell structure to biomimetics and nanotechnology. *Angew. Chem. Int. Ed.* **38**, 1034-1054 (1999).
51. Zhang, Y., Li, Y., Wang, D. & Dai, H. Imaging as-grown single-walled carbon nanotubes originated from isolated catalytic nanoparticles. *Appl. Phys. A* **74**, 325-328 (2002).





# CHAPTER III<sup>i</sup>. Crystallization and preliminary X-ray characterization of a ferritin from the hyperthermophilic archaeon and anaerobe *Pyrococcus furiosus*



## ABSTRACT

Crystals of the title protein have been produced and preliminary structural analysis has been carried out. The crystals belong to the orthorhombic space group  $C222_1$ , with unit-cell parameters  $a = 258.1$ ,  $b = 340.1$ ,  $c = 266.5$  Å. The protein forms a 24-mer of 20 kDa subunits, which assemble with 432 non-crystallographic symmetry. A total of 36 monomers are found in the asymmetric unit, corresponding to one and a half 24-mers.

---

<sup>i</sup> This chapter has been published as Matias PM, Tatur J, Carrondo MA & Hagen WR. Crystallization and preliminary X-ray characterization of a ferritin from the hyperthermophilic archaeon and anaerobe *Pyrococcus furiosus*. *Acta Cryst.* F61, 503-506 (2005)





## INTRODUCTION

Ferritin is the generic name for a class of small (*circa* 20 kDa) helical proteins that ubiquitously occur in the three domains of life, both in aerobic and anaerobic cells. Ferritins spontaneously polymerize into a 24-meric hollow sphere-like structure (inner diameter 8 nm and outer diameter 12 nm), which can be homopolymeric or, in higher eukaryotes, can be made up of two (H and L) <sup>1</sup> or three (H, L, M) homologous subunits <sup>2</sup>. A ferritin homologue known as Dps (for DNA-protecting protein during starvation) forms smaller hollow spheres (inner diameter 4.5 nm and outer diameter 9 nm) as 12-mers <sup>3</sup>. Ferritins are thought to function physiologically as reversible stores of iron (and possibly of oxoanions and of other metal ions) and/or as protecting systems against oxidative damage of cell components, notably DNA <sup>4</sup>. Ferritins can be viewed as enzymes as they catalyze the oxidation of Fe(II) and the formation of a Fe(III) mineral core in their interior. Each subunit carries a ferroxidase active centre consisting of a  $\mu$ -oxo bridged dinuclear iron cluster. Proteins from the subclass of bacterioferritins additionally have heme groups sandwiched between two subunits, presumably functioning in electron transfer <sup>5</sup>. In recent years, interest in ferritins has increased remarkably in view of their putative technological application in nanoscience, environmental remediation, fuel cells and magnetic information storage <sup>6-8</sup>.

Here, we report the crystallization and preliminary structure analysis of PffTn, the ferritin from *Pyrococcus furiosus*. *P. furiosus* is a marine strictly anaerobic fermentative hyperthermophilic archaeon with an optimal growth temperature of 373 K. A putative ferritin gene has been cloned and overexpressed in *Escherichia coli* and the purified protein is an active non-heme ferritin forming a 24-meric structure that can incorporate up to 2700 Fe ions (as determined by chemical analysis) into a superparamagnetic core when incubated with Fe(II) under air. This protein exhibits the highest thermostability known among ferritins: its core-formation activity is fully retained after incubation at 373 K for 8 hours or autoclaving at 393 K for 20 minutes <sup>9</sup>. While a number of

crystallographic structures are available for ferritins, bacterioferritins and Dps from several species <sup>10</sup>, archaeal structural data are limited to a ferritin from the sulfate-reducing thermophile *Archaeoglobus fulgidus* (PDB code 1sq3 <sup>11</sup>) and a Dps-like ferritin from the mesophilic halophile *Halobacterium salinarum* (PDB codes 1tjo, 1tk6, 1tko, 1tkp <sup>12</sup>). In *A. fulgidus* ferritin, a novel 23 symmetry was found, which opens four large pores through which it may be possible for large molecules to enter the protein <sup>11</sup>. Contrarily, in the current study on *P. furiosus* ferritin (PfFtn) the more common quaternary structure among ferritins with 432 non-crystallographic symmetry was observed, indicating that the 23 symmetry found in *A. fulgidus* is not a general trait among archaeal ferritins. The high thermostability of PfFtn will probably be explained from structural data. The mechanism of iron incorporation into ferritins is under debate. In the hyperthermophilic PfFtn, pre-steady-state kinetics of iron uptake can be slowed drastically at ambient temperatures (our unpublished results), which may allow following of the iron-incorporation pathway in protein crystals.

## **EXPERIMENTAL PROCEDURES AND RESULTS**

### **Protein production**

*P. furiosus* DSM 3638 cells were grown as described in <sup>13</sup>. Genomic DNA was isolated with sodium dodecyl sulfate and sodium lauryl sarcosine, and extraction was performed with phenol/chloroform/isoamylalcohol <sup>14</sup>. The putative ferritin gene was PCR-amplified using 5 ng of genomic DNA, 15 pmol of each primer (forward primer 5'-CCATATGTTGAGCGAAAGAATGC-3' and reverse primer 5'-GTCGACTTACTCTCCTCCCTG-3'), 15 nmol dNTPs, 50 nmol MgSO<sub>4</sub> and 1.25 U of *Pfx* polymerase in a total volume of 50 ml. The PCR program consisted of a melting step at 368 K for 5 minutes followed by 30 cycles of 368 K for 1 minute, 329 K for 1 minute and 345 K for 1.5 minutes and a final extension step at 345 K for 10 minutes. The amplified gene was cloned into pCR 2.1-TOPO vector (Invitrogen). The fidelity of the ferritin gene-containing clone was confirmed by DNA

sequencing (Base-Clear). The plasmid pCR 2.1-TOPO was isolated with QIA Spin miniprep Kit (Qiagen), restriction-digested with *NdeI* and *SalI* (Roche) and cloned into the same restriction sites of the vector pET24a(+) (Novagen). The resulting clone was transformed into competent *E. coli* DH5 $\alpha$ -T1<sup>R</sup> cells (Invitrogen). The construct produced was expressed in BL21-CodonPlus (DE3)-RIL cells (Stratagene). The pre-culture of the transformed cells was cultivated aerobically at 310 K and 200 rev/min in 100 ml LB medium<sup>14</sup>, 50 mg/ml chloramphenicol and 20 mg/ml kanamycin overnight. The pre-culture was transformed in TB medium<sup>14</sup> in a 1:20 ratio for 2 hours and induced with 1 mM IPTG. The cells were harvested by centrifugation after an additional 5 hours of growth. The cells were washed in 20 mM Tris-HCl buffer pH 8 and DNase, RNase and 0.5 mM PMSF were added. The cells were broken with a Cell Disruptor (Constant Systems). The cell-free extract was subjected to heat treatment (353 K, 10 min) and clarified by centrifugation. The supernatant was loaded onto a HiLoad Superdex 200 26/60 column (Amersham Biosciences) equilibrated with 20 mM Tris-HCl buffer pH 8 and 0.15 M NaCl. The fractions exhibiting ferroxidase activity were pooled and concentrated (Amicon, YM-100).

### **Iron incorporation and determination**

Ferritin iron loading was performed by adding a freshly and anaerobically prepared aqueous solution of iron sulfate containing 0.1% HCl (v/v) to a solution of apoferritin in 50 mM HEPES pH 7 under aerobic conditions. Core-formation activity was monitored at 315 nm using  $\epsilon = 2200 \text{ M}^{-1} \text{ cm}^{-1}$ <sup>15</sup>.

Iron in the protein samples was determined based on the methods of Hennessy *et al.*<sup>16</sup> and Pierik *et al.*<sup>17</sup> by chelating it with ferrene and reading the absorption of the iron-ferrene complex at 593 nm,  $\epsilon = 35\,500 \text{ M}^{-1} \text{ cm}^{-1}$ .

### **Crystallization**

Crystals of PfFtn were produced aerobically using the hanging-

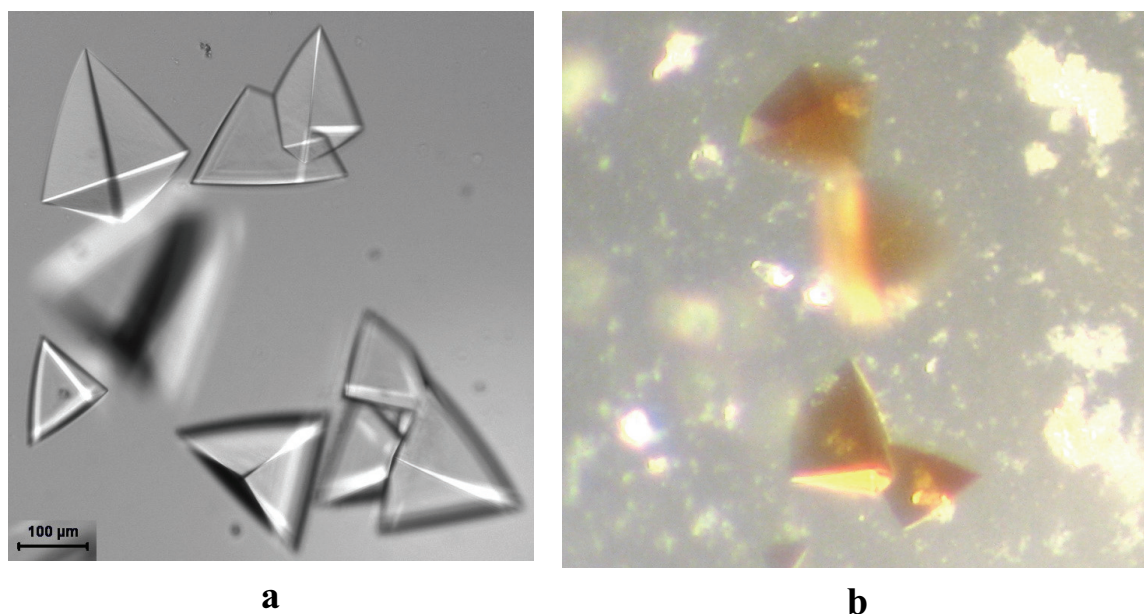


**Figure 3.1.** Crystals of *P. furiosus* ferritin. **a** As-isolated, ~17 Fe atoms per 24-mer. **b** Iron-containing ferritin, ~1000 Fe atoms per 24-mer. The color of the iron-loaded protein solution and crystals prepared from it depends on the amount of iron loaded and varies from light yellow to brown

drop vapour-diffusion method at room temperature. Commercially available screens (Crystal Screen 1 and SaltRx, Hampton Research) were used for crystallization screening. The best crystals were obtained with 2 M ammonium sulfate (Crystal Screen 1, solution 32; Fig. 3.1). Further optimization attempts by varying the pH and concentration of ammonium sulfate and the concentration of the protein did not produce better crystals. Several other crystallization conditions produced small crystals, spherulites or needles. Optimization of those conditions was attempted by seeding or factorial experiments, but did not lead to any improvement of the results. The crystals used for data collection were grown against 0.5 ml of 2 M ammonium sulfate reservoir solution, with drops containing 2 ml of 5 mg/ml protein solution in 50 mM HEPES pH 7 and an equal amount of the reservoir solution. The crystals of the ‘as isolated’ ferritin, containing *circa* 17 Fe atoms per 24-mer, grew in three weeks and those loaded with ~1000 Fe atoms per 24-mer (as estimated from the amount of loaded iron prior to crystallization) in four months. The crystals exhibited pyramidal shapes with base side and height of 150–250 μm (Fig. 3.1).

### **X-ray data collection and preliminary crystallographic analysis**

Cryoprotecting conditions were established in-house and consisted of briefly dipping the crystals into a modified crystallization solution containing 20% glycerol prior to flash-freezing them at 110 K in a nitrogen-gas stream using an Oxford Cryosystems low-temperature device.

Diffraction data from an ‘as-isolated’ Pfftn crystal were collected at ESRF beamline ID14-2 from a single flash-frozen crystal at 100 K. The diffraction images were integrated with the program *MOSFLM*<sup>18</sup>. The processed data were scaled, merged and converted to structure factors using the CCP4 program suite<sup>19</sup>. Data-processing statistics are summarized in Table 1. The diffraction data obtained is not very strong [ $I/\sigma(I) = 5.4$  overall], consistent with the relatively high merging R factor (0.115 for data to 3.0 Å). In addition, the scaling results revealed signs of crystal decay arising from radiation damage in the X-ray beam after only little more than 6-7 min exposure to the beam. Fine  $\phi$ -slicing (0.25°) was also necessary during data collection in order to minimize spatial overlaps on the detector surface, owing to the unfavorable orientation of the crystal in the loop, with the longest cell axis,  $c$ , making a 38° angle with the spindle.

A loaded Pfftn crystal with ~1000 Fe atoms per 24-mer was also tested on the X-ray beam. However, this crystal was smaller and diffraction could only be observed to about 6 Å.

Cell-volume considerations led to the conclusion that there might be between one and three 24-mers in the asymmetric unit, corresponding to values of  $V_M$ <sup>20</sup> between 6.1 and 2.0 Å<sup>3</sup>/Da, with an estimated solvent content ranging between 80 and 39%.

The self-rotation Patterson maps (Fig. 3.2) show peaks consistent with 432 point-group symmetry, typical of a 24-mer quaternary arrangement for the ferritins.

### **Structure determination by molecular replacement**

The determination of the three-dimensional structure of Pfftn was

**Table 3.1.** X-ray diffraction data-collection and processing statistics. Values in parentheses refer to the last resolution shell,  $3.16 \geq d \geq 3.00 \text{ \AA}$ 

Beamline	ESRF ID14-EH2
Detector	ADSC Quantum 4
Wavelength ( $\text{\AA}$ )	0.933
Space group	C222 <sub>1</sub>
Unit cell ( $\text{\AA}$ )	a 258.1 b 340.1 c 266.5
Resolution range ( $\text{\AA}$ )	83.3 - 3.0
Observations (unique reflections)	731,509 (225,192)
% Completeness	97.4 (98.8)
Redundancy	3.2 (3.2)
$R_{\text{merge}}^a$	0.115 (0.316)
$I/\sigma(I)$	5.4 (2.3)
Estimated $B_{\text{overall}}$ ( $\text{\AA}^2$ )	60.2

<sup>a</sup>  $R_{\text{merge}} = \sum_{\text{hkl}} \sum_i |I_{\text{hkl},i} - \langle I_{\text{hkl}} \rangle| / \sum_{\text{hkl}} \sum_i I_{\text{hkl},i}$ , where  $\langle I_{\text{hkl}} \rangle$  the mean intensity of the set of symmetry-related reflections denoted by  $I_{\text{hkl},i}$

undertaken by the molecular-replacement (MR) method using the program *PHASER*<sup>21</sup> and the homologous ferritin from the thermophilic bacterium *Thermotoga maritima* (PDB code 1vlg) as the search model. The sequence of this 164-amino-acid ferritin has 89 amino-acid residues identical with that of PfFtn (174 amino acids), corresponding to 51% homology, and the only insertions or deletions occur at the termini of the protein chains. The MR calculations were carried out using the standard *PHASER* protocol as implemented through the CCP4 graphical user interface, with reflection data to 3.2  $\text{\AA}$  resolution. Because no strong peaks were observed in a Patterson map calculated using the native PfFtn diffraction data, there was no indication of any translational symmetry between 24-mers in the asymmetric unit and therefore in the first *PHASER* calculation only one 24-mer was considered as the search model. Indeed, the self-rotation function indicated that one or more of the fourfold NCS rotation axes in the 24-mer might be parallel or even

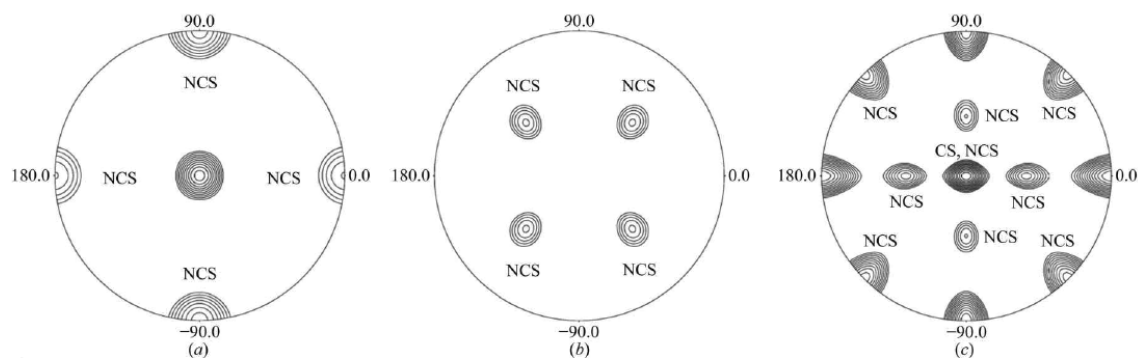


**Figure 3.2.** Self-rotation Patterson function plots for Pfftn in the resolution range  $3.5 \leq d \leq 15 \text{ \AA}$  with integration range  $5 \leq R \leq 20 \text{ \AA}$ . Peaks in the sections shown at  $k = 90^\circ$  (a),  $k = 120^\circ$  (b) and  $k = 180^\circ$  (c) give the orientation of the crystallographic twofold and non-crystallographic twofold, threefold and fourfold (NCS) rotation axes in the crystal structure. The maximum value was normalized to 100 and the contours drawn at five-unit intervals, starting at 40. Drawings were prepared with programs *POLARRFN*, *NPO* and *XPLOT84DRIVER*<sup>19</sup>

coincident with a crystallographic twofold axis. Therefore, it was assumed that two 12-mers (each corresponding to half of a 24-mer) might be present in the asymmetric unit, fulfilling this condition. In each case, the second half of the 24-mer would then be generated by the corresponding crystallographic twofold rotation. The 12-mer search model was constructed from the published structure coordinates of the ferritin from *T. maritima*. The MR calculations with *PHASER* gave a strong solution, but inspection of crystal packing on a three-dimensional graphics workstation revealed that the search model was incomplete. Only one of the 24-mers was actually found to be lying on a crystallographic twofold axis along cell edge b. Another 24-mer is located in general positions, of which only half was accounted for by the search model. The *PHASER* calculations were repeated using the two previously located 12-mer positions to look for the missing 12-mer. A single solution was found, with Z score 86.5, which completed the model. The second-best solution, with Z score 74.9, was rejected owing to  $C^\alpha$  clashing. The asymmetric unit of the Pfftn crystal structure was therefore found to contain one and a half 24-mers (36 monomers). It is interesting to note that the 24-mer that lies a special position, with one of

its NCS fourfold axes coincident with a crystallographic twofold axis along cell edge b, has the other two orthogonal NCS fourfolds slightly misaligned with the other two crystallographic unit-cell directions. On the other hand, the 24-mer lying in general positions has its NCS fourfold axes slightly ( $\sim 10^\circ$ ) offset from those of the first 24-mer. This arrangement explains the lack of a strong peak in the native Patterson map arising from non-crystallographic translation symmetry between the 24-mers, which should be present if the NCS fourfold axes from both 24-mers were exactly parallel, as in the case of bacterioferritin from *Desulfovibrio desulfuricans* ATCC 27774<sup>22</sup>. Furthermore, it also explains the differences observed in the intensity of the peaks in the self-rotation Patterson maps which arise from the NCS symmetry twofold and fourfold rotation axes (see Fig. 3.2), since the observed pattern results from the combination of two 432 NCS patterns, one from each 24-mer, which are slightly misaligned with respect to each other.

Despite the success of the MR calculations, we believe that because of the low resolution of the diffraction data and low homology of the search model, as well as the complexity of the structure, experimental phase information is needed in order to obtain the best possible structural model from the data. To that end, a MAD experiment at the Fe K absorption edge will be carried out at the earliest opportunity.

**Acknowledgments** The authors wish to thank the ESRF (Grenoble, France) for financial and technical support during data collection.

## REFERENCES

1. Crichton, R. R. *Inorganic biochemistry of iron metabolism: from molecular mechanisms to clinical consequences* (John Wiley & Sons, Chichester, 2001).
2. Ha, Y., Shi, D., Small, G. W., Theil, E. C. & Allewell, N. M. Crystal structure of bullfrog M ferritin at 2.8 Å resolution: analysis of subunit interactions and the binuclear metal center. *J. Biol. Inorg. Chem.* **4**, 243-256 (1999).
3. Grant, R. A., Filman, D. J., Finkel, S. E., Kolter, R. & Hogle, J. M. The crystal structure of Dps, a ferritin homolog that binds and protects DNA. *Nat*



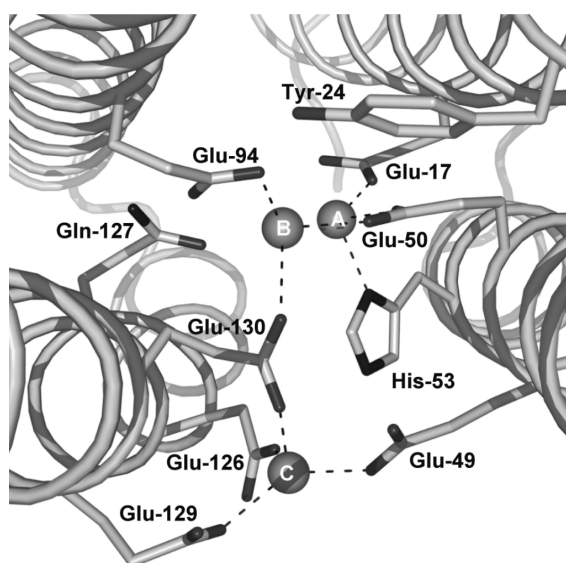
- Struct Biol* **5**, 294-303 (1998).
4. Smith, J. L. The physiological role of ferritin-like compounds in bacteria. *Crit Rev Microbiol* **30**, 173-185 (2004).
  5. Stiefel, E. I. & Watt, G. D. Azotobacter cytochrome b557.5 is a bacterioferritin. *Nature* **279**, 81-83 (1979).
  6. Hosein, H. A., Strongin, D. R., Allen, M. & Douglas, T. Iron and cobalt oxide and metallic nanoparticles prepared from ferritin. *Langmuir* **20**, 10283-10287 (2004).
  7. Sleytr, U. B., Messner, P., Pum, D. & Sára, M. Crystalline bacterial cell surface layers (S layers): from supramolecular cell structure to biomimetics and nanotechnology. *Angew. Chem. Int. Ed.* **38**, 1034-1054 (1999).
  8. Zhang, N., Fengyi, L., Fu, Q. J. & Tsang, S. C. Naturally occurring ferritin as a novel catalyst for selective hydroxylation of phenol. *React. Kinet. Catal. Lett.* **71**, 393-404 (2000).
  9. Tatur, J., Hagedoorn, P. L., Overeijnder, M. L. & Hagen, W. R. A highly thermostable ferritin from the hyperthermophilic archaeal anaerobe *Pyrococcus furiosus*. *Extremophiles* **10**, 139-148 (2006).
  10. Carrondo, M. A. Ferritins, iron uptake and storage from the bacterioferritin viewpoint. *EMBO J.* **22**, 1959-1968 (2003).
  11. Johnson, E., Cascio, D., Sawaya, M. R., Gingery, M. & Schröder, I. Crystal structures of a novel tetrahedral open pore ferritin from the hyperthermophilic archaeon *Archaeoglobus fulgidus*. *Structure* **13**, 637-648 (2005).
  12. Zeth, K., Offermann, S., Essen, L. O. & Oesterhelt, D. Iron-oxo clusters biomineralizing on protein surfaces: structural analysis of *Halobacterium salinarum* DpsA in its low- and high-iron states. *Proc. Natl. Acad. Sci. USA* **101**, 13780-13785 (2004).
  13. Arendsen, A. F., Veenhuizen, P. T. & Hagen, W. R. Redox properties of the sulfhydrogenase from *Pyrococcus furiosus*. *FEBS Lett.* **368**, 117-121 (1995).
  14. Sambrook, J., Fritsch, E. F. & Maniatis, T. *Molecular Cloning: A Laboratory Manual* (Cold Spring Harbor Laboratory Press, Cold Spring Harbor, NY, 1989).
  15. Bonomi, F., Kurtz, D. M. & Cui, X. Ferroxidase activity of recombinant *Desulfovibrio vulgaris* rubrerythrin. *J. Biol. Inorg. Chem.* **1**, 67-72 (1996).
  16. Hennessy, D. J., Reid, G. R., Smith, F. E. & Thompson, S. L. Ferrene - a new spectrophotometric reagent for iron. *Can. J. Chem.* **62**, 721-724 (1984).

17. Pierik, A. J., Wolbert, R. B., Mutsaers, P. H., Hagen, W. R. & Veeger, C. Purification and biochemical characterization of a putative [6Fe-6S] prismane-cluster-containing protein from *Desulfovibrio vulgaris* (Hildenborough). *Eur. J. Biochem.* **206**, 697-704 (1992).
18. Leslie, A. G. W. in *Joint CCP4 and ESF-EACMB Newsl on Protein Crystallogr* 27-33 (1992).
19. Collaborative Computational Project Number 4. The CCP4 suite: programs for protein crystallography. *Acta Crystallogr Sect D* **50**, 760-763 (1994).
20. Matthews, B. W. Solvent content of protein crystals. *J Mol Biol* **33**, 491-7 (1968).
21. Storoni, L. C., McCoy, A. J. & Read, R. J. Likelihood-enhanced fast rotation functions. *Acta Crystallogr Sect D* **60**, 432-438 (2004).
22. Coelho, A. V., Macedo, S., Matias, P. M., Thompson, A. W., LeGall, J. & Carrondo, M. A. Structure determination of bacterioferritin from *Desulfovibrio desulfuricans* by the MAD method at the Fe K-edge. *Acta Cryst. D* **57**, 326-329 (2001).





# CHAPTER IV<sup>i</sup>. Crystal structure of the ferritin from the hyperthermophilic archaeal anaerobe *Pyrococcus furiosus*



## ABSTRACT

The crystal structure of the ferritin from the archaeon, hyperthermophile and anaerobe *Pyrococcus furiosus* (PfFtn) is presented. While many ferritin structures from bacteria to mammals have been reported, until now only one was available from archaea, the ferritin from *Archaeoglobus fulgidus* (AfFtn). The PfFtn 24-mer exhibits the 432 point-group symmetry that is characteristic of most ferritins, which suggests that the 23 symmetry found in the previously reported AfFtn is not a common feature of archaeal ferritins. Consequently, the four large pores that were found in AfFtn are not present in PfFtn. The structure has been solved by molecular replacement and refined at 2.75-

---

<sup>i</sup> This chapter has been published as Tatur J, Hagen WR & Matias PM. Crystal structure of the ferritin from the hyperthermophilic archaeal anaerobe *Pyrococcus furiosus*. *JBIC* 12 (5), 615-630 (2007)

Å resolution to  $R = 0.195$  and  $R_{\text{free}} = 0.247$ . The ferroxidase center of the aerobically crystallized ferritin contains one iron at site A and shows sites B and C only upon iron or zinc soaking. Electron paramagnetic resonance studies suggest this iron depletion of the native ferroxidase center to be a result of a complexation of iron by the crystallization salt. The extreme thermostability of PfFtn is compared with that of eight structurally similar ferritins and is proposed to originate mostly from the observed high number of intrasubunit hydrogen bonds. A preservation of the monomer fold, rather than the 24-mer assembly, appears to be the most important factor that protects the ferritin from inactivation by heat

## INTRODUCTION

Ferritin is a protein involved in metal homeostasis by reversible storage of iron and presumably also in protection against oxidative stress by scavenging reactive oxygen species. It is a small protein of approximately 20 kDa and its main structural motif is a bundle of four parallel  $\alpha$ -helices and a fifth short  $\alpha$ -helix tilted towards the bundle axis and masking the one end of the cylindrical bundle. The functional ferritin molecule is an approximately 500 kDa hollow spherical assembly of 24 subunits, with outer and inner diameters of 12 and 8 nm, respectively. The 24-meric ferritin agglomerate may be a homopolymer or, in higher eukaryotes, a heteropolymer consisting of homologous subunits designated as H, M and/or L. Ferritin subunits, except the L-type subunit, incorporate a ferroxidase center (FC) that consists of a  $\mu$ -oxo bridged dinuclear iron group and is responsible for iron oxidation. Additionally, a third iron site is observed in the subunits of some bacterial ferritins<sup>1,2</sup>. The binuclear iron cluster of the FC and the third iron site are referred to as A, B and C iron sites, respectively. Some ferritins, also called bacterioferritins (BFRs), enclose 12 heme groups that are located between homodimeric subunit pairs, and may be involved in electron transfer<sup>3</sup>. The homologous protein DNA protection during starvation (DPS) and also called a “small ferritin,” is a spherical 12-subunit assembly with smaller dimensions (outer and inner diameters of 9 and 4.5 nm, respectively) and iron storage capacity (500 iron atoms vs. 3,000 in ferritin) than ferritins<sup>4</sup>. While iron is believed to be the main cationic substrate of ferritins, zinc accumulation in ferritin has also been reported<sup>5</sup>.

Ferritins occur in a wide variety of organisms, from prokaryotes to mammals. In humans, their function is related to iron deficiencies or iron-overload disorders such as thalassemia, sickle cell anemia, hemochromatosis and pulmonary hemosiderosis<sup>6-9</sup>. Understanding the mechanism of the action of ferritin will be of great value in the treatment of iron-related diseases. Besides its medical relevance, this knowledge is also of fundamental scientific interest, especially in case of anaerobes.

To date, an insight into the iron-uptake reaction has only been achieved for aerobic organisms. In these organisms, Fe(II) ions are oxidized, possibly together with phosphate oxoanions, and stored inside a ferritin shell as a soluble Fe(III) mineral, believed to be a ferrihydrite mineral with approximate composition  $\text{Fe}_2\text{O}_3 \cdot 0.5\text{H}_2\text{O}$ . Ferric ions from the core can be reduced and released from the ferritin molecule when needed by a cell. Nevertheless, the chemical nature of the physiological reductants for iron release and in the case of anaerobes that of the physiological oxidants for iron uptake have not yet been established.

Crystal structures of ferritins from bacteria, fungi, plants, insects and vertebrates are available, whereas those from archaea are limited to a ferritin from the sulfate-reducing anaerobe and thermophile *Archaeoglobus fulgidus* (AfFtn) (Protein Data Bank, PDB, codes 1sq3 and 1s3q) <sup>2</sup> and a DPS protein from *Halobacterium salinarum* (PDB codes 1tjo, 1tk6, 1tko and 1tkp) <sup>10</sup>.

In AfFtn, a novel 23 point-group symmetry of the 24-mer assembly was found, which is unusual for ferritins and was only known previously in 12-meric assemblies, such as the DPS proteins <sup>10,11</sup> and also in the ferritin from the bacterium *Listeria innocua* <sup>12</sup>. As a result, four oversized triangular pores about 45-Å wide are present in the protein shell of AfFtn <sup>2</sup>.

*Pyrococcus furiosus* is a strict anaerobe and hyperthermophilic archaeon, living optimally at 100°C. It was isolated from the hot marine springs off the beach of Porto di Levante in Vulcano, Italy. *P. furiosus* is a fermentative heterotroph that grows on starch, maltose, or peptone and yeast extract and produces CO<sub>2</sub>, acetate, alanine, H<sub>2</sub> and H<sub>2</sub>S. The expression of the native ferritin from *P. furiosus* (PfFtn) has been confirmed by N-terminal sequencing of the purified protein and the recombinant ferritin has been over-produced in *Escherichia coli* in order to afford extensive biochemical studies <sup>13</sup>.

Herein we present the 3D structure of PfFtn, refined at 2.75-Å resolution. In contrast to the previously reported first structure of an archaeal AfFtn, the functional PfFtn 24-mer has the typical 432 point-



group symmetry observed in other ferritins and BFRs. There are no four large pores such as were found in AfFtn. Instead, the characteristic threefold and fourfold channels are present in PfFtn.

The extreme thermostability of PfFtn, which *in vitro* can withstand 1 day of incubation at 100°C, has been analyzed at the structural level, in comparison with structurally related ferritins. Although *P. furiosus* grows at the highest temperature, 100°C, among the organisms used in thermostability analysis, our results suggest that the ferritin from *Thermotoga maritima* (TmFtn), which has an optimal growth temperature of 80°C, may be even more thermostable than PfFtn. The hyperthermal stability of PfFtn and other ferritins appears to result mainly from the preservation of the monomer fold rather than the 24-mer assembly, owing to a high number of intramolecular hydrogen bonds between main-chain atoms, and between main-chain and side-chain atoms.

The FC stability was analyzed by electron paramagnetic resonance (EPR). Without further experiments, the lack of FC iron sites B and C in nonsoaked PfFtn crystals obtained does not allow any conclusions supporting or contradicting the FC as a stable catalytic cofactor.

## **MATERIALS AND METHODS**

### **Protein production and crystallization**

PfFtn was obtained and purified as previously described<sup>13</sup>. Ferritin iron loading prior to crystallization was performed by adding a freshly and anaerobically prepared aqueous solution of 20 mM iron sulfate, containing 0.1% HCl, to a solution of apoferritin in 50 mM N-(2-hydroxyethyl)piperazine-N'-ethanesulfonic acid (Hepes), pH 7, under aerobic conditions. Crystals of PfFtn were produced using the hanging drop vapor diffusion method at room temperature<sup>14</sup>. The crystals used for data collection were grown against 0.5 ml of 2 M ammonium sulfate reservoir solution, with drops containing 2 µl of 5 mg/ml protein solution in 50 mM Hepes, pH 7, and an equal amount of the reservoir solution. The crystals of the as-isolated ferritin, containing approximately 17 Fe

per 24-mer, grew in 3 weeks and those loaded with approximately 1,000 Fe atoms per 24-mer prior to crystallization grew in 4 months. The crystals exhibited an irregular pyramidal shape, with base side and height between 150 and 250  $\mu\text{m}$ . The iron content of as-isolated ferritin was determined with ferrene as previously described<sup>14</sup> by measuring the absorption of the iron–ferrene complex at 593 nm,  $\epsilon = 35500 \text{ M}^{-1}\text{cm}^{-1}$ .

Iron soaking of ferritin crystals was performed by transferring them to a 10–20- $\mu\text{l}$  drop of a solution with composition 20 mM  $\text{FeSO}_4$ , 2 mM  $\text{Na}_2\text{S}_2\text{O}_4$ , 25% glycerol and 2 M ammonium sulfate, for 15 min. Zinc soaking with  $\text{ZnCl}_2$  was carried out in a similar fashion, with the exception that dithionite ( $\text{Na}_2\text{S}_2\text{O}_4$ ) was omitted from the solution.

### **X-ray data collection**

Cryoprotecting conditions consisted of briefly dipping the crystals into a modified crystallization solution containing 20% glycerol in the case of the as-crystallized and Fe-loaded crystals, and 25% glycerol in the case of the Fe-soaked and Zn-soaked crystals, prior to flash-freezing at  $-173^\circ\text{C}$  in a nitrogen-gas stream, using an Oxford Cryosystems low-temperature device.

Diffraction data from an as-crystallized, an Fe-soaked and a Zn-soaked crystal of as-isolated PfFtn, as well as from a loaded PfFtn crystal, with approximately 1,000 Fe per 24-mer, were collected at the ESRF beamline BM-14, from flash-frozen single crystals at  $-173^\circ\text{C}$ . Two datasets were collected from the Zn-soaked crystal: the first at the Zn K-edge (9.6760 keV, 1.2810 Å, Zn peak) as determined from a fluorescence scan, and the second (9.500 keV, 1.305 Å, Zn low-E rm) on the low-energy side of the absorption edge. The diffraction images were integrated with the program MOSFLM<sup>15</sup>. The processed data were scaled, merged and converted to structure factors using the CCP4 program suite<sup>16</sup>. Data-processing statistics are summarized in Table 4.1.

### **Structure determination of as-isolated and Fe-loaded PfFtn**

Previously<sup>14</sup>, the 3D structure of PfFtn was solved by the

molecular replacement (MR) method, using the program PHASER<sup>17</sup> and the homologous TmFtn (PDB entry 1vlg) as the search model. The sequence of this 165 amino acid ferritin shares a 51% amino acid sequence identity (88 amino acid residues) with that of Pfftn (174 amino acids), and the only insertions or deletions occur at the termini of the subunit chains. However, despite the success of the MR calculations we believed that, because of the low resolution of the diffraction data, relatively low amino acid sequence identity with the search model, as well as the complexity of the structure, experimental phase information would be needed in order to obtain the best possible structural model from the data. To that end, the first BM-14 dataset was collected at a long wave-length (7.0000 keV, 1.7712 Å) from a crystal of as-isolated Pfftn with the intention of using S-SAD in phasing, whereas a second dataset was collected just above the Fe K-absorption edge (7.1500 keV, 1.7340 Å) from an Fe-loaded Pfftn crystal, with the aim of using Fe-SAD in phasing and also for better location of the incorporated Fe atoms. However, neither dataset could provide the desired independent phase information, owing to complications that arose from radiation damage, which prevented us from collecting the highly redundant dataset required for application of the S-SAD method to the first dataset, as well as the lack of a sufficiently high ordered Fe content, which limited the usefulness of the anomalous dispersion data obtained from the second dataset.

Therefore, the 3D structure of Pfftn was solved by repeating the MR calculations previously described<sup>14</sup> with the new “as-isolated” 2.75-Å dataset, using the standard PHASER protocol as implemented through the CCP4 graphical user interface, with reflection data up to 3.25-Å resolution. Previously, we had established<sup>14</sup> that the asymmetric unit of the Pfftn crystal structure contained 36 monomers, arranged as 1.5 24-mers. The search model used was half of a TmFtn 24-mer, constructed from the PDB 1vlg coordinates without the Fe sites, and three such models were searched for in the crystal structure of Pfftn. The MR calculations with PHASER gave a single solution. Prior to

**Table 4.1.** X-ray diffraction data collection and processing statistics

Beamline	ESRF BM-14		ESRF BM-14		ESRF BM-14		ESRF BM-14		ESRF BM-14	
Detector	MAR	225	MAR	225	MAR	225	MAR	225	MAR	225
	CCD		CCD		CCD		CCD		CCD	
Crystal	As-isolated		Fe-loaded		FeSO <sub>4</sub> soak		ZnSO <sub>4</sub> soak, Zn peak		ZnSO <sub>4</sub> soak, Zn low-E rm	
Wavelength (Å)	1.7712		1.7340		1.4585		1.2810		1.305	
Space group	C222 <sub>1</sub>		C222 <sub>1</sub>		C222 <sub>1</sub>		C222 <sub>1</sub>		C222 <sub>1</sub>	
Unit cell (Å)	a	255.00	b	254.32	c	254.30	a	255.37	b	255.69
	b	341.42	c	343.16	a	342.88	c	342.06	b	342.36
	c	265.52	a	266.26	b	266.22	c	265.99	a	266.21
Resolution range (Å)	58.2 – 2.75 (2.90 – 2.75)		63.2 – 2.95 (3.11 – 2.95)		42.0 – 2.80 (2.95 – 2.80)		42.9 – 2.80 (2.95 – 2.80)		42.9 – 2.80 (2.95 – 2.80)	
Observations	1,685,078 (151,184)		903,956 (85,605)		1,011,149 (102,079)		1,082,567 (111,068)		1,086,719 (111,952)	
Unique reflections	295,335 (42,009)		237,583 (32,389)		280,407 (38,583)		279,537 (37,607)		280,474 (37,777)	
% Completeness (Overall)	99.7 (97.8)		98.1 (92.2)		99.1 (94.1)		98.7 (91.6)		98.7 (91.9)	
Redundancy	5.7 (3.6)		3.8 (2.6)		3.6 (2.6)		3.9 (3.0)		3.9 (3.0)	
R <sub>merge</sub>	0.085 (0.300)		0.113 (0.532)		0.081 (0.354)		0.075 (0.288)		0.077 (0.344)	
I/σ(I)	16.5 (3.1)		10.8 (1.6)		8.2 (2.0)		8.8 (2.5)		8.6 (1.9)	
% Anomalous Completeness	98.0 (88.3)		89.2 (71.1)		94.4 (64.8)		97.7 (85.4)		97.6 (85.5)	
Anomalous Redundancy	2.9 (1.9)		2.0 (1.5)		1.8 (1.6)		1.9 (1.5)		2.0 (1.5)	
R <sub>anom</sub>	0.043 (0.204)		0.078 (0.414)		0.058 (0.294)		0.063 (0.252)		0.059 (0.288)	
Estimated B <sub>overall</sub> (Å <sup>2</sup> )	53.3		62.7		60.5		54.3		58.5	

Values in *parantheses* refer to the last resolution shell

model rebuilding, electron-density map improvement was carried out both by using Arp/wArp<sup>18</sup> in atom update and refinement mode as well as by using DM<sup>19</sup> with 36-fold noncrystallographic symmetry (NCS) averaging. In this way, the initial PHASER figure of merit of 0.502 for the full resolution range of the 2.75-Å dataset was improved to 0.697

(Arp/wArp) and 0.849 (DM). Rebuilding of the protein chain to take into account the differences in sequence and chain length between TmFtn and PfFtn was carried out with the program TURBO<sup>20</sup> using one monomer and the 36-fold averaged electron-density map obtained from the DM calculations. The coordinates for each of the remaining 35 monomers were obtained from those of the first by applying the appropriate NCS transformations, followed by model correction with TURBO using the electron-density maps obtained from both the DM and the Arp/wArp calculations. In these maps, peaks corresponding to Fe occupation of the A sites only in the FC were observed, and therefore only 36 iron sites (one per monomer), were included in the model.

The structure of the Fe-loaded PfFtn was also determined by MR with PHASER using a similar procedure; however, the  $|F_o|$  density map, as well as an anomalous electron density map, calculated with MR phases, showed that only the A site in the FC was occupied by Fe atoms. Since the “as-isolated” dataset had higher resolution and better quality, further work on the “Fe-loaded” dataset was abandoned.

### **Structure refinement of as-isolated PfFtn**

Refinement was carried out with the program REFMAC<sup>21</sup> using medium main-chain and weak side-chain NCS restraints between the 18 dimers in the asymmetric unit. At a later stage, a translation–libration–screw (TLS) rigid-body motion refinement<sup>22</sup> was made prior to restrained refinement of atomic positions and thermal motion parameters. One rigid body was defined for each of the 36 independent monomers. In the final refinement stages, a total of 832 solvent molecules were located with Arp/wArp<sup>23</sup>. On the basis of their B factors, observed electron density and interactions with neighboring protein residues, 791 were assigned to water molecules, while the remaining 41 were modeled as sulfate ions. Individual restrained B factors were refined for all non-hydrogen atoms and, for consistency with the structure refinements of the Fe-soaked and Zn-soaked crystals (see below), only tight NCS restraints (0.1 Å positional and 1.0 Å<sup>2</sup>

thermal parameter) were applied to all the protein residues involved in the FC metal coordination, instead of defining the coordination geometry for each individual protein–metal bond as in the earlier stages of refinement.

The final values of  $R$  and  $R_{\text{free}}$  were 0.195 and 0.247, respectively. Neither TLS rigid-body refinement nor full NCS restraints (i.e., extending over the whole monomer and relating all the chains in the asymmetric unit) were used in the final refinement, as they were seen to lead to higher values of both  $R$  and  $R_{\text{free}}$ .  $R_{\text{free}}$ <sup>24</sup> was calculated from a randomly chosen subset of the data, containing approximately 5% of the total number of independent reflections. Throughout the refinement, the model was periodically checked and corrected with TURBO against  $2|F_o| - |F_c|$  and  $|F_o| - |F_c|$  electron-density maps. The refinement statistics are included in Table 4.2. The maximum-likelihood estimate of the overall coordinate error, obtained with REFMAC, was 0.20 Å. For all 36 independent monomers in the PfFtn crystal structure, only the first 168 residues were included in the model. Although some electron density was visible beyond Gly168, it was not possible to build any more C-terminal residues into it, and it is likely that the C-terminal tail is disordered in all the independent PfFtn monomers. On the basis of a B-value comparison with the protein residues directly coordinating the iron atoms, it was realized that at least 17 out of the 36 metal sites were not fully occupied, and were assigned occupation factors of 0.8 (0.7 in one case). In addition, 788 side-chain atoms could not be seen in either  $2|F_o| - |F_c|$  or  $|F_o| - |F_c|$  electron-density maps and were therefore given zero occupancy during the refinement.

The structure was analyzed with PROCHECK<sup>25</sup> and its stereochemical quality parameters were within their respective confidence intervals. A Ramachandran<sup>26</sup>  $\varphi, \psi$  plot showed that of the 5544 non-glycine and non-proline residues, 11 (0.20%) were found to lie in the generously allowed regions and only one (0.02%) outlier was observed. All these residues with more unusual  $\varphi, \psi$  conformations were located in a loop region containing Lys145, for which the electron

**Table 4.2.** Refinement and structure analysis statistics for PfFtn

Crystal	As-isolated, as-crystallized	Fe-soaked	Zn-soaked
Resolution (Å)	56.8 – 2.75	42.0 – 2.80	42.8 – 2.80
No. reflections in work set/test set	280,375 / 14,914	266,173 / 14,187	265,356 / 14,134
$R_{\text{work}} / R_{\text{free}}$	0.195 / 0.247	0.197 / 0.249	0.201 / 0.251
Number of atoms			
Protein – total number of atoms	49,824	49,824	49,824
Protein – atoms with zero occupancy	788	718	720
Fe/Zn atoms	36	108	108
Water molecules (sulfate ions)	791 (41)	413 (26)	162 (44)
Mean $B$ -factors (Å <sup>2</sup> )			
Protein main-chain (side-chain)	32.6 (34.6)	38.0 (39.9)	30.9 (32.7)
Fe/Zn atoms	57.5	53.2	36.9
Water molecules (sulfate ions)	26.5 (67.1)	29.0 (76.8)	21.9 (74.0)
Root mean square deviations from ideal values			
Bond lengths (Å)	0.014	0.014	0.015
Bond angles (°)	1.44	1.46	1.48
Mean positional error (Å)	0.20	0.22	0.22
PROCHECK Ramachandran analysis			
Total nr. analyzed residues	5544	5544	5544
Nr. (%) residues in core regions	5255 (94.79)	5241 (94.53)	5239 (94.50)
Nr. (%) residues in allowed regions	277 (5.00)	285 (5.14)	289 (5.21)
Nr. (%) residues in generous regions	11 (0.20)	10 (0.18)	9 (0.16)
Nr. (%) residues in disallowed regions	1 (0.02)	8 (0.14)	7 (0.13)
PROCHECK G-factors			
Mean (range) dihedral	0.00 (-0.13 to 0.07)	-0.04 (-0.23 to 0.03)	-0.04 (-0.21 to 0.09)
Mean (range) covalent	0.38 (0.32 – 0.45)	0.38 (0.29 – 0.46)	0.36 (0.26 – 0.44)
Mean (range) overall	0.15 (0.07 – 0.19)	0.12 (0.00 – 0.18)	0.12 (0.01 – 0.17)

density was generally poor. The final atomic coordinates were deposited with the PDB <sup>27</sup>, to be released upon publication, with the accession code 2jd6.

### **Structure determination and refinement of the Fe-soaked and Zn-soaked PfFtn crystals**

In view of the very small changes in cell parameters observed in comparison with those of the as-isolated crystal, the structures of the Fe-soaked and Zn-soaked crystals of PfFtn were determined directly by using the final refined coordinates of the as-isolated structure, omitting the iron sites and the solvent atoms. Ten cycles of rigid-body refinement were first carried out, followed by a TLS rigid-body motion refinement<sup>22</sup> prior to restrained refinement of atomic positions and thermal motion parameters. At this stage, the  $2|F_o| - |F_c|$  or  $|F_o| - |F_c|$  electron-density maps were inspected with COOT<sup>28</sup> for inclusion of the FC A, B and C metal sites in the models. Because of the complexity of the metal coordination in the FC, the low resolution of the diffraction data and the realization that some of the FC metal sites were not fully occupied (see “Discussion” for details), tight NCS restraints (0.1 Å positional and 1.0 Å<sup>2</sup> thermal parameter) were applied to all the protein residues involved in the FC metal coordination, instead of defining the coordination geometry for each individual protein–metal bond.

In the final refinement of the Fe-soaked crystal structure, 423 solvent molecules and 26 sulfate ions were located with Arp/wArp<sup>23</sup> and included in the model, and individual restrained B factors were refined for all non-hydrogen atoms. On the basis of a B-value comparison with the protein residues directly coordinating the iron atoms, it was realized that not all metal sites were fully occupied: all the B sites and one C site were assigned an occupation of 0.5. The final values of R and R<sub>free</sub> were 0.197 and 0.249. The refinement statistics are listed in Table 4.2. The structure was analyzed with PROCHECK<sup>25</sup> and its stereochemical quality parameters were within their respective confidence intervals. A Ramachandran<sup>26</sup>  $\varphi, \psi$  plot showed that of the 5544 non-glycine and non-proline residues, ten (0.18%) were found to lie in the generously allowed regions and only eight (0.14%) outliers were observed. With three exceptions, all these residues with more unusual  $\varphi, \psi$  conformations were located in a loop region containing Lys145, for which the electron



density was generally poor.

In the final refinement of the Zn-soaked crystal structure, 162 solvent molecules and 44 sulfate ions were located with Arp/wArp<sup>23</sup> and included in the model, and individual restrained B factors were refined for all non-hydrogen atoms. A B-value comparison with the protein residues directly coordinating the metal atoms, combined with the observation of a mixed iron/zinc population at the A sites (see below for details) led us to postulate a mixed (50:50 Zn/Fe) occupancy for the A sites, which was modeled as a Zn atom with 0.9 occupancy. Also, the B sites were modeled as partially occupied by zinc (50%) and the C sites as partially occupied by iron (50%). The final values of R and  $R_{\text{free}}$  were 0.201 and 0.251. The refinement statistics are included in Table 4.2. The structure was analyzed with PROCHECK<sup>25</sup> and its stereochemical quality parameters were within their respective confidence intervals. A Ramachandran<sup>26</sup>  $\varphi, \psi$  plot showed that of the 5544 non-glycine and non-proline residues, nine (0.16%) were found to lie in the generously allowed regions and only seven (0.13%) outliers were observed. With two exceptions, all these residues with more unusual  $\varphi, \psi$  conformations were located in a loop region containing Lys145, for which the electron density was generally poor.

As for the as-isolated structure, neither TLS rigid-body refinement nor full NCS restraints were used in the final refinement of the Fe-soaked or Zn-soaked structures, as they were seen to lead to higher values of both R and  $R_{\text{free}}$ .  $R_{\text{free}}$ <sup>24</sup> was calculated from a randomly chosen subset of the data, containing approximately 5% of the total number of independent reflections, and with the same h,k,l indices as for the “as-isolated” data. These test-set reflections were not chosen in thin resolution shells. However, while it is true that the 24-mers have very high NCS, in all three refined crystal structures the  $R_{\text{free}}/R_{\text{work}}$  ratios are typical for the data resolution and refinement parameters used,<sup>29</sup> and therefore there is no indication that the more simplistic test-set choice may have introduced a bias in the  $R_{\text{free}}$  values. Throughout the refinement, the models were periodically checked and corrected with

COOT<sup>28</sup> against  $2|F_o| - |F_c|$  and  $|F_o| - |F_c|$  electron-density maps. Since the asymmetric unit of both structures contains 36 monomers, and each monomer contains one FC with three metal sites, a total of 108 metal atoms are present in the model. In addition, 718 side-chain atoms could not be seen in either  $2|F_o| - |F_c|$  or  $|F_o| - |F_c|$  electron-density maps for the Fe-soaked structure (720 for the Zn-soaked structure) and were given zero occupancy during the refinement. The final atomic coordinates were deposited with the PDB<sup>27</sup>, to be released upon publication, with the accession codes 2jd7 (Fe-soaked structure) and 2jd8 (Zn-soaked structure).

## RESULTS AND DISCUSSION

### Structure of the PfFtn monomer

The PfFtn monomer exhibits the typical four-helical bundle fold which is encountered in ferritins, BFRs, DPS proteins and rubrerythrins. According to the DSSP algorithm<sup>30</sup> the four helices comprise residues 4–34 (helix A), 37–64 (helix B), 83–111 (helix C) and 114–144 (helix D). A short, C-terminal  $\alpha$ -helix (helix E, residues 148–160), bordering one of the cylindrical bundle openings, followed by a tail without any secondary structure also occurs in the PfFtn monomer fold (Fig. 4.1a, b). For convenience of terminology, the two extremities of the cylindrical  $\alpha$ -helical bundle will be further referred to as the open side and the E-helix sides of the monomer.

The PfFtn monomer is built of hydrophobic amino acids at its open and E-helix sides and polar and hydrophilic residues in the middle of the subunit, similarly to the subunits from other ferritins. The open side of the monomer contains three leucine residues (Leu10, Leu104 and Leu120), two phenylalanine residues (Phe57 and Phe123), Met6, Tyr60 and Ile101, whereas the E-helix side has three phenylalanine residues (Phe87, Phe31 and Phe39), Trp42 and Met27 (denoted by asterisks in Fig. 4.2). The residues defining the open and E-helix sides of the monomer are conserved among PfFtn, the ferritin from *E. coli* (EcFtnA), AfFtn and human H chain ferritin (HuHF) in terms of their polarities,

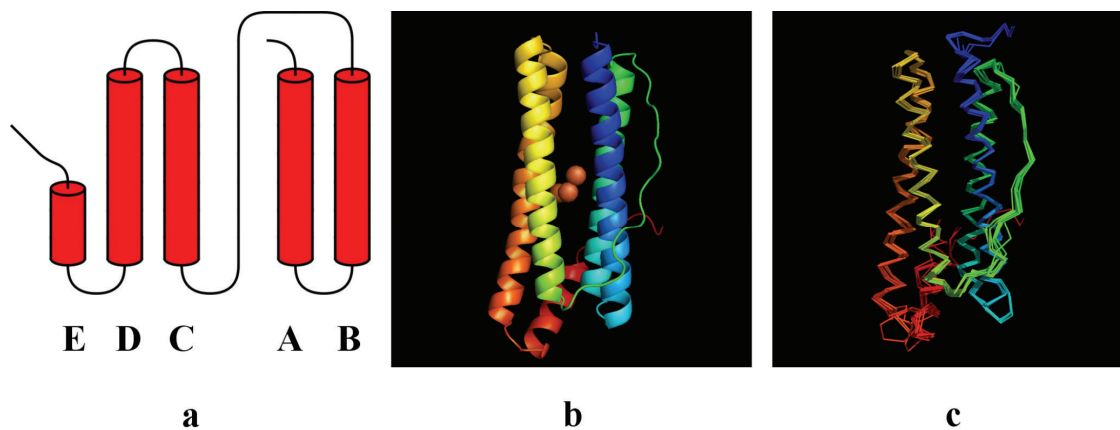


**Figure 4.1.** **a** Topology diagram of the ferritin from *Pyrococcus furiosus* (PfFtn). **b** Ribbon diagram of PfFtn showing the location of the ferroxidase center sites A, B and C (orange spheres) near the center of the four-helical bundle. **c** Superposition of the PfFtn C $^{\alpha}$  chain with those of its eight closest homologous structures. In **b** and **c**, the molecule colors change from blue to red in the N-terminal to C-terminal direction. **b, c** Prepared with PyMOL<sup>31</sup>

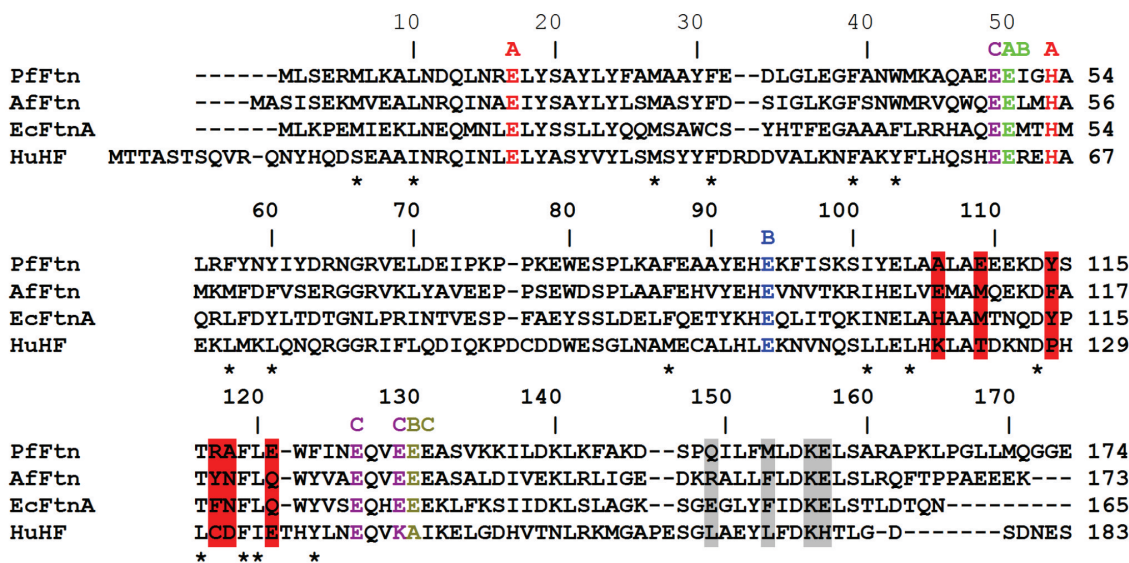


**Figure 4.2.** Amino acid sequence alignment of PfFtn, the ferritin from *Archaeoglobus fulgidus* (AfFtn), the ferritin from *Escherichia coli* (EcFtnA) and human H chain ferritin (HuHF). Asterisks show the residues around the open and E-helix sides of the monomer; A, B and C denote the residues coordinating the iron sites of the ferroxidase center (FC); red bars highlight the main residues located around the threefold channels and gray bars those around the fourfold channels. The alignment was prepared with ClustalW<sup>32</sup>

apart from Phe123, which in other ferritins is a tyrosine.

The central part of the subunit comprises the negatively charged and polar amino acids involved in metal binding. These are Glu17, Glu49, Glu50, Glu94, Glu126, Glu129 and Glu130 and His53, which are shown in figure 4.2 with A, B or C labels to denote the iron site they coordinate (see “The FC”). In addition, Tyr24 and Gln127, which in EcFtnA<sup>1</sup> indirectly contribute to the A and B sites via hydrogen bonds to Glu94 and Glu17, are also oriented towards the FC in Pfftn. It has been noted<sup>2</sup> that Gly67, Ser84 and Gly147 (in AfFtn numbering) are conserved among AfFtn, EcFtnA and HuHF, and define the BC loop and the end of D helix, respectively. In the case of Pfftn, only Ser84 is conserved, while the two glycine residues are changed into Asn65 and Lys145.

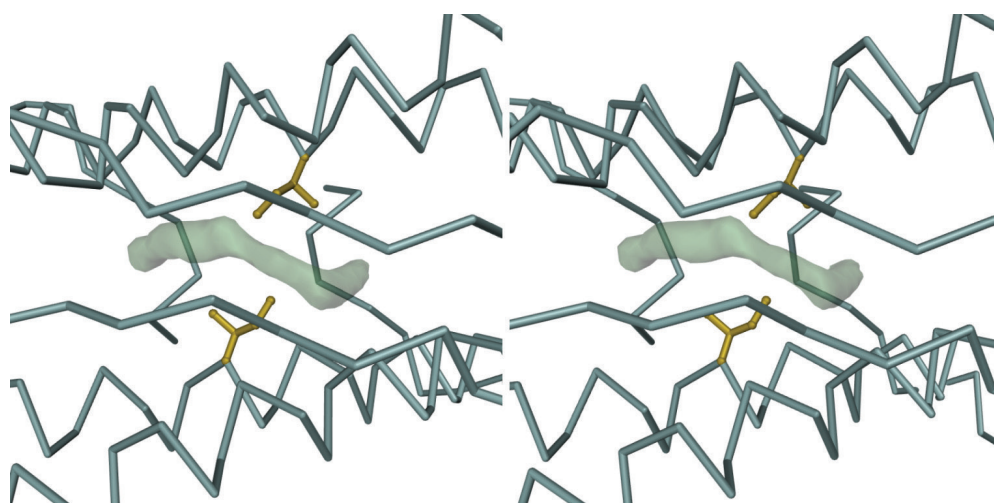


**Figure 4.3.** Stereoview of a dimer interface in the as-isolated Pfftn structure, showing a difference electron density feature, drawn at the 2.5 map root mean square (RMS) level, which results from a disordered chain of water molecules trapped within a hydrophobic pocket centered around Ile51. This feature is observed in all dimers of all Pfftn structures investigated. The bulk of the Pfftn dimer is represented by its C $\alpha$  trace (blue-gray). The side chains (including C $\alpha$  atoms) of the Ile51 residues in both monomers are represented in ball-and-stick mode and are colored gold. The view is down the noncrystallographic twofold symmetry axis of the dimer, looking towards the inside of the Pfftn 24-mer. The figure was prepared with DINO<sup>33</sup>

### **A surface hydrophobic pocket at the Pfftn dimer interface**

A large surface pocket, largely lined by hydrophobic residues, was located at the Pfftn dimer interface. Interestingly, one of these is Ile51, corresponding to Met 57 in the BFR from *Desulfovibrio desulfuricans*

ATCC 27774<sup>34</sup>, which binds the heme group. In-stead of a heme, the pocket appears to be occupied by a disordered string of water molecules (Fig. 4.3) which form a continuous region of electron density. This feature was observed for all the Pfftn structures investigated. A similar situation was reported by Yu *et al.*<sup>35</sup> for the hydrophobic cavity of human interleukin 1 $\beta$ .

### **Subunit structure comparison**

In order to compare the Pfftn structure with the structures of other known ferritins, a protein structure comparison against the PDB using the secondary structure matching (SSM) tool at the European Bioinformatics Institute (<http://www.ebi.ac.uk/msd-srv/ssm>)<sup>36</sup> was performed. This resulted in 377 hits, which, after elimination of duplicate protein chains, were seen to correspond to 63 different protein structures. A multiple structural alignment was then carried out with a subset of eight SSM hits, listed in Table 4.3 and shown as a superposition of C $^{\alpha}$  chains in figure 4.1c. The members of this subset were chosen such that the percentage of their aligned residues was equal to or greater than 25%, all five secondary structure elements ( $\alpha$ -helices) were aligned, the Q score, of their pairwise SSM alignment with Pfftn was greater than 0.5, and considering only one crystal form of each different protein structure from each organism. This subset includes representatives from archaea, bacteria and eukarya. The structural alignment showed Pfftn to be highly similar to TmFtn, followed by AfFtn and EcFtnA (Table 4.3). The deviations occur mostly in loop regions: AB loop from Glu32 to Leu34, end of the BC loop from Lys78 to Pro83, CD loop and helix D up to Phe123 and DE loop from Lys145 to Leu151 (in Pfftn numbering).

### **Structure of the Pfftn 24-mer and comparison with AfFtn**

A highly conserved quaternary structure appears among all known ferritins — a spherical tetraeicosameric assembly with 432 point-group symmetry. An interesting exception to this rule is the recently reported

**Table 4.3.** Proteins with known 3D-structure most closely homologous to PFFtn

PDB ID	Protein name	Source organism	Chain length	Identity %	Identity SS-Aligned %	Q score <sup>a</sup>	RMSD (Å)
1vlg	Ferritin (TM1128)	<i>Thermotoga maritima</i>	176	55	55.3	0.92	0.49
1s3q	Ferritin	<i>Archaeoglobus fulgidus</i>	173	50	48.2	0.94	0.53
1krq	Ferritin	<i>Campylobacter jejuni</i>	167	39	39.2	0.81	1.02
1eum	Ferritin ECFTNA	<i>Escherichia coli</i>	165	38	38.4	0.86	0.90
1r03	Mitochondrial Ferritin	<i>Homo sapiens</i>	182	40	30.6	0.68	1.55
2fha	H ferritin K86Q mutant	<i>Homo sapiens</i>	183	37	29.4	0.62	1.98
1mfr	M ferritin	<i>Rana catesbeiana</i>	176	36	29.6	0.68	1.67
1rcg	L ferritin	<i>Rana catesbeiana</i>	173	32	25.0	0.61	2.03

*PDB* Protein Data Bank, *SS* secondary structure, RMSD root mean square deviation

<sup>a</sup> Parameter that takes the alignment length and the RMSD between the superimposed atoms into account, and varies from 0 in case of poor matches to 1 in case of identical proteins

structure of the AfFtn 24-mer <sup>2</sup>, which exhibited 23 point-group symmetry, normally an attribute of the dodecameric DPS proteins. Even though PFFtn and AfFtn are highly similar archaeal ferritins (50 and 70% amino acid sequence identity and similarity, respectively), the PFFtn 24-mer has the canonical 432 point-group symmetry instead of the 23 point-group symmetry found in the AfFtn 24-mer. Although there may be other archaeal tetraeicosameric ferritins with 23 point-group symmetry like AfFtn, our structure clearly suggests that it is not a feature of all archaeal ferritins.

When comparing the two quaternary structures (Fig. 4.4), it can be seen that the 432 and 23 arrangements in PFFtn and AfFtn result from a different organization of the four fundamental units, hexamers formed by three dimers around a 90° vertical turn from a threefold NCS rotation axis. The 23 arrangement leads to the appearance of four outsized

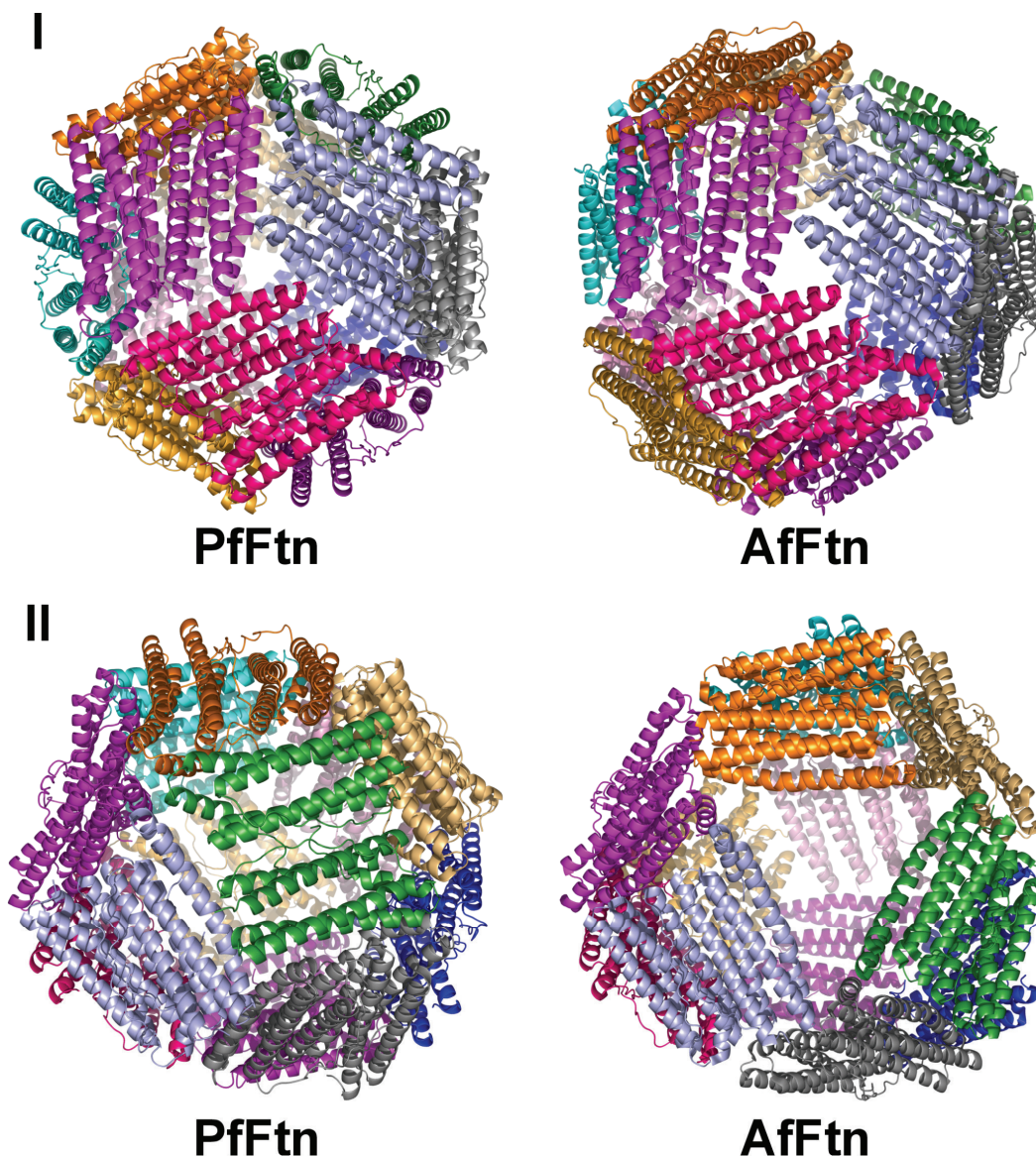


**Figure 4.4.** Ribbon diagrams of the PfFtn and AfFtn 24-mers. *I* View down a 3-fold axis, showing one “fundamental hexamer”; *II* View rotated by *ca.* 90° about a vertical axis, showing the different hexamer arrangement, which leads to the appearance of large pores in AfFtn. The figure was prepared with PyMOL <sup>31</sup>

triangular pores about 45-Å wide in the protein shell of AfFtn <sup>2</sup>, which are absent in the 432 arrangement of PfFtn and all other known structures of tetraeicosameric bacterial ferritins.

### **Threefold and fourfold channels**

The eight threefold channels are formed by helices C and D from three adjacent dimers, in such a way that, with respect to the hollow tetraeicosameric protein shell, the C-terminal ends of helices C define

the outer entrance to the channel and the N-termini of helices D define the inner entrance (Fig. 4.5). The Pfftn threefold channel is lined by a mix of hydrophobic and hydrophilic amino acids Ala106 and Glu109 at the outer side of the channel, Tyr114 and Arg117 in the middle and Ala118 and Glu121 at the inner entrance of the channel (Fig. 4.5). In general, and similarly to EcFtnA and AfFtn, this channel is less hydrophilic than in vertebrate H and L chain ferritins, suggesting a rather hydrophobic threefold channel in microbial ferritins in comparison with vertebrate ferritins. Nevertheless, when compared with that in EcFtnA and AfFtn, the threefold channel in Pfftn is more similar to that of HuHF, in the sense that it is more negatively charged at its inner entrance and more positively charged in its central region (Fig. 4.5).

On the basis of the crystallographic, kinetic, mutagenesis and electrostatic calculations studies on HuHF 9,37-39, the threefold channels were proposed to be involved in the entry of iron ions into the ferritin molecule. The inhibition of iron uptake in HuHF upon Asp131 and Glu134 substitutions 37 and the coordination of Ca<sup>2+</sup> by Asp131 and Glu134 40 have been observed in this protein. The inner narrow entrance of the threefold channel in Pfftn resembles that of HuHF, suggesting that a similar mechanism is possible in Pfftn. Nevertheless, the mutations of His118 and Cys130 also influenced the iron-binding capacity of HuHF and inhibited the binding of different metals by the channel to different extents. The different amino acid arrangements in the threefold channel of the various ferritins suggests the possibility of different iron incorporation mechanisms.

The six fourfold channels, formed around the four-fold symmetry axes of the Pfftn 24-mer, are lined, from the outside to the inside of the protein shell, by Gln149, Met153, Lys156 and Glu157 (Fig. 4.5). Owing to a nozzle-like shape formed by Gln149, the Pfftn four-fold channel is longer (approximately 16 Å) than its counterparts in EcFtnA (approximately 14 Å) and HuHF (approximately 12 Å). In Pfftn, Lys145 in the DE loop, which forms an outer gate to the fourfold channel, occurs in place of EcFtnA Gly145 or HuHF Gly159, making



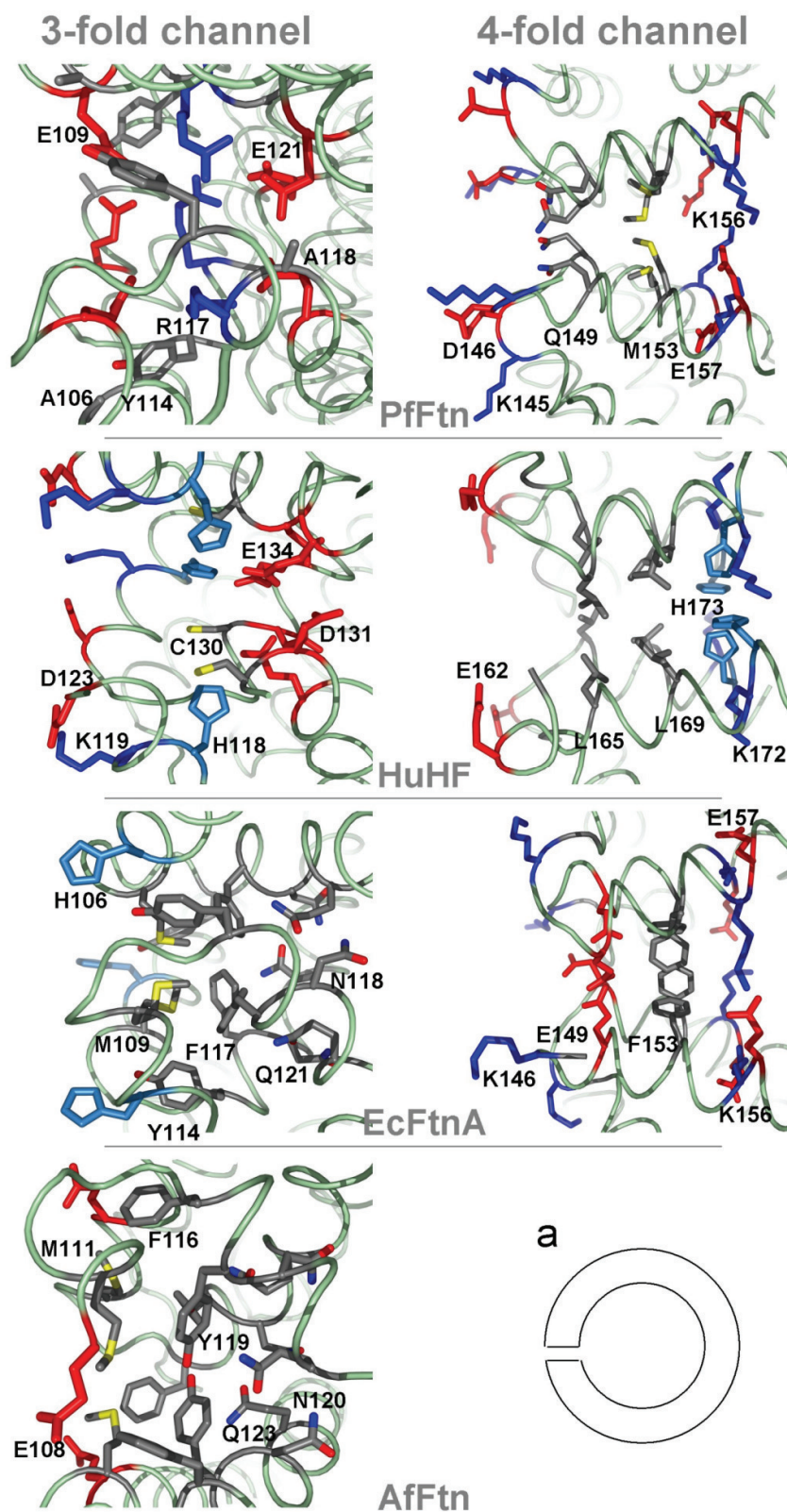


**Figure 4.5.** Profile view of the threefold (left column) and fourfold (right column) channels in PfFtn, AfFtn, EcFtnA and HuHF. The exterior of the shell lies on the left side and the inner cavity on the right side of each cartoon as shown schematically in a. The red residues correspond to acidic Glu and Asp residues and the blue ones to positive Lys, Arg and His residues, and highlight the arrangement of positive and negative amino acids along the channels. The figure was prepared with PyMOL <sup>31</sup>

this gate more polar and charged in Pfftn. In addition, the DE loop and its amino acids are somewhat oriented outwards from the fourfold channel, resulting in a hourglass shape of this channel, which is less strongly developed in EcFtnA and even less so in HuHF, where the pore has an almost cylindrical shape. The outer entrance of the Pfftn fourfold channel is polar and hydrophilic, the region inside the channel is nonpolar and the inner entrance is polar again. The fourfold channels in EcFtnA have a similar arrangement of polar residues at both channel entrances and are nonpolar in the middle, while in HuHF they are mostly apolar with Leu165 and Leu169 and polar His173 on the inner side of the channel (Fig. 4.5). In electrostatic terms, the Pfftn fourfold channel is similar to that of both EcFtnA and HuHF; the outer entrance of it is uncharged as in HuHF and the inner entrance has a compensated charge from the sequence of positive Lys156 and negative Glu157 as in EcFtnA.

### **The FC**

The active site responsible for the oxidation of Fe(II) to Fe(III) in ferritins, the FC, is located in the central part of each subunit (Fig. 4.1b). It is generally believed that in most ferritins the initial stages of the core formation take place via the FC. Subsequently, iron incorporation and removal is thought to occur pre-dominantly through one or the other of the channels formed around the threefold and fourfold symmetry axes of the 24-mer. In this discussion, the nomenclature for the FCs in ferritins and BFRs presented in a recent review<sup>41</sup> will be followed. The FC in Pfftn is of the FtnA (EcFtnA) type, which is strictly conserved in all the closest prokaryote structural homologues of Pfftn besides EcFtnA (Table 4.4). The EcFtnA FC contains three metal binding sites (A, B and C), in contrast with the HuHF and *E. coli* BFR FC, which only contain two (A and B). The FC of the as-crystallized Pfftn showed iron bound to site A only. Iron binding to sites B and C was observed only after soaking the Pfftn crystals in Fe(II).

In Pfftn, iron site A is coordinated by Glu17, Gly50 and His53,

**Table 4.4.** The ferroxidase center in Pfftn and its homologous crystallized ferritins

PDB ID	Protein name	Source organism	Resolution (Å)	FC type	Metal site occupation
--	Ferritin	<i>Pyrococcus furiosus</i>	2.75	FtnA	A (Fe) A,B,C(Fe,Zn)
1s3q	Ferritin	<i>Archaeoglobus fulgidus</i>	2.10	FtnA	A,B (Zn) <sup>a</sup> A,B,C (Fe)
1vlg	Ferritin (TM1128)	<i>Thermotoga maritima</i>	2.00	FtnA	A (Fe)
1krq	Ferritin	<i>Campylobacter jejuni</i>	2.70	FtnA	A,B (Ow?) <sup>b</sup>
1eum	Ferritin ECFTNA	<i>Escherichia coli</i>	2.05	FtnA	A,B (Zn) <sup>c</sup> A,B,C (Fe)
1r03	Mitochondrial ferritin	<i>Homo sapiens sapiens</i>	1.70	HuHF	--
2fha	H ferritin K86Q mutant	<i>Homo sapiens sapiens</i>	1.90	HuHF	--
1mfr	M ferritin	<i>Rana catesbeiana</i>	2.80	HuHF	--
1rcg	L ferritin	<i>Rana catesbeiana</i>	2.20	---	--

FC ferroxidase center

<sup>a</sup> Zn in 1s3q and Fe in 1sq3<sup>2</sup>

<sup>b</sup> 1krq contains 4 water molecules, two of which are located at the FC, in positions corresponding to A and B sites. They might be low-occupancy metal sites but there's no indication of whether it is a native or a soaked crystal

<sup>c</sup> 1eum corresponds to the native structure<sup>1</sup>; these sites were located in the Zn<sup>2+</sup> and Fe<sup>3+</sup> derivatives, respectively, for which no coordinates were deposited in the PDB.

iron site B by Glu50, Glu94 and Glu130, and iron site C by Glu49, Glu126, Glu129 and Glu130. Site B is 3.0 Å distant from site A. Site C is located 7.5 and 6.3 Å away from sites A and B, respectively (Table 4.5, Fig. 4.6). Glu17 and Glu94 appear to be monodentate ligands; therefore, sites A and B are coordinated by side chains from three amino acids, while site C is coordinated by side chains from four amino acids. The final  $2|F_o| - |F_c|$  electron density around the FC of a selected Pfftn monomer in the as-isolated, Fe-soaked and Zn-soaked crystal structures are represented in Fig. 4.7a–c, respectively.

For the Fe-loaded crystal structure, the anomalous difference Fourier map, calculated with the phases obtained from the final “as-isolated” refinement (Fig. 4.7d), shows a very small occupancy of site

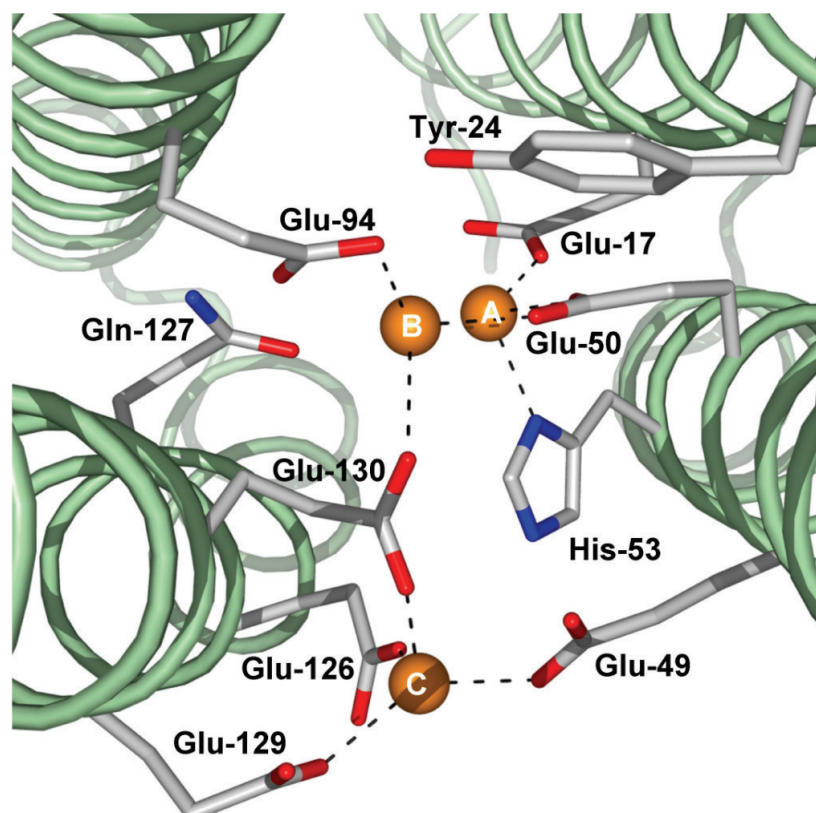


**Figure 4.6.** View of the FC down the Pfftn subunit from the E-helix side. The three metal sites are annotated as A, B and C. Metal occupation of sites B and C is observed only upon crystal soaking in Zn or Fe. The dashed lines correspond to the coordination geometries described in Table 4.5. The figure was prepared with PyMOL<sup>31</sup>

B. This map is very similar to that obtained from the MR phases (not shown). In the Fe-soaked crystal, the anomalous difference Fourier map calculated at the end of the refinement showed that sites A and C have a clearly higher Fe occupancy than site B (Fig. 4.7e).

In the Zn-soaked crystal, the anomalous difference Fourier maps obtained from the two datasets collected (just above and 176 eV below the Zn K-absorption edge) clearly show some iron occupation of sites A and C (Fig. 4.7h), whereas zinc populates sites A and B (Fig. 4.7f, i). The dispersive Fourier map calculated using the two datasets (Fig. 4.7i) shows Zn peaks at sites A and B but since no diffraction data were recorded at the inflexion point of the Zn K-absorption edge, this map is noisier and no conclusions can be drawn about any Zn occupation of site C. Since the as-isolated structure only showed Fe occupation of FC site A, we conclude that the Fe occupation of site C in the Zn-soaked

**Table 4.5.** Coordination geometry statistics of the ferroxidase center in Pfftn

Bonds <sup>a</sup>	Distance, Å		
	“As-isolated” <sub>b</sub>	Fe-soak <sup>b</sup>	Zn-soak <sup>b</sup>
M <sub>A</sub> ... Glu 17 Oε1	2.24 (0.09) [2.00 – 2.46]	2.21 (0.08) [2.00 – 2.47]	2.18 (0.07) [2.01 – 2.32]
M <sub>A</sub> ... Glu 50 Oε1	2.26 (0.11) [2.09 – 2.47]	2.24 (0.09) [2.09 – 2.55]	2.22 (0.07) [2.02 – 2.38]
M <sub>A</sub> ... His 53 Nδ1	2.12 (0.09) [1.97 – 2.41]	2.28 (0.09) [2.12 – 2.47]	2.21 (0.08) [2.08 – 2.40]
M <sub>A</sub> ... M <sub>B</sub>		3.02 (0.19) [2.62 – 3.63]	2.93 (0.18) [2.54 – 3.49]
M <sub>A</sub> ... M <sub>C</sub>		7.41 (0.10) [7.18 – 7.63]	7.51 (0.11) [7.30 – 7.77]
M <sub>B</sub> ... Glu 50 Oε2		2.21 (0.12) [1.93 – 2.45]	2.16 (0.12) [1.92 – 2.50]
M <sub>B</sub> ... Glu 94 Oε2		2.34 (0.14) [2.12 – 2.70]	2.40 (0.10) [2.18 – 2.65]
M <sub>B</sub> ... Glu 130 Oε1		2.87 (0.16) [2.47 – 3.14]	2.81 (0.20) [2.41 – 3.21]
M <sub>B</sub> ... M <sub>C</sub>		6.29 (0.20) [5.81 – 6.77]	6.25 (0.15) [5.93 – 6.55]
M <sub>C</sub> ... Glu 49 Oε1		2.11 (0.08) [1.92 – 2.36]	2.29 (0.11) [2.13 – 2.56]
M <sub>C</sub> ... Glu 126 Oε1		2.06 (0.09) [1.87 – 2.26]	2.31 (0.16) [1.84 – 2.53]
M <sub>C</sub> ... Glu 129 Oε1		2.31 (0.10) [2.12 – 2.58]	2.02 (0.10) [1.81 – 2.26]
M <sub>C</sub> ... Glu 130 Oε2		1.89 (0.08) [1.72 – 2.04]	1.89 (0.09) [1.66 – 2.07]

<sup>a</sup> M stands for metal (Fe in as-isolated and in Fe-soak; Zn or Fe in Zn-soak)

<sup>b</sup> For each column, the numbers listed are the mean value, calculated from the 36 independent distances in the asymmetric unit, followed by the corresponding standard deviation in *parentheses*, and finally the minimum and maximum values in the population, enclosed in square brackets.

structure results from iron initially present in site A, displaced to site C by the Zn soak. This is an interesting new result, since the previous Zn-soaked and Fe-soaked structures reported for AfFtn <sup>2</sup> and EcFtnA <sup>1</sup> were obtained from apoferritin crystals.

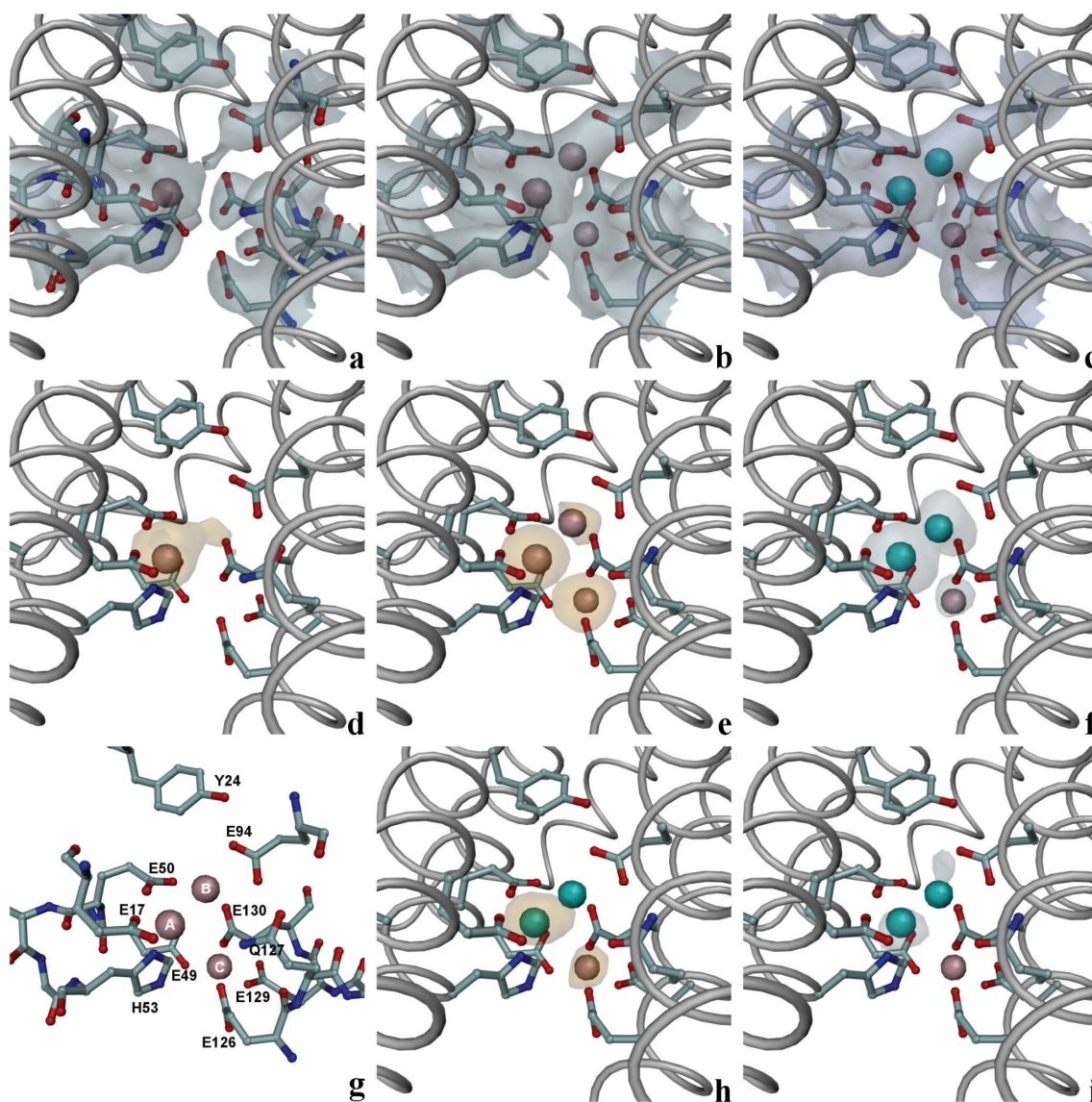


**Figure 4.7.** Details of the FC of a selected monomer in the structures of as-isolated, Fe-loaded, Fe-soaked and Zn-soaked PfFtn crystals. **a** Final  $2|F_o| - |F_c|$  electron-density map for the as-isolated PfFtn, contoured at 1.2 map RMS. **b** Final  $2|F_o| - |F_c|$  electron-density map for the Fe-soaked PfFtn, contoured at 1.2 map RMS. **c** Final  $2|F_o| - |F_c|$  electron-density map for the Zn-soaked PfFtn, contoured at 1.2 map RMS. **d** Anomalous Fourier map for the Fe-loaded PfFtn, contoured at 3.0 map RMS. **e** Anomalous Fourier map for the Fe-soaked PfFtn, contoured at 3.0 map RMS. **f** Anomalous Fourier map for the Zn-soaked PfFtn using the peak data, contoured at 3.0 map RMS. **g** Labeled view of the residues and metal sites in the Fe-soaked FC. **h** Anomalous Fourier map for the Zn-soaked PfFtn using the low-energy remote data, contoured at 3.0 map RMS. **i** Dispersive Fourier map for the Zn-soaked PfFtn, contoured at 2.8 map RMS. The anomalous electron-density maps were calculated using as amplitudes the anomalous difference coefficients obtained from each dataset, and the phases (rotated by  $90^\circ$ ) obtained from the respective final structure refinement, except for the “Fe-loaded” data, for which the phases were

ated” refinement. The Zn-dispersive Fourier map was calculated by first scaling together the peak and low-energy remote datasets with CCP4 SCALEIT<sup>16</sup> and then using as coefficients the difference  $F(\text{low-energy remote}) - F(\text{peak})$  and the phases from the final “Zn-soak” refinement. **a–c** show that the occupation of site B in the

that the occupation of site B in the as-isolated crystal is negligible; **d** shows a small residual occupancy of site B in the Fe-loaded structure and no evidence of site C occupancy; **e** shows a site B occupancy clearly lower than those of sites A and C in the Fe-soaked structure; **f**, **h** and **i** show that in the Zn-soaked structure, part of the originally present Fe in site A has been displaced to site C by the Zn ions, that site B is occupied by Zn only, and that site C is very likely occupied by Fe only. All panels were drawn with the same orientation. In all panels except **g** the bulk of Pfftn monomer is represented as a gray tube onto which the side chains (including C $\alpha$  atoms) of the FC residues have been overlaid in ball-and-stick representation (carbon atoms blue-gray, oxygen atoms red, nitrogen atoms blue, iron atoms pink and zinc atoms cyan). In **g**, only the residues near the FC are represented in ball-and-stick mode, and are labeled for easier identification of the residues mentioned in the text. The figure was prepared with DINO<sup>33</sup>

### **FC stability**

Interestingly, while mutagenesis studies have shown both sites A and B to be important for iron uptake and oxidation in ferritins<sup>41</sup>, in the crystallized proteins the occupancy of the both sites was found only in BFR from *D. desulfuricans* ATCC 27774<sup>34</sup>. The Pfftn FC followed the common trend, and as mentioned already the occupation of FC sites B and C was only observed in Fe-soaked or Zn-soaked crystals. This contradicted our EPR studies that showed a fully developed dinuclear iron FC EPR signal in the sample prior to crystallization<sup>42</sup>. In order to check the integrity of the Pfftn FC, we loaded three samples of apo Pfftn with iron and incubated them for 1 day and 2 months at 4°C in air and, mimicking the crystallization conditions, for 2 months in a 2 M ammonium sulfate solution at room temperature. The FC EPR signal from each sample was measured after titration to 130 mV, which is the potential at which the mixed-valence Pfftn EPR signal is maximum<sup>42</sup>. The amplitude of the FC signal from the sample incubated for 2 months in air was noticeably but not drastically smaller than that of the sample incubated for 1 day (Fig. 4.8). However, the FC EPR signal amplitude of the sample incubated for 2 months in a 2 M ammonium sulfate solution was fivefold smaller than that from the sample incubated for 2 months in air (Fig. 4.8). The coordination distance from Glu130 to site B (Table 4.5) is quite long (more than 2.8 Å); therefore, site B may be rather labile, which could account for its lower occupation in the Fe-soaked and Zn-soaked crystals, as well as for the easy removal of its iron atom by

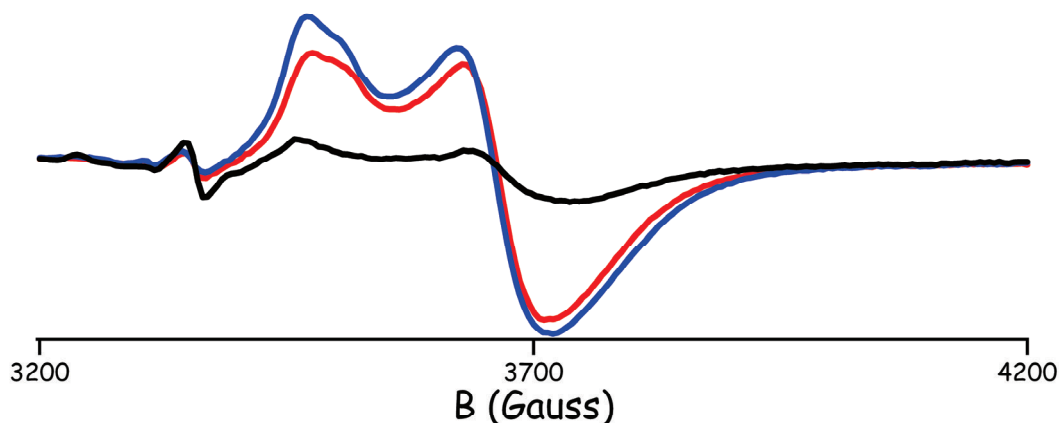


**Figure 4.8.** The Fe(III)–O–Fe(II) FC electron paramagnetic resonance (EPR) signal of 6  $\mu$ M PfFtn 24-mer, titrated to 130 mV. The decrease in the amplitude of the signal depending on incubation time and the presence of crystallization solution in the sample illustrates the stability of the center. Prior to EPR measurement, the three samples tested were incubated, respectively, for 1 day after loading with iron (blue line), for 2 months (red line) and for 2 months in the presence of a crystallization solution, 2 M ammonium sulfate (black line)

the precipitating agent ammonium sulfate during crystallization of the as-isolated ferritin.

There is an ongoing discussion in the literature on whether the FC iron sites A and B are transient in the process of iron uptake–oxidation–translocation into the protein core, or whether they form a stable cofactor<sup>41</sup>. In the current experiment, the decrease in the amplitude of the FC EPR signal in the sample incubated in air for 2 months appears to be too small to be caused by iron translocation into the protein cavity. Instead, as shown by the sample incubated for 2 months in ammonium sulfate, the most likely cause for the lack of the B iron site in the as-crystallized PfFtn is iron complexation and removal by the crystallization agent.

### **Thermostability**

The thermal stability of a protein can often be described as equilibrium between the protein's folded and unfolded state, and frequently correlates with the growth temperature of the organism. Analysis of thermostability factors is often made via comparison of the genome/protein sequences from the hyperthermophiles, thermophiles and mesophiles, or via mutagenesis. In the literature, a number of factors



have been proposed to be involved in thermostability. These include salt bridges, hydrogen bonds, van der Waals interactions, distribution of amino acids, higher  $\beta$ -strand content, more charged amino acids, fewer uncharged polar amino acids, more hydrophobic  $\beta$ -branched amino acids and others<sup>43-49</sup>. However, no single consistent set of determining factors has emerged from the different studies that have been carried out to date; therefore, it appears that protein thermal stability is the cumulative result of various factors.

Ferritins are large and highly symmetrical agglomerates of 24 single subunits. This suggests that these proteins possess forces that keep the big structure together. Horse spleen ferritin has been shown to resist inactivation by up to 10 M urea<sup>50</sup> and temperatures up to 93°C<sup>51</sup>.

PfFtn has been shown to be an extremely thermostable protein. No melting temperature could be found with differential scanning calorimetry up to 120°C and the protein could withstand incubation at 100 °C for 1 day or autoclaving at 120°C for half an hour without loss of its iron-uptake activity<sup>13</sup>. There are no data in the literature regarding the thermostability of other thermophilic and hyperthermophilic ferritins.

In our analysis of PfFtn thermostability (summarized in Table 4.6), and given that no thermostability data are available in the literature on ferritins from microorganisms other than *P. furiosus*, we assumed that it is the most thermostable ferritin among those shown in Table 4.6, and we used the optimal growth temperature of the organism as a measure of relative thermostability for the other ferritins listed in Table 4.6. However, it should be noted that the denaturation temperature of a protein may be higher than the optimal growth temperature of the organism where it is produced.

The hydrogen bonds were calculated with HBPLUS<sup>52</sup> using default parameters, and were divided into three classes: between main-chain atoms only (MM); between main-chain and side-chain atoms (MS); and between side-chain atoms only (SS). The salt bridges were determined as a subset of SS hydrogen bonds, considering interactions between side chains of negatively charged Asp/Glu residues with side

**Table 4.6.** Hydrogen bonds and salt bridges in the PfFtn 24-mer and its closest structural homologues, calculated with HBPLUS

PDB ID	Source organism <sup>a</sup>	Total H-bonds <sup>b</sup>	MM		MS		SS		Salt bridges <sup>c</sup>	
			Intra	Inter	Intra	Inter	Intra	Inter	Intra	Inter
--	<i>Pyrococcus furiosus</i> (100°C)	4630	3377	24	439	72	544	174	172	67
1vlg	<i>Thermotoga maritima</i> (80°C)	4767	3237	30	540	117	633	210	189	120
1s3q	<i>Archaeoglobus fulgidus</i> (80°C)	4457	2788	24	412	80	453	176	114	134
1krq	<i>Campylobacter jejuni</i> (42°C)	4632	3360	24	648	72	384	144	72	72
1eum	<i>Escherichia coli</i> (37°C)	4720	3320	24	836	32	412	96	60	4

*MM* hydrogen bonds between main-chain atoms only, *MS* hydrogen bonds between main-chain and side-chain atoms, *SS* hydrogen bonds between side-chain atoms only

*Intra* and *Inter* correspond to intramolecular (within the same monomer) and intermolecular (between neighboring monomers) hydrogen bonds

<sup>a</sup> optimal growth temperature in parentheses

<sup>b</sup> calculated using default program parameters

<sup>c</sup> a subset of SS H-bonds, considering interactions between side-chains of negatively charged Asp/Glu residues with side-chains of positively charged Arg/His/Lys residues.

chains of positively charged Arg/His/Lys residues. Furthermore, a distinction between intramolecular (within the same monomer) and intermolecular (between neighboring monomers) hydrogen bonds was made. The MM bonds are mostly intramolecular and are responsible for the stability of the secondary structure elements ( $\alpha$ -helices). The intramolecular MS and SS hydrogen bonds contribute to stabilize the 3D fold of the monomeric subunits. The intermolecular MS and SS hydrogen bonds are those that contribute most to the stability of the 24-mer.

A surprising result of this calculation was that the total number of hydrogen bonds in the ferritin 24-mers was quite similar. If we exclude the lowest number (4457 for AfFtn) which can possibly be attributed to

its unusual quaternary structure, PfFtn actually has the lowest total number of hydrogen bonds, two fewer than the ferritin from *Campylobacter jejuni* (CjFtn), 90 fewer than EcFtnA and 137 fewer than TmFtn. There is no clear single trend in the data listed in Table 4.6, which only emphasizes the complex nature of the structural factors governing thermostability, even within a group of closely related structures. However, a careful inspection shows some interesting features, which may have a bearing on the structural basis for the different thermostabilities of the different ferritins listed in Table 4.6. The most striking single feature in Table 4.6 is the marked increase in intramolecular salt bridges between the ferritins of mesophilic (EcFtnA and CjFtn) and hyperthermophilic (AfFtn, TmFtn and PfFtn) organisms. Indeed, a similar but less clear trend is observed for the SS hydrogen bonds overall. These structural features could explain the higher resistance to thermal inactivation in the latter. However, this trend by itself does not validate our initial assumption that PfFtn is the most thermostable ferritin in the group. A secondary trend can be perceived for the main-chain intramolecular hydrogen bonds in the hyperthermophilic organisms (AfFtn, TmFtn and PfFtn), which is greatest in PfFtn, and may offset the effect of a lower number of intramolecular salt bridges in comparison with TmFtn. Therefore, the most important factor that protects PfFtn and other ferritins from thermal denaturation appears to be the preservation of the monomer fold, rather than the 24-mer assembly.

## CONCLUSIONS

In this study, we reported the crystal structure of PfFtn. High sequence similarity between PfFtn, TmFtn and AfFtn suggests a separate group of thermostable ferritins. PfFtn is the second archaeal ferritin structure to be reported, following that of AfFtn. In spite of the high sequence identity (50%) between these two proteins, their quaternary structures are significantly different. PfFtn exhibited the 432 symmetry commonly found in other known ferritins, whereas AfFtn showed the 23

symmetry similar to dodecameric DPS proteins. The 23 symmetry of the AfFtn 24-mer resulted in four triangular pores with an approximate size of 45 Å, making large openings in the AfFtn shell. Therefore, the 23 symmetry of the AfFtn 24-mer remains an exception among ferritins, and further research is required to explain such an unusual conformation.

Three iron sites were observed in the FC of PfFtn monomer. Site A was present in the as-crystallized protein and sites B and C were observed only upon crystal soaking with either Fe or Zn ions. Combining these results with our measurements of the FC EPR signal prior to crystallization, where samples were incubated in air for 1 day and 2 months, and for 2 months in 2 M ammonium sulfate (the crystallization solution), we conclude that the lack of iron atoms at the B site is very likely due to their complexation by ammonium sulfate, and that the absence of these sites in the as-crystallized protein cannot be taken *per se* as evidence of a transient nature of the FC, in PfFtn and other ferritins.

The possible iron entry and exit routes of PfFtn, the threefold and fourfold channels, are similar to those from bacterial ferritins in the sense that the threefold channel is less hydrophilic and the fourfold channel is more polar than the channels of mammalian H and L chain ferritins.

The hyperthermostability of PfFtn was analyzed at the structural level by comparing the number of salt bridges and hydrogen bonds in PfFtn with those in AfFtn, TmFtn, CjFtn and EcFtnA. Although there are no data on the thermal stability of other thermostable ferritins, our results suggest that TmFtn, the ferritin from *T. maritima*, a bacterium which grows optimally at 80°C, is probably more thermostable than PfFtn. Owing to a high number of intramolecular hydrogen bonds between main-chain atoms, and between main-chain and side-chain atoms, the main factor contributing to the high thermostability of PfFtn as well as the other structurally similar ferritins from hyperthermophilic microorganisms appears to be the preservation of the monomer fold rather than the 24-mer structure.

**Acknowledgments** The authors are grateful to Ian Tickle (Astex Therapeutics, Cambridge, UK) for helpful suggestions and to Emile Bol (Delft University of Technology, Delft, The Netherlands) for advice on PyMOL. The authors would like to acknowledge the staff of the EMBL Grenoble Outstation, in particular Martin Walsh and Hassan Belrhali for technical assistance with the measurements at the EMBL-CRG BM 14 beamline. Financial support is acknowledged from the European Union—Research Infrastructure activity under the FP6 “Structuring the European Research Area” I3 program and from the Council for Chemical Sciences of the Netherlands Organization for Scientific Research (CW-NWO) under project no. 700.51.301.

## REFERENCES

1. Stillman, T. J., Hempstead, P. D., Artymiuk, P. J., Andrews, S. C., Hudson, A. J., Treffry, A., Guest, J. R. & Harrison, P. M. The high-resolution X-ray crystallographic structure of the ferritin (EcFtnA) of *Escherichia coli*; comparison with human H ferritin (HuHF) and the structures of the Fe(3+) and Zn(2+) derivatives. *J Mol Biol* **307**, 587-603 (2001).
2. Johnson, E., Cascio, D., Sawaya, M. R., Gingery, M. & Schröder, I. Crystal structures of a novel tetrahedral open pore ferritin from the hyperthermophilic archaeon *Archaeoglobus fulgidus*. *Structure* **13**, 637-648 (2005).
3. Stiefel, E. I. & Watt, G. D. Azotobacter cytochrome b557.5 is a bacterioferritin. *Nature* **279**, 81-83 (1979).
4. Crichton, R. R. *Inorganic biochemistry of iron metabolism: from molecular mechanisms to clinical consequences* (John Wiley & Sons, Chichester, 2001).
5. Webb, J., Macey, D. J. & Talbot, V. Identification of ferritin as a major high molecular weight zinc-binding protein in the tropical rock oyster, *Saccostrea cucullata*. *Arch Environ Contam Toxicol* **14**, 403-407 (1985).
6. Lonnerdal, B., Bryant, A., Liu, X. & Theil, E. C. Iron absorption from soybean ferritin in nonanemic women. *Am J Clin Nutr* **83**, 103-7 (2006).
7. Jacobs, A. & Worwood, M. *Iron in biochemistry and medicine, II* (Academic Press, London, 1980).
8. Powers, J. M. p53-mediated apoptosis, neuroglobin overexpression, and globin deposits in a patient with hereditary ferritinopathy. *J Neuropathol Exp Neurol* **65**, 716-21 (2006).
9. Takahashi, T. & Kuyucak, S. Functional properties of threefold and fourfold channels in ferritin deduced from electrostatic calculations. *Biophys J* **84**, 2256-63 (2003).

10. Zeth, K., Offermann, S., Essen, L. O. & Oesterhelt, D. Iron-oxo clusters biomineralizing on protein surfaces: structural analysis of *Halobacterium salinarum* DpsA in its low- and high-iron states. *Proc. Natl. Acad. Sci. USA* **101**, 13780-13785 (2004).
11. Grant, R. A., Filman, D. J., Finkel, S. E., Kolter, R. & Hogle, J. M. The crystal structure of Dps, a ferritin homolog that binds and protects DNA. *Nat Struct Biol* **5**, 294-303 (1998).
12. Ilari, A., Stefanini, S., Chiancone, E. & Tsernoglou, D. The dodecameric ferritin from *Listeria innocua* contains a novel intersubunit iron-binding site. *Nat Struct Biol* **7**, 38-43 (2000).
13. Tatur, J., Hagedoorn, P. L., Overeijnder, M. L. & Hagen, W. R. A highly thermostable ferritin from the hyperthermophilic archaeal anaerobe *Pyrococcus furiosus*. *Extremophiles* **10**, 139-148 (2006).
14. Matias, P. M., Tatur, J., Carrondo, M. A. & Hagen, W. R. Crystallization and preliminary X-ray characterization of a ferritin from the hyperthermophilic archaeon and anaerobe *Pyrococcus furiosus*. *Acta Crystallogr Sect F* **61**, 503-506 (2005).
15. Leslie, A. G. W. in *Joint CCP4 and ESF-EACMB Newsl on Protein Crystallogr* 27-33 (1992).
16. Collaborative Computational Project Number 4. The CCP4 suite: programs for protein crystallography. *Acta Crystallogr Sect D* **50**, 760-763 (1994).
17. Storoni, L. C., McCoy, A. J. & Read, R. J. Likelihood-enhanced fast rotation functions. *Acta Crystallogr Sect D* **60**, 432-438 (2004).
18. Perrakis, A., Harkiolaki, M., Wilson, K. S. & Lamzin, V. S. ARP/wARP and molecular replacement. *Acta Crystallogr Sect D* **57**, 1445-1450 (2001).
19. Cowtan, K. in *Joint CCP4 and ESF-EACBM Newsl on Protein Crystallogr* 34-38 (1994).
20. Roussel, A., Fontecilla-Camps, J. C. & Cambillau, C. XV IUCr Congress Abstracts 66-67 (Bordeaux, France, 1990).
21. Murshudov, G. N., Vagin, A. A. & Dodson, E. J. Refinement of macromolecular structures by the maximum-likelihood method. *Acta Crystallogr Sect D* **53**, 240-255 (1997).
22. Schomaker, V. & Trueblood, K. N. On the rigid-body motion of molecules in crystals. *Acta Crystallogr Sect B* **24**, 63-76 (1968).
23. Lamzin, V. S. & Wilson, K. S. Automated refinement of protein models.

- Acta Crystallogr Sect D* **49**, 129-147 (1993).
24. Brünger, A. T. Free R value: A novel statistical quantity for assessing the accuracy of crystal structures. *Nature* **355**, 472-474 (1992).
  25. Laskowski, R. A., MacArthur, M. W., Moss, D. S. & Thornton, J. M. PROCHECK - a program to check the stereochemical quality of proteins. *J Appl Crystallogr* **26**, 283-291 (1993).
  26. Ramachandran, G. N. & Sasisekharan, V. Conformation of polypeptides and proteins. *Adv Prot Chem* **23**, 283-438 (1968).
  27. Berman, H. M., Westbrook, J., Feng, Z., Gilliland, G., Bhat, T. N., Weissig, H., Shindyalov, I. N. & Bourne, P. E. The Protein Data Bank. *Nucl Acids Res* **28**, 235-242 (2000).
  28. Emsley, P. & Cowtan, K. Coot: model-building tools for molecular graphics. *Acta Crystallogr Sect D* **60**, 2126-32 (2004).
  29. Tickle, I. J., Laskowski, R. A. & Moss, D. S. Rfree and the rfree ratio. I. Derivation of expected values of cross-validation residuals used in macromolecular least-squares refinement. *Acta Crystallogr Sect D* **54**, 547-57 (1998).
  30. Kabsch, W. & Sander, C. Dictionary of protein secondary structure: pattern recognition of hydrogen-bonded and geometrical features. *Biopolymers* **22**, 2577-2637 (1983).
  31. DeLano, W. L. The PyMOL molecular graphics system. (DeLano Scientific, San Carlos, 2002). <http://pymol.sourceforge.net/>
  32. Combet, C., Blanchet, C., Geourjon, C. & Deleage, G. NPS@: Network Protein Sequence Analysis. *Trends Biochem Sci* **25**, 147-150 (2000).
  33. Philippsen, A. (2003). DINO: Visualizing Structural Biology. <http://www.dino3d.org>
  34. Macedo, S., Romao, C. V., Mitchell, E., Matias, P. M., Liu, M. Y., Xavier, A. V., LeGall, J., Teixeira, M., Lindley, P. & Carrondo, M. A. The nature of the di-iron site in the bacterioferritin from *Desulfovibrio desulfuricans*. *Nat Struct Biol* **10**, 285-290 (2003).
  35. Yu, B., Blaber, M., Gronenborn, A. M., Clore, G. M. & Caspar, D. L. Disordered water within a hydrophobic protein cavity visualized by x-ray crystallography. *Proc Natl Acad Sci U S A* **96**, 103-8 (1999).
  36. Krissinel, E. & Henrick, K. Secondary-structure matching (SSM), a new tool for fast protein structure alignment in three dimensions. *Acta Crystallogr Sect*

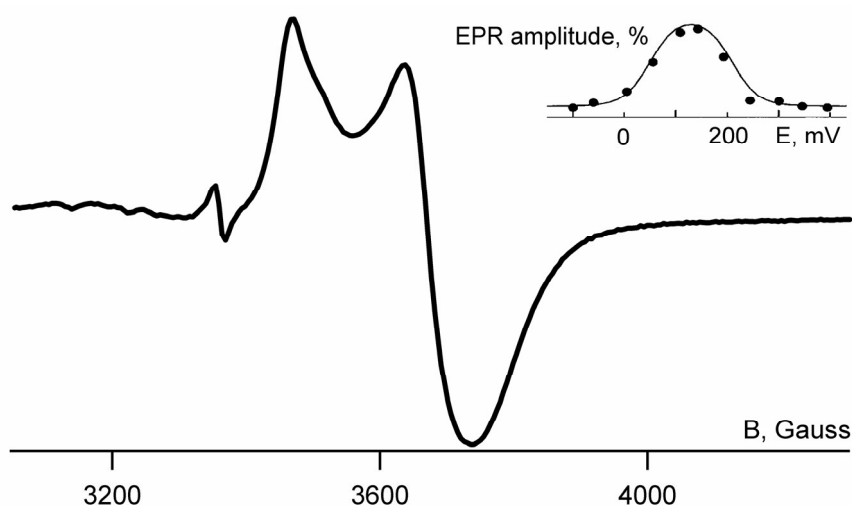
- D* **60**, 2256-2268 (2004).
37. Levi, S., Santambrogio, P., Corsi, B., Cozzi, A. & Arosio, P. Evidence that residues exposed on the three-fold channels have active roles in the mechanism of ferritin iron incorporation. *Biochem J* **317** (Pt 2), 467-73 (1996).
  38. Rice, D. W., Ford, G. C., White, J. L., Smith, J. M. A. & Harrison, P. M. in Theil, E. C., Eichhorn, G. L. & Marzilli, L. G. (eds.) *Advances in Inorganic Biochemistry* 39-50 (Elsevier, New York, 1983).
  39. Wardeska, J. G., Viglione, B. & Chasteen, N. D. Metal ion complexes of apoferritin. Evidence for initial binding in the hydrophilic channels. *J Biol Chem* **261**, 6677-6683 (1986).
  40. Lawson, D. M., Artymiuk, P. J., Yewdall, S. J., Smith, J. M., Livingstone, J. C., Treffry, A., Luzzago, A., Levi, S., Arosio, P., Cesareni, G., Thomas, C. D., Shaw, W. V. & Harrison, P. M. Solving the structure of human H ferritin by genetically engineering intermolecular crystal contacts. *Nature* **349**, 541-544 (1991).
  41. Lewin, A., Moore, G. R. & Le Brun, N. E. Formation of protein-coated iron minerals. *Dalton Trans*, 3597-3610 (2005).
  42. Tatur, J. & Hagen, W. R. The dinuclear iron-oxo ferroxidase center of *Pyrococcus furiosus* ferritin is a stable prosthetic group with unexpectedly high reduction potentials. *FEBS Lett* **579**, 4729-4732 (2005).
  43. Vogt, G. & Argos, P. Protein thermal stability: hydrogen bonds or internal packing? *Fold Des* **2**, S40-6 (1997).
  44. Kannan, N. & Vishveshwara, S. Aromatic clusters: a determinant of thermal stability of thermophilic proteins. *Protein Eng* **13**, 753-61 (2000).
  45. Eidsness, M. K., Richie, K. A., Burden, A. E., Kurtz, D. M., Jr. & Scott, R. A. Dissecting contributions to the thermostability of *Pyrococcus furiosus* rubredoxin: beta-sheet chimeras. *Biochemistry* **36**, 10406-10413 (1997).
  46. Vetriani, C., Maeder, D. L., Tolliday, N., Yip, K. S., Stillman, T. J., Britton, K. L., Rice, D. W., Klump, H. H., Robb, F. T. Protein thermostability above 100 degrees C: a key role for ionic interactions. *Proc Natl Acad Sci U S A* **95**, 12300-12305 (1998).
  47. Kumar, S., Tsai, C. J. & Nussinov, R. Factors enhancing protein thermostability. *Protein Eng* **13**, 179-191 (2000).
  48. Chakravarty, S. & Varadarajan, R. Elucidation of determinants of protein stability through genome sequence analysis. *FEBS Lett* **470**, 65-69 (2000).



49. Suhre, K. & Claverie, J. M. Genomic correlates of hyperthermostability, an update. *J Biol Chem* **278**, 17198-202 (2003).
50. Liu, X., Jin, W. & Theil, E. C. Opening protein pores with chaotropes enhances Fe reduction and chelation of Fe from the ferritin biomineral. *Proc Natl Acad Sci U S A* **100**, 3653-8 (2003).
51. Stefanini, S. Cavallo, S., Wang, C. Q., Tataseo, P., Vecchini, P., Giartosio, A. & Chiancone, E. Thermal stability of horse spleen apoferritin and human recombinant H apoferritin. *Arch Biochem Biophys* **325**, 58-64 (1996).
52. McDonald, I. K. & Thornton, J. M. Satisfying hydrogen bonding potential in proteins. *J Mol Biol* **238**, 777-93 (1994).



# CHAPTER V<sup>i</sup>. The dinuclear iron-oxo ferroxidase center of *Pyrococcus furiosus* ferritin is a stable prosthetic group with unexpectedly high reduction potentials



## ABSTRACT

Recombinant ferritin from *P. furiosus* expressed in *Escherichia coli* exhibits in EPR monitored redox titrations a mixed valence ( $\text{Fe}^{3+}$ - $\text{Fe}^{2+}$ )  $S=1/2$  signal at intermediate potentials that is a high-resolution homolog of the ferroxidase signal previously described for reconstituted horse spleen apoferritin. *P. furiosus* reconstituted apoferritin reduced to intermediate potentials exhibits the same mixed-valence signal, which integrates to close to one spin per subunit. The reduction potentials of +210 and +50 mV imply that the iron dimer is a stable prosthetic group with three redox states.

<sup>i</sup> This chapter has been published as

Tatur J, & Hagen WR. The dinuclear iron-oxo ferroxidase center of *Pyrococcus furiosus* ferritin is a stable prosthetic group with unexpectedly high reduction potentials. *FEBS Lett*, 579, 4729-4732 (2005)



## INTRODUCTION

Ferritins are small alpha-helical proteins that polymerize into 24-mers, or 12-mers, in the shape of a hollow shell of inner diameter 8 nm, or 4.5 nm. Ferritins occur ubiquitously in nature possibly in all forms of life. They are structurally subdivided into ferritins *per se*, bacterioferritins with a heme group, and so called ‘DNA protecting proteins from starved cells’, Dps’s, which form 12-mers. All ferritins have the catalytic capacity to oxidize Fe(II) ions and to form, inside their shell, a ‘ferrihydrite’ mineral core of *circa* 500 (12-mer) to 3000 (24-mer) Fe(III) ions and oxygen with approximate composition  $\text{Fe}_2\text{O}_3 \cdot 0.5\text{H}_2\text{O}$ . The core may also contain oxoanions, notably phosphate, and metal ions other than iron, notably manganese. Fe(III) from the core is re-mobilized and released by reduction. Ferritins may function *in vivo* in iron homeostasis, through storage and release, and/or in protection against oxidative stress<sup>1,2</sup>.

Mainly on the basis of crystallographic studies it is now generally accepted that all ferritins carry a dinuclear iron-oxo center in their intrasubunit ferroxidase site<sup>3-5</sup>. Furthermore, eukaryotic ferritins have been proposed to employ protein based redox groups, presumably radicals, for their action<sup>6-8</sup>.

There are several methods to study the redox chemistry of enzymes. The most common one is the thermodynamic equilibrium method of stepwise chemical reduction/oxidation in homogeneous solution in the presence of redox mediator dyes, with spectroscopic monitoring of the prosthetic groups<sup>9</sup>. Limited resolution of optical spectra and interference of colored mediators usually makes EPR spectroscopy the monitor of choice. Remarkably, although ferritins have been studied with EPR for almost four decades, EPR monitored redox titrations have never been reported. However, intermediates in core formation have been followed with EPR<sup>7</sup>, Mössbauer<sup>10,11</sup>, and XANES spectroscopy<sup>12</sup>. Also, coulometric and voltammetric studies of ferritins have been reported<sup>6,8,13-17</sup>.

Here, we explore the possibility to study redox properties of iron clusters of ferritin via equilibrium EPR redox titrations of the

*Pyrococcus furiosus* ferritin.

## MATERIALS AND METHODS

*Pyrococcus furiosus* ferritin was obtained after overexpression in *Escherichia coli* as previously described<sup>18</sup>. The ‘as isolated’ protein in 50 mM Hepes, pH 7.5, and 0.25 M NaCl contains *circa* 0.7 iron ion per subunit. This preparation was used in reductive (sodium dithionite) and oxidative (potassium ferricyanide), dye-mediated titrations following<sup>9</sup>. EPR spectroscopy was done on a Bruker ER 200 D spectrometer and spectral simulation using the *g*-strain formalism was as described in<sup>19</sup>. The apo-ferritin (< 0.04 Fe per subunit) was prepared by reductive demetallation in the presence of 2,2’-bipyridyl<sup>10</sup>. From apoprotein the mixed valence protein was prepared by aerobic incubation with Fe(II) followed by anaerobiosis, and then anaerobic addition of Fe(II) as described in<sup>20,21</sup>. Incubation time was 15 minutes in all cases. Alternatively, apoprotein was loaded for 0.5-48 hours with 48 Fe(II) under air and subsequently partially reduced with sodium dithionite in the presence of dye mediators to an intermediate potential of *circa* +130 mV.

## RESULTS

### A high-resolution S=1/2 signal from (Fe<sup>3+</sup>-Fe<sup>2+</sup>)

When *P. furiosus* ferritin as isolated is titrated with substoichiometric additions of dithionite in the presence of mediators a signal appears at intermediate redox potentials, which subsequently disappears at low potential. The signal shown in figure 5.1A has a number of properties that identify it as coming from a mixed valence dinuclear iron-oxo cluster: (i) all *g*-values are below 2; (ii) the signal is not saturable with high microwave power, up to 200 mW, down to a temperature of 9 K; (iii) the linewidth is relatively broad; (iv) the signal rapidly broadens with increasing temperature; it is broadened beyond detection above 20-25 K (not shown).

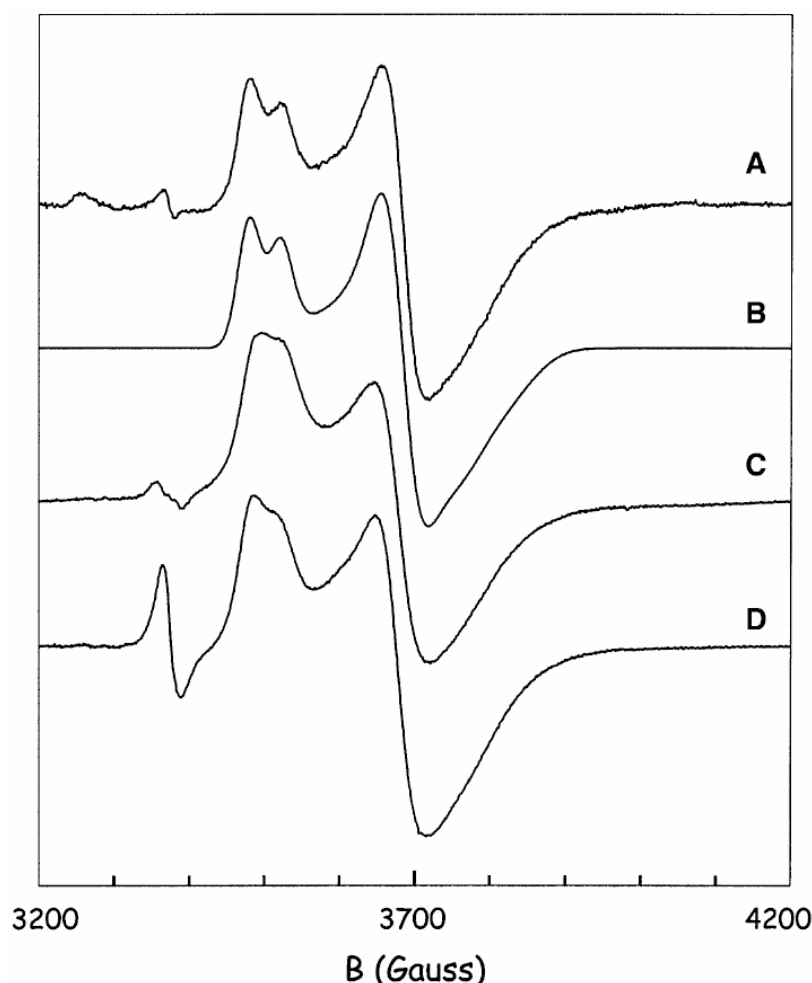


**Figure 5.1.** EPR spectrum of the  $S=1/2$  signal from the mixed-valence dinuclear iron-oxo cluster in *P. furiosus* ferritin. Trace A: ferritin ‘as isolated’ reductively titrated to +144 mV; trace B: simulation of trace A; trace C: apo-ferritin with one Fe(III) and two Fe(II) per subunit; trace D: apo-ferritin with two Fe(III) per subunit reductively titrated to +145 mV. EPR conditions: microwave frequency, 9428 MHz; microwave power, 80 mW; modulation frequency, 100 kHz; modulation power, 12.5 Gauss; temperature, 9-11 K. Simulation parameters for trace B were  $g$ -values 1.80, 1.838, 1.946 (component I) and 1.77, 1.838, 1.923 (component II); line widths in  $g$ -value units 0.020, 0.013, 0.010; the intensity ratio of component II over I was 0.7

A similar signal has been described repeatedly for horse spleen ferritin upon an aerobic/anaerobic incubation sequence with Fe(II), however, that signal has a significantly greater line width resulting in a single, asymmetrical line<sup>7,20,21</sup>. The *P. furiosus* signal does not only have a well resolved axiality (i.e.,  $g_z - g_{xy} \gg$  linewidth) but it even bears indication of extra lines suggestive of signal multiplicity and/or magnetic interaction. The signal can be reasonably accounted for by simulation (Fig. 5.1B) assuming two slightly different rhombic species of comparable intensity.

### **Three distinct ways to make the (Fe<sup>3+</sup>-Fe<sup>2+</sup>) cluster**

The first way to create the mixed-valence state is the titration of as isolated proteins just described.

The second way follows the original procedure on horse spleen ferritin to incubate apoprotein aerobically with 0.5 Fe(II)/subunit, and then incubate with 5 Fe(II)/subunit anaerobically<sup>20</sup>. We applied this procedure to *P. furiosus* apo-ferritin (<0.04 Fe/subunit) by adding different ratios of Fe(II)/subunit in the aerobic and subsequent anaerobic incubation, namely: 0.25+5, 1+2, 1+1, 2+1, 5+0.25. In all cases a mixed-valence cluster signal was found, however, the integrated EPR intensity (*circa* 0.64, 0.86, 0.04, 0.17, 0.54 spins per subunit) did not appear to bear a simple relation to the ratio of ferric/ferrous iron, perhaps suggesting a kinetic bottleneck in cluster formation via this protocol. The spectrum of highest intensity obtained with 1Fe(III)+2Fe(II) is given in figure 5.1C, and it can be seen to be virtually identical in shape to the spectrum of reductively titrated ‘as isolated’ ferritin.

As a third way to produce the mixed-valence cluster, apo-ferritin was incubated aerobically with two Fe(II) per subunit for various times of 0.5-48 hours, and each individual sample was subsequently reductively titrated in the presence of mediators to a potential of *circa* +130 mV. The resulting spectrum is in trace D of figure 5.1, and it is again virtually identical to the spectrum of titrated ‘as isolated’ ferritin. The double integral amounts to  $0.9 \pm 0.1$  S=1/2 per subunit and its intensity is within experimental error independent of the time of incubation with Fe(II) from 0.5 to 48 hours. These results suggest to ascribe the observed EPR signal to the one-electron reduced ferroxidase center in *P. furiosus* ferritin. As a further check, we carried out a two-dimensional binding experiment: ferritin was loaded aerobically with different amounts of Fe(II) and each individual sample of this binding curve was transferred to be the starting solution for a redox titration to produce samples in the mixed-valence state for monitoring by EPR spectroscopy. The overall result of 28 separate redox titrations is given in figure 5.2. This composite experiment affords considerable scatter in



the final data, however, the trend of figure 5.2 (solid line) is consistent with a stoichiometry of approximately 48 ferroxidase irons per ferritin, i.e., two Fe per subunit.

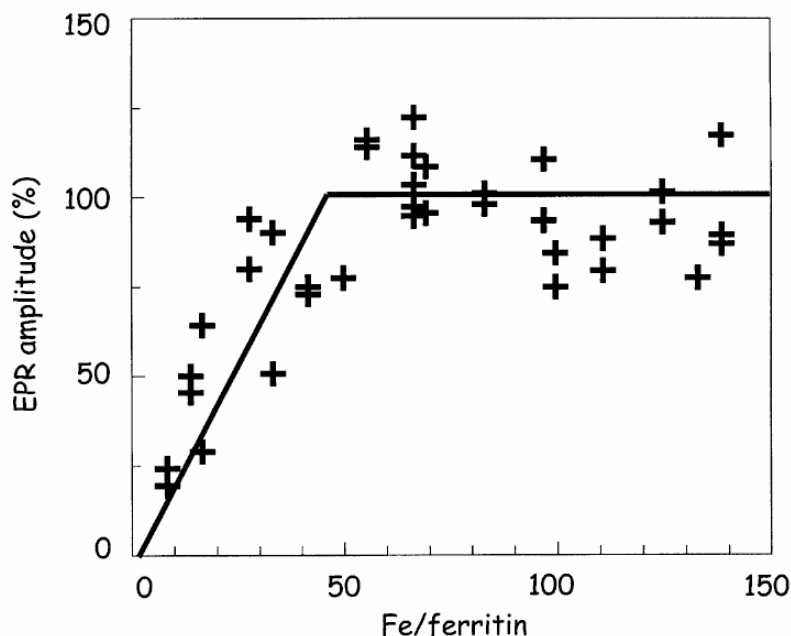


**Figure 5.2.** Derived curve for the binding of iron to the putative ferroxidase site in *P. furiosus* apo-ferritin. The protein was first aerobically incubated with varying amounts of Fe(II); subsequently, each sample was individually anaerobically titrated in the presence of mediators to a potential of *circa* +130 mV. The amplitude of the EPR signal from the mixed valence dinuclear iron center is plotted versus added iron indicating saturation at *circa* two Fe per subunit

### **A novel half-integer high-spin signal assigned to a modified (Fe<sup>3+</sup>-Fe<sup>2+</sup>) cluster**

During the equilibrium-titration of the ‘as isolated’ ferritin a second signal is observed at intermediate potentials. The field span of the signal is much wider than that of the mixed-valence S=1/2 signal. This broad signal is reminiscent of the EPR signature of the superparamagnetic core in Fe-loaded ferritins<sup>22</sup>. However, the present signal is essentially different on two counts: (i) it is observed at low temperatures and disappears at high temperatures; (ii) it is observed at intermediate potentials and disappears at high potentials. The signal has an unusual temperature dependence, which is shown in figure 5.3. At the low temperature of 6.8 K, the spectrum appears to consist of a single asymmetrical line with an effective g-value approximately 4 and a high-

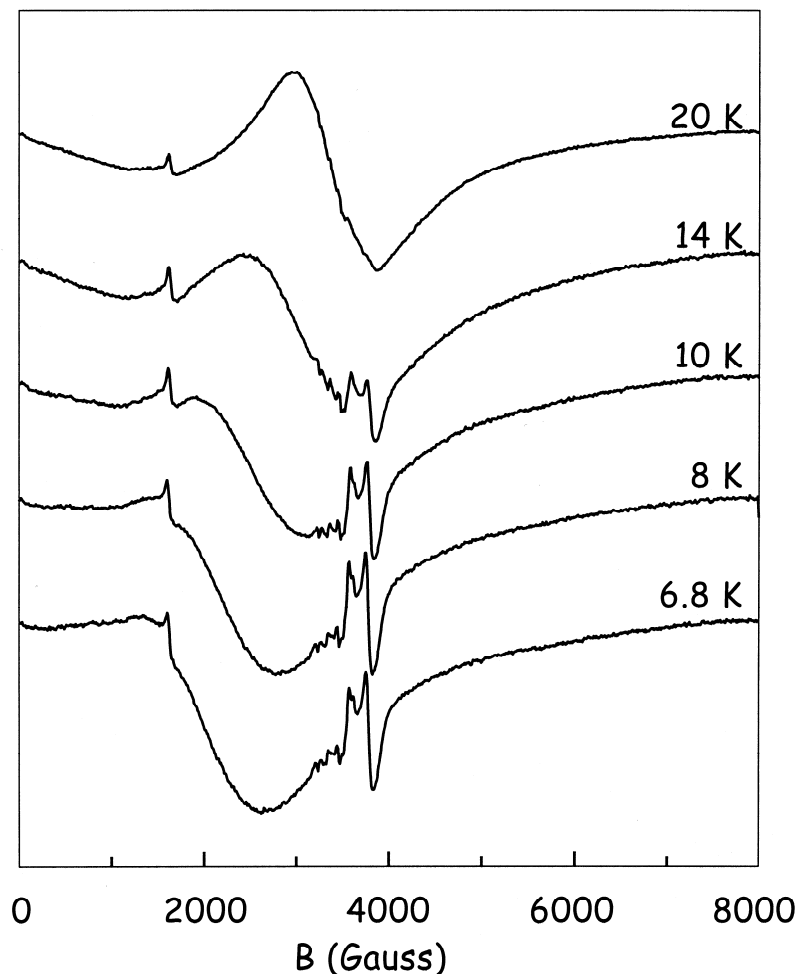


**Figure 5.3.** Temperature dependence of the broad, high-spin signal from partially reduced *P. furiosus* ferritin. EPR conditions: microwave frequency, 9642 GHz; microwave power, 80 mW; modulation frequency, 100 kHz; modulation power 12.5 Gauss, temperature, 6.8-44 K

field wing extending to *circa* 8000 Gauss. With increasing temperature the spectrum becomes less asymmetric and the effective  $g$ -value moves towards higher field to approach *circa*  $g = 2$  at 20 K. There is no intensity when the spectrometer is switched to parallel-mode, indicating that the origin of the signal is not an integer spin system. The complete set of spectra would be consistent with more than one spin system ( $S=3/2$  and  $S=1/2$ ) over a relatively limited temperature range, such as a spin ladder from a metal cluster with relatively small exchange coupling.

The broad signal could be from a different form of the ferroxidase center or it could be from a small core structure (i.e., not large enough to exhibit superparamagnetism). Against this latter interpretation argues the

following observation: when apoprotein is loaded with up to 8 Fe per subunit, either via the aerobic/anaerobic incubation method or by aerobic incubation followed by reductive titration, the broad signal is not observed. The signal is also not found after incubations of apoprotein with mixtures of iron/manganese or iron/phosphate (not shown). The signal is, therefore, putatively ascribed to a modified ( $\text{Fe}^{3+}\text{-Fe}^{2+}$ ) center resulting from ferritin biosynthesis and partial iron loading in the heterologous host *E. coli*.

### **Redox potentials from ( $\text{Fe}^{3+}\text{-Fe}^{3+}$ ) to ( $\text{Fe}^{2+}\text{-Fe}^{2+}$ )**

The ‘as isolated’ protein was titrated reductively with sodium dithionite and oxidatively with potassium ferricyanide at ambient temperature (22°C) and pH 7.5. The amplitude of the EPR signals from the putative ferroxidase mixed-valence cluster and from the broad signal are plotted versus solution potential in figure 5.4. The subsequent potentials for the one-electron reduction of ( $\text{Fe}^{3+}\text{-Fe}^{3+}$ ) to ( $\text{Fe}^{3+}\text{-Fe}^{2+}$ ) and of ( $\text{Fe}^{3+}\text{-Fe}^{2+}$ ) to ( $\text{Fe}^{2+}\text{-Fe}^{2+}$ ) are  $E_{m,7.5} = +210$  and  $+50$  mV, and are, therefore, sufficiently separated to afford almost full (92%) development of the EPR amplitude around  $+130$  mV. This observation is the basis for the experiments described above, in which individual samples are step-potential titrated to *circa*  $+130$  mV for maximal development of the mixed valence ferroxidase signal. The  $2 \times 1$  electron reduction of the center is fully reversible. Partial reoxidation of the fully reduced cluster with ferricyanide affords the mixed-valence signal, which disappears again upon further oxidation. An earlier attempt to reach the mixed-valence state with dithionite <sup>21</sup> probably failed because more than substoichiometric reductant was added.

The plot of EPR amplitude versus redox potential of the broad signal is remarkably similar to the signal presumably from the ferroxidase center. There are two reduction potentials each slightly shifted to more positive values compared to the ferroxidase signal:  $E_{m,7.5} = +240$  and  $+90$  mV. Thus, also the cluster giving rise to the broad signal has three accessible redox states in the potential range studied

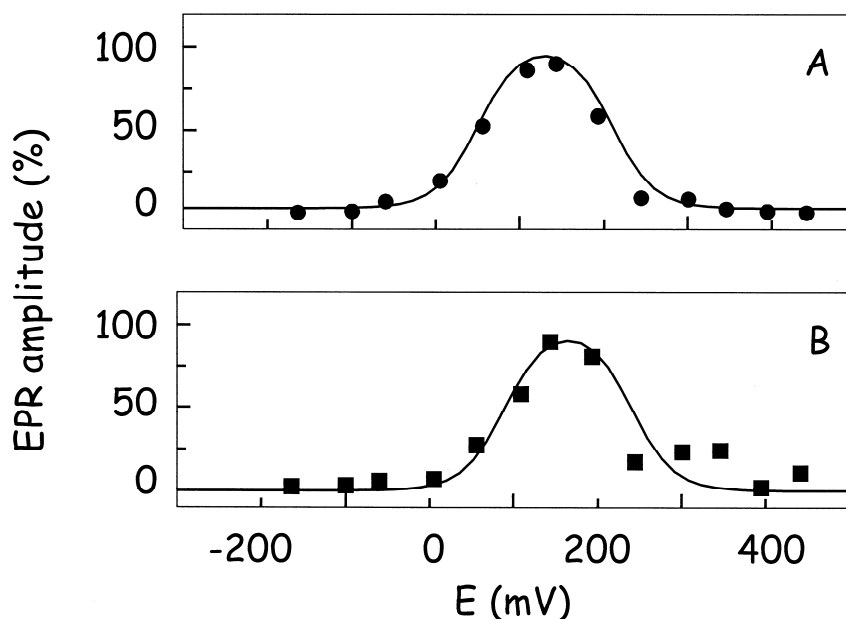


**Figure 5.4.** EPR monitored redox titration of *P. furiosus* ferritin. The ferroxidase signal (upper trace) was measured as in figure 5.1 and its amplitude ( $g_z$ -peak to  $g_{xy}$ -trough) was plotted. The broad signal (lower trace) was measured as in figure 5.3 at a temperature of 26 K

consistent with its putative assignment to a modified ferroxidase center.

## DISCUSSION

Equilibrium redox titration of proteins in homogeneous solution monitored by spectroscopy is a well established<sup>9</sup> and widely employed methodology to determine redox properties of prosthetic groups. The storage and release of iron in ferritin are redox processes that have been extensively studied over several decades, however, to our knowledge bulk redox titrations of ferritin have never been reported. A possible reason for this could be the expectation that reduction of ferritin would always result in release of iron. On the other hand, X-ray crystallographic studies have firmly established that ferritins contain metal centers that are not part of the inner core, but rather are associated with well defined coordination sites provided by the internal of the protein subunit, and it seems reasonable to expect that nature does not synthesize and break down these centers on the same time scale as the iron in the storage pool. In other words, it can be expected that the ferroxidase center is a stable structure over the time course of

enzymological experimentation. The present study suggests that the dinuclear iron-oxo center can be reduced and reoxidized on a time scale of minutes to hours without loss of integrity. To what extent this may also hold for core structures remains to be explored.

The mode of iron release from ferritin, and in particular the source of reducing equivalents, is not known. The lowest reduction potential of the ferroxidase center in *P. furiosus* ferritin is +50 mV. Under the assumption that reduction (and subsequent release) of core iron takes place through the redox-catalytic action of the ferroxidase center, this would imply that a relatively mild reductant, for example a rubredoxin, would be sufficient to wire iron release from ferritin to cell metabolism. However, this conclusion is at variance with results of earlier studies in which electrochemical reduction of iron loaded ferritins showed that core reduction occurs at much more negative potentials typically in the range of  $-0.2$  to  $-0.5$  V<sup>8,13-17</sup>. Therefore, core reduction cannot take place through the redox-catalytic action of the ferroxidase center unless the redox potential of core iron would be modified by - yet to be identified – factors such as Fe(II) complexing agents.

**Acknowledgements** This research has been financially supported by the Council for Chemical Sciences of the Netherlands Organization for Scientific Research (CW-NWO) under project number 700.51.301.

## REFERENCES

1. Chasteen, N. D. & Harrison, P. M. Mineralization in ferritin: an efficient means of iron storage. *J Struct Biol* **126**, 182-194 (1999).
2. Chiancone, E., Ceci, P., Ilari, A., Ribacchi, F. & Stefanini, S. Iron and proteins for iron storage and detoxification. *BioMetals* **17**, 197-202 (2004).
3. Stillman, T. J., Hempstead, P. D., Artymiuk, P. J., Andrews, S. C., Hudson, A. J., Treffry, A., Guest, J. R. & Harrison, P. M. The high-resolution X-ray crystallographic structure of the ferritin (EcFtnA) of *Escherichia coli*; comparison with human H ferritin (HuHF) and the structures of the Fe(3+) and Zn(2+) derivatives. *J Mol Biol* **307**, 587-603 (2001).
4. Macedo, S., Romao, C. V., Mitchell, E., Matias, P. M., Liu, M. Y., Xavier, A. V., LeGall, J., Teixeira, M., Lindley, P. & Carrondo, M. A. The nature of

- the di-iron site in the bacterioferritin from *Desulfovibrio desulfuricans*. *Nat Struct Biol* **10**, 285-290 (2003).
5. Zeth, K., Offermann, S., Essen, L. O. & Oesterhelt, D. Iron-oxo clusters biomineralizing on protein surfaces: structural analysis of *Halobacterium salinarum* DpsA in its low- and high-iron states. *Proc. Natl. Acad. Sci. USA* **101**, 13780-13785 (2004).
  6. Watt, R. K., Frankel, R. B. & Watt, G. D. Redox reactions of apo mammalian ferritin. *Biochemistry* **31**, 9673-9679 (1992).
  7. Sun, S. & Chasteen, N. D. Rapid kinetics of the EPR-active species formed during initial iron uptake in horse spleen apoferritin. *Biochemistry* **33**, 15095-15102 (1994).
  8. Johnson, J. L., Norcross, D. C., Arosio, P., Frankel, R. B. & Watt, G. D. Redox reactivity of animal apoferritins and apoheteropolymers assembled from recombinant heavy and light human chain ferritins. *Biochemistry* **38**, 4089-4096 (1999).
  9. Dutton, P. L. Redox potentiometry: determination of midpoint potentials of oxidation-reduction components of biological electron-transfer systems. *Methods in Enzymology* **54**, 411-435 (1978).
  10. Bauminger, E. R., Harrison, P. M., Hechel, D., Nowik, I. & Treffry, A. Mössbauer spectroscopic investigation of structure-function relations in ferritins. *Biochim. Biophys. Acta* **1118**, 48-58 (1991).
  11. Pereira, A. S., Tavares, P., Lloyd, S. G., Danger, D., Edmondson, D. E., Theil, E. C. & Huynh, B. H. Rapid and parallel formation of Fe<sup>3+</sup> multimers, including a trimer, during H-type subunit ferritin mineralization. *Biochemistry* **36**, 7917-7927 (1997).
  12. Joo, M. S., Tourillon, G., Sayers, D. E. & Theil, E. C. Rapid reduction of iron in horse spleen ferritin by thioglycolic acid measured by dispersive X-ray absorption spectroscopy. *Biol. Met.* **3**, 171-175 (1990).
  13. Imai, N., Umezawa, Y., Arata, Y. & Fujiwara, S. An electrochemical study of the iron storage protein ferritin. *Biochim. Biophys. Acta* **626**, 501-506 (1980).
  14. Watt, G. D., Frankel, R. B. & Papaefthymiou, G. C. Reduction of mammalian ferritin. *Proc. Natl. Acad. Sci. USA* **82**, 3640-3643 (1985).
  15. Jacobs, D. L., Watt, G. D., Frankel, R. B. & Papaefthymiou, G. C. Redox reactions associated with iron release from mammalian ferritin. *Biochemistry* **28**, 1650-1655 (1989).

16. Chasteen, N. D., Ritchie, I. M. & Webb, J. Stepped potential microcoulometry of ferritin. *Anal. Biochem.* **195**, 296-302 (1991).
17. Marken, F., Patel, D., Madden, C. E., Millward, R. C. & Fletcher, S. The direct electrochemistry of ferritin compared with the direct electrochemistry of nanoparticulate hydrous ferric oxide. *New. J. Chem.* **26**, 259-263 (2002).
18. Matias, P. M., Tatur, J., Carrondo, M. A. & Hagen, W. R. Crystallization and preliminary X-ray characterization of a ferritin from the hyperthermophilic archaeon and anaerobe *Pyrococcus furiosus*. *Acta Crystallogr Sect F* **61**, 503-506 (2005).
19. Hagen, W. R., Hearshen, D. O., Harding, L. J. & Dunham, W. R. Quantitative numerical analysis of g strain in the EPR of distributed systems and its importance for multicenter metalloproteins. *J. Magn. Reson.* **61**, 233-244 (1985).
20. Chasteen, N. D., Antanaitis, B. C. & Aisen, P. Iron deposition in apoferritin. Evidence for the formation of a mixed valence binuclear iron complex. *J. Biol. Chem.* **260**, 2926-2929 (1985).
21. Hanna, P. M., Chen, Y. & Chasteen, N. D. Initial iron oxidation in horse spleen apoferritin. Characterization of a mixed-valence iron(II)-iron(III) complex. *J Biol Chem* **266**, 886-893 (1991).
22. Weir, M. P., Peters, T. J. & Gibson, J. F. Electron spin resonance studies of splenic ferritin and haemosiderin. *Biochim. Biophys. Acta* **828**, 298-305 (1985).





## CHAPTER VI. Ferritin-like proteins of *Pyrococcus furiosus*

### ABSTRACT

*Pyrococcus furiosus* is an anaerobic and hyperthermophilic archaeon that thrives at 100°C. Ferritin is a protein that stores iron and protects the DNA from oxidative stress. Until recently ferritin has been considered as a prerequisite of aerobic organisms. The electron acceptor during the iron storage process is oxygen in case of aerobic organisms and a yet to be identified electron partner in case of anaerobic organisms. Similar to the unknown electron acceptor, the role of ferritin in anaerobic organisms is also not clear. Earlier we showed that the wild type anaerobe *P. furiosus* expresses H chain ferritin. Here we analyze the genome of *P. furiosus* and identify more putative ferritin-like proteins. The genes encoding the ferritin-like proteins of *P. furiosus* (PF1190, 93, 95, 96) are located in one DNA region and might represent a gene cluster that plays a role in oxidative stress protection and high thermal stability of *P. furiosus*. From these genes, PF1195 is likely to be BFR-A type ferritin.

Relative species of *P. furiosus*, namely *P. abyssi* and *P. horikoshii*, contain genes that are highly similar to PF1195 and PF1190 (BFR-A type) and not to the earlier characterized PfFtn (H-type), a dissimilarity that might be linked to the organisms' different habitats.



## INTRODUCTION

*P. furiosus* is a marine archaeon, anaerobe and hyperthermophile that was isolated off the shore of a volcanic island in southern Italy <sup>1</sup>. The archaeon was characterized as a strict anaerobe that lives on starch, maltose, peptone, or tryptone, plus yeast extract and excretes CO<sub>2</sub>, H<sub>2</sub>, H<sub>2</sub>S (if grown on S<sup>0</sup>) and acetate. *P. furiosus* contains ferritin. Ferritin is a protein that takes up iron in the presence of oxygen in case of aerobes and in the presence of a yet to be identified electron acceptor in case of anaerobes. Recently more physiological functions of ferritins have been suggested such as oxidative stress shield (not only via iron sequestration), binding to microtubules, defense against oxidative stress caused by irradiation, and DNA binding and protection <sup>2-7</sup>. The ferritin protein consists of 24 subunits that are arranged in the form of a hollow sphere in 432 symmetry. There are several types of ferritins such as heme and non-heme ferritins as well as ferritins with or without the catalytic center – the so called ferroxidase center. The non-heme ferritins are divided into H, L, and M types whose chains can be hetero or homo arranged. Thus, the non-heme ferritin structure can vary from H<sub>24</sub>L<sub>0</sub> to H<sub>0</sub>L<sub>24</sub>. The H ferritins comprise ferroxidase centers (FC), i.e. the diiron centers where Fe(II) oxidizes to Fe(III) during the iron uptake reaction. There is one FC site per each H-chain subunit. Although the L ferritins, that lack the FC sites, also take up and store iron, their kinetics is slower than that of H ferritins. The heme ferritins, also called BFR proteins (or bacterioferritins, because they have initially been isolated from bacteria), contain heme groups harbored between every two adjacent subunits. BFR proteins are of H type, e.g. they possess the FC sites. Additionally, BFR-A and BFR-B are ferritins that possess one or the other group of ligands - heme or FC site ligands. Ferritins can store up to 3000 irons in the inner cavity of their spherical protein coat.

The DPS proteins (DPS stands for DNA protection during starvation) are spherical proteins that consist of 12 subunits, which are arranged in 23 symmetry. The DPS-like protein (DPSL) is another recently discovered group of the ferritin family of proteins. The metal

centers of DPSL protein from *S. solfataricus* are located within the subunit as in ferritins, while those of DPS proteins are at the inter-subunits interface. Similar to ferritins, the role of DPS proteins is iron storage, removal of oxidative species, and DNA protection.

*P. furiosus* expresses ferritin (PfFtn), a fact that does not seem obvious for an anaerobe at first sight. Moreover, it expresses the DPSL protein too <sup>8</sup> and the expression of this protein has been shown to be upregulated as a result of gamma irradiation <sup>9</sup>. In the present work, we identify another group of hypothetical ferritin-like proteins in *P. furiosus*. This result supports the hypothesis of multiple physiological functions of ferritin-like proteins in the organisms, and in case of hyperthermophiles seems to be an integrated system that affords thermal stability and prevents DNA damage.

## DISCUSSION

*P. furiosus* contains ferritin (PfFtn), (ordered locus name PF0742, Swiss-Prot <sup>10,11</sup> accession number Q8U2T8). It has been heterologously overproduced and characterized as described in chapters II to V <sup>12-14</sup>. PfFtn is a homo 24-mer ferritin consisting of H-type subunits. Interestingly, *P. abyssi* and *P. horikoshii*, relative species of *P. furiosus*, do not contain a gene similar to the one encoding PfFtn. They contain other genes, whose sequences are similar to BFR-A, and are highly similar (55-59 % identity) to genes PF1195 and PF1190 from *P. furiosus* (PAB0624 / PH1057 and PAB1750 / PH0568, respectively), whose expression products have yet to be studied. The reason why *P. abyssi* and *P. horikoshii* do not contain an H-type ferritin similar to PfFtn, but do seem to possess BFR like proteins, is not clear but could be associated with the region of inhabitation of the species. Contrary to *P. abyssi* and *P. horikoshii* that settle at 2 and 1.4 km below sea level <sup>15,16</sup>, *P. furiosus* is a resident of shallow marine grounds and might be exposed to oxygen more readily than its counterparts from the deep sea floor, therefore, requiring a system for faster iron kinetics, such as H-type ferritin. H chain ferritin (and not L chain) has also been shown to protect

lens epithelial cells from oxidation caused by UVB irradiation<sup>5</sup>.

While PF1195 and PF1190 situate close to each other in the *P. furiosus* genome, the similar genes in *P. abyssi* and *P. horikoshii* genomes are distantly located. It has been proposed that differences among *P. furiosus*, *P. abyssi* and *P. horikoshii* species, such as genomic deletions, insertions, displacements and rearrangements<sup>17</sup>, that have occurred since the divergence of these species, could be associated with the hyperthermal environment of the species and high rate of DNA break/repair<sup>9,18</sup>.

The other gene, PF1196 is located next to PF1195 in the *P. furiosus* genome<sup>i</sup>. Genes PF1190, PF1195 and PF1196 are similar in the sense that their protein products are predicted to possess BFR-like ferroxidase center ligands and to have similar secondary helical structure. Figure 6.1 shows alignment of the amino acid sequences of these proteins with BFR and FtnA from *E. coli*. White residues highlighted in red are the conserved amino acids. All of them except Leu 10 are the ligands of the ferroxidase center in BFR from *E. coli*. The last amino acid motif ExxH coordinating the ferroxidase centers in BFRs is changed into QxxE as in bacterial H chain ferritins and is highlighted in orange in the figure 6.1.

Running Blast programs on EBI<sup>19</sup>, ExPASy<sup>10,11</sup> and TIGR<sup>20</sup> bioinformatics servers results in annotations of PF1195, PF1196 and PF1190 as hypothetical, rubrerythrin or rubrerythrin-related proteins. Additionally to these common annotation, BLAST against PF1196 results in a few ferritins and BFRs annotations, and against PF1190 in DNA break repair and chromosome segregation proteins. BLAST against PF1195 returns nearly 20 hits of bacterioferritins, mostly at TIGR web service (Table 6.1). We expect that PF1195 is a BFR-A type ferritin and represents at least one more ferritin protein of *P. furiosus* besides the already discovered PfFtn (PF0742)<sup>12</sup>. Gene PF1192 could not be aligned with PF1190, PF1195 and PF1196.

However, because BLAST against this protein returns annotations

---

<sup>i</sup> Accession numbers are in the legend to figure 6.1

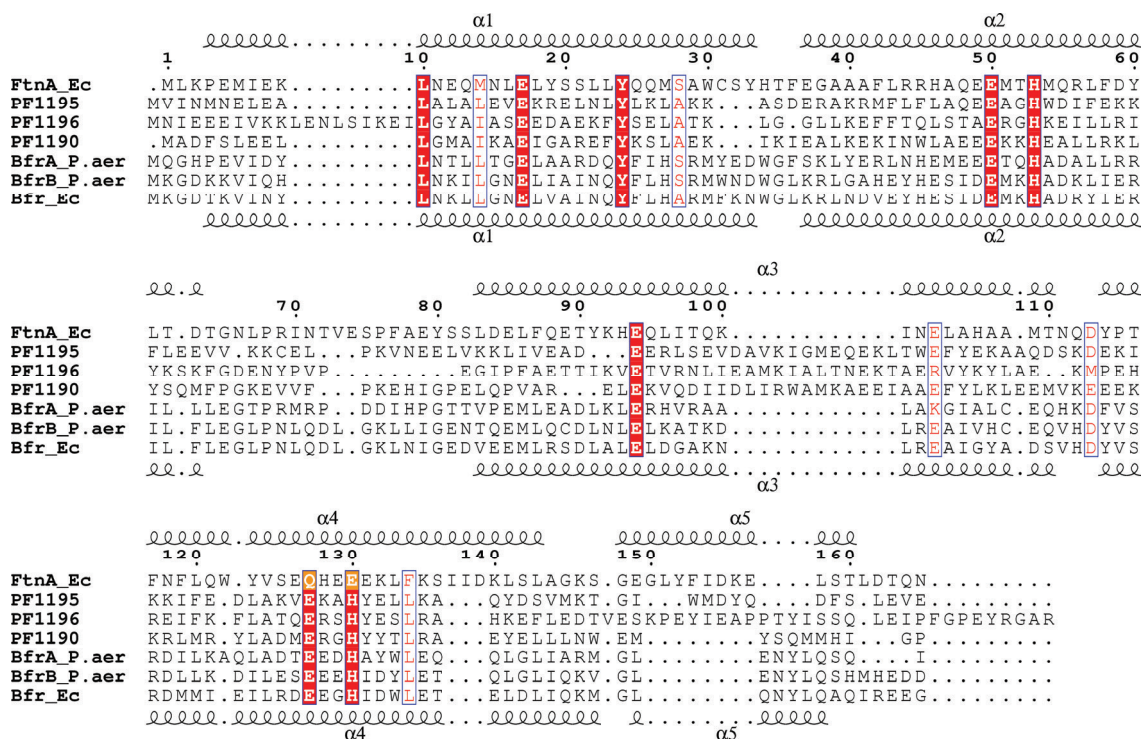


**Figure 6.1.** Alignment of the amino acids sequences of *P. furiosus* proteins PF1195 (GenBank ID: NP\_578924.1), PF1196 (GenBank ID: NP\_578925.1) and PF1190 (GenBank ID: NP\_578919.1), *P. aeruginosa* BFR A (Swiss-Prot<sup>10,11</sup> ID Q9HWF9) and BFR B (Swiss-Prot<sup>10,11</sup> Q9HY79) proteins, and *E. coli* BFR (Swiss-Prot<sup>10,11</sup> P0ABD3) and FtnA proteins (Swiss-Prot<sup>10,11</sup> P0A998). Amino acids at the positions 17, 24, 50, 53, 94, 127 and 130 on this figure are ligands of the ferroxidase center in BFRs and bacterial H chain ferritins. Alignment has been prepared with T-coffee<sup>21,22</sup> and ESPript<sup>23</sup>

such as rubrerythrin/related, ferritin and DPS, and BFR protein, and because the protein has a four helical structure similar to that of ferritins, we believe that PF1192 also belongs to the ferritin family of proteins. BLAST against PF1194 returns the majority of hits as ferric uptake regulator (FUR) protein, an enzyme that positively regulates ferritin and superoxide dismutase<sup>24</sup>. Genes encoding PF1190, PF1192, PF1194, PF1195, and PF1196 are located close to PF1193, which is a DPS-like protein of *P. furiosus*<sup>8,25</sup> and together they form a cluster of putative ferritin-like/DNA-binding-protecting helical proteins (yellow arrows in the figure 6.2). The need for such a system that provides efficient DNA protection is logical in the case of hyperthermophiles that thrive under extreme conditions<sup>3</sup>.



**Figure 6.2.** Genes region view. Yellow blocks represent genes encoding ferritin family proteins. The blue block stands for a hypothetical protein. PF1193 and PF1197 have already been identified as a DPSL protein<sup>8</sup> and NAD(P)H:Rubredoxin oxidoreductase<sup>26</sup>, respectively. PF1194 and PF1195 are highly probably FUR and BFR-A ferritin, correspondingly

**Table 6.1.** Most frequent annotations of genes PF1190-PF1197 obtained with BLAST program

<i>PF1190 – rubrerythrin/related protein, DNA break repair, chromosome segregation protein</i>
<i>PF1191 - chromosome assembly protein, bacteriocin, protease, signal transduction</i>
<i>PF1192 – rubrerythrin/related, ferritin and DPS, BFR, methyltransferase</i>
<i>PF1193 – DPSL protein<sup>8</sup></i>
<i>PF1194 - ferric uptake regulator protein (FUR), highly conserved</i>
<i>PF1195 – BFR type ferritin, highly conserved</i>
<i>PF1196 - rubrerythrin/related, ferritin, BFR</i>
<i>PF1197 – NAD(P)H:Rubredoxin oxidoreductase<sup>26,27</sup></i>

The fact that *P. furiosus* possess a number of genes encoding ferritin-like proteins also supports hypotheses of additional physiological reactions of ferritins besides metal uptake. These include nutritional and oxidative stress protection of organisms, binding and protection of DNA from UV or X-ray irradiation, also inside of nuclei<sup>5,28</sup>, binding to microtubules<sup>7</sup>, and chaperone activity<sup>2,29</sup>. These various functions of ferritin can be expected from structural similarities and/or cooperative action of this globular protein with an SMC (structural maintenance of chromosome) protein, frataxin<sup>30</sup>, artemin<sup>2</sup>, microtubule binding protein, DNA binding proteins<sup>28</sup>, and DNA break repair proteins.

## REFERENCES

1. Fiala, G. & Stetter, K. O. *Pyrococcus furiosus* sp. nov. represents a novel genus of marine heterotrophic archaeobacteria growing optimally at 100°C. *Arch microbiol* 145, 56-61 (1986).
2. Chen, T., Villeneuve, T. S., Garant, K. A., Amons, R. & MacRae, T. H. Functional characterization of artemin, a ferritin homolog synthesized in *Artemia* embryos during encystment and diapause. *Febs J* 274, 1093-101 (2007).
3. Peak, M. J., Robb, F. T. & Peak, J. G. Extreme resistance to thermally induced DNA backbone breaks in the hyperthermophilic archaeon *Pyrococcus furiosus*. *J Bacteriol* 177, 6316-8 (1995).
4. Smith, J. L. The physiological role of ferritin-like compounds in bacteria. *Crit Rev Microbiol* 30, 173-185 (2004).
5. Goralska, M., Holley, B. L. & McGahan, M. C. Overexpression of H- and L-ferritin subunits in lens epithelial cells: Fe metabolism and cellular response to UVB irradiation. *Investigative Ophthalmology and Visual Science* 42, 1721-1727 (2001).
6. Hasan, M. R., Morishima, D., Tomita, K., Katsuki, M. & Kotani, S. Identification of a 250 kDa putative microtubule-associated protein as bovine ferritin. Evidence for a ferritin-microtubule interaction. *Febs J* 272, 822-31 (2005).
7. Hasan, M. R., Koikawa, S., Kotani, S., Miyamoto, S. & Nakagawa, H. Ferritin forms dynamic oligomers to associate with microtubules in vivo: implication for the role of microtubules in iron metabolism. *Exp Cell Res* 312, 1950-60 (2006).
8. Ramsay, B., Wiedenheft, B., Allen, M., Gauss, G. H., Lawrence, C. M., Young, M. & Douglas, T. Dps-like protein from the hyperthermophilic archaeon *Pyrococcus furiosus*. *J Inorg Biochem* 100, 1061-8 (2006).
9. Williams, E., Lowe, T. M., Savas, J. & Diruggiero, J. Microarray analysis of the hyperthermophilic archaeon *Pyrococcus furiosus* exposed to gamma irradiation. *Extremophiles* 11, 19-29 (2007).
10. Boeckmann, B., Bairoch, A., Apweiler, R., Blatter, M. C., Estreicher, A., Gasteiger, E., Martin, M. J., Michoud, K., O'Donovan, C., Phan, I., Pilbout, S. & Schneider, M. The SWISS-PROT protein knowledgebase and its supplement TrEMBL in 2003. *Nucleic Acids Res* 31, 365-70 (2003).



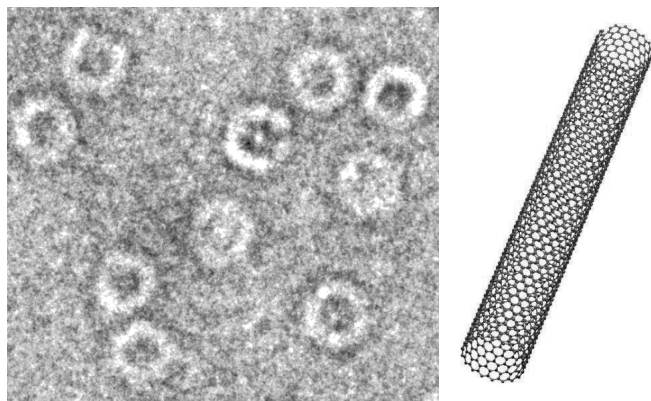
11. Gasteiger, E., Gattiker, A., Hoogland, C., Ivanyi, I., Appel, R. D. & Bairoch, A. ExPASy: The proteomics server for in-depth protein knowledge and analysis. *Nucleic Acids Res* 31, 3784-8 (2003).
12. Tatur, J., Hagedoorn, P. L., Overeijnder, M. L. & Hagen, W. R. A highly thermostable ferritin from the hyperthermophilic archaeal anaerobe *Pyrococcus furiosus*. *Extremophiles* 10, 139-148 (2006).
13. Tatur, J. & Hagen, W. R. The dinuclear iron-oxo ferroxidase center of *Pyrococcus furiosus* ferritin is a stable prosthetic group with unexpectedly high reduction potentials. *FEBS Lett* 579, 4729-4732 (2005).
14. Tatur, J., Hagen, W. R. & Matias, P. M. Crystal structure of the ferritin from the hyperthermophilic archaeal anaerobe *Pyrococcus furiosus*. *J Biol Inorg Chem* 12, 615-630 (2007).
15. Gonzalez, J. M., Masuchi, Y., Robb, F. T., Ammerman, J. W., Maeder, D. L., Yanagibayashi, M., Tamaoka, J. & Kato, C. *Pyrococcus horikoshii* sp. nov., a hyperthermophilic archaeon isolated from a hydrothermal vent at the Okinawa Trough. *Extremophiles* 2, 123-130 (1998).
16. Erauso, G., Reysenbach, A.-L., Godfroy, A., Meunier, J.-R., Crump, B., Partensky, F., Baross, J. A., Marteinson, V., Barbier, G., Pace, N. R. & Prieur, D. *Pyrococcus abyssi* sp. nov., a new hyperthermophilic archaeon isolated from a deep-sea hydrothermal vent. *Arch Microbiol* 160, 338-349 (1993).
17. Zivanovic, Y., Lopez, P., Philippe, H. & Forterre, P. *Pyrococcus* genome comparison evidences chromosome shuffling-driven evolution. *Nucleic Acids Res* 30, 1902-10 (2002).
18. Maeder, D. L., Weiss, R. B., Dunn, D. M., Cherry, J. L., Gonzalez, J. M., DiRuggiero, J. & Robb, F. T. Divergence of the hyperthermophilic archaea *Pyrococcus furiosus* and *P. horikoshii* inferred from complete genomic sequences. *Genetics* 152, 1299-1305 (1999).
19. European Bioinformatics Institute (EBI). <http://www.ebi.ac.uk>
20. The Institute for Genomic Research (TIGR). <http://www.tigr.org>
21. Poirot, O., O'Toole, E. & Notredame, C. Tcoffee@igs: A web server for computing, evaluating and combining multiple sequence alignments. *Nucleic Acids Res* 31, 3503-6 (2003).
22. Notredame, C., Higgins, D. G. & Heringa, J. T-Coffee: A novel method for fast and accurate multiple sequence alignment. *J Mol Biol* 302, 205-17 (2000).

23. Gouet, P., Courcelle, E., Stuart, D. I. & Metoz, F. ESPript: analysis of multiple sequence alignments in PostScript. *Bioinformatics* 15, 305-8 (1999).
24. Masse, E. & Gottesman, S. A small RNA regulates the expression of genes involved in iron metabolism in *Escherichia coli*. *Proc Natl Acad Sci U S A* 99, 4620-5 (2002).
25. Wiedenheft, B., Mosolf, J., Willits, D., Yeager, M., Dryden, K. A., Young, M. & Douglas, T. An archaeal antioxidant: characterization of a Dps-like protein from *Sulfolobus solfataricus*. *Proc Natl Acad Sci U S A* 102, 10551-6 (2005).
26. Ma, K. & Adams, M. W. A hyperactive NAD(P)H:Rubredoxin oxidoreductase from the hyperthermophilic archaeon *Pyrococcus furiosus*. *J Bacteriol* 181, 5530-3 (1999).
27. Grunden, A. M., Jenney, F. E., Jr., Ma, K., Ji, M., Weinberg, M. V. & Adams, M. W. In vitro reconstitution of an NADPH-dependent superoxide reduction pathway from *Pyrococcus furiosus*. *Appl Environ Microbiol* 71, 1522-30 (2005).
28. Surguladze, N., Thompson, K. M., Beard, J. L., Connor, J. R. & Fried, M. G. Interactions and reactions of ferritin with DNA. *J Biol Chem* 279, 14694-702 (2004).
29. Chen, T., Amons, R., Clegg, J. S., Warner, A. H. & MacRae, T. H. Molecular characterization of artemin and ferritin from *Artemia franciscana*. *Eur J Biochem* 270, 137-45 (2003).
30. Bencze, K. Z., Kondapalli, K. C., Cook, J. D., McMahon, S., Millan-Pacheco, C., Pastor, N. & Stemmler, T. L. The structure and function of frataxin. *Crit Rev Biochem Mol Biol* 41, 269-91 (2006).





# CHAPTER VII<sup>i</sup>. Production of nanotubes in technologically substantial amounts using ferritin



## ABSTRACT

Nanotubes offer attractive possibilities for industrial applications. However, acquiring industrially relevant amounts of nanotubes is limited by technological and financial difficulties in the production of nanoparticles, the nucleation seeds for nanotube growth. Use of the iron storage protein ferritin affords a straightforward technique for the production of nanoparticles with the Chemical Vapor Deposition (CVD) method, but the nanotubes yield is low. Here, we show that the yield of the ferritin-derived nanotubes can be increased dramatically from what has been achieved so far in CVD. This new method is realized by first emptying the protein cage and subsequent iron loading into the ferritin molecule. The reason for previous low yields of nanotubes is probably a heterogeneous structure of the mineral core of natural ferritins containing phosphate and possibly other oxoanions and metals. We also recommend a new ferritin that has been recombinantly overproduced in *E. coli* to an extremely high yield of 25 % of the total cell protein as an easily available material for a large nanoparticle fabrication.

---

<sup>i</sup> This chapter is the result of the collaborative work with C. Meyer, A. Chepelienskii, and C. Dekker from Molecular Biophysics group, Kavli Institute of NanoSciences, Delft University of Technology, The Netherlands.



## INTRODUCTION

Carbon nanotubes are hollow cylinders composed of carbon atoms (Fig. 7.1). The unique combination of the properties of carbon nanotubes such as their small size, hollow fiber-like shape, stiffness, semiconductivity or metallic characteristics make them an attractive material for industrial applications. They have been shown to be usable as reinforcement or cross linking material, field-effect transistors, electron wires, single molecule channels, nanoprobes, biosensors and carriers in gene delivery<sup>1-3</sup>.

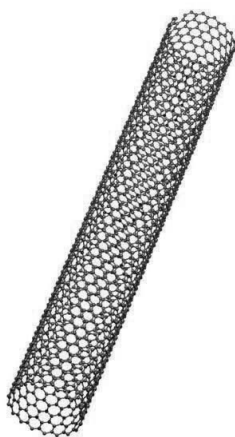


**Figure 7.1.** Model of a carbon nanotube

<http://www.ewels.info/img/science/nanotubes/tube.angled.jpg>

Currently, nanotubes can be produced via chemical vapor deposition, arc discharge or laser ablation methods. Laser ablation of graphite produces single wall carbon nanotubes, however, the synthesis does not result in pure nanotubes and purification is required. Arc discharge was the first method to be used for production of nanotubes. It is financially more favorable than laser ablation, but more expensive than chemical vapor deposition. Furthermore, it does not result in a high production yield of the nanotubes.

In chemical vapor deposition (CVD) the nanotubes are produced using a substrate, e.g. Al or Ni nanoparticle, that is heated to 900°C and flashed with carbon containing gas (such as acetylene or methane) and a process gas (such as nitrogen, hydrogen or ammonia). In this process, the growth of nanotubes starts at, and extends from the nanoparticle.

Advantages of this method are that it is the least expensive from the three, the tubes can be grown directly on the support, without the need for collection chamber as in other two methods, and the direction of the nanotube growth on the chip can be controlled, e.g. perpendicular or along the support. Disadvantages of the method are a need for nanoparticles and the low uniformity of the nanotube wall.

Ferritin is a hollow spherical protein whose natural function is the storage of iron in its cavity in the form of a mineral core or in other words, a nanoparticle. The inner and outer diameter of the ferritin shell is 8 and 12 nm, respectively. Ferritin-derived nanoparticles have been used for nanotubes production<sup>4</sup>. The carbon nanotubes from ferritin derived iron cores had a higher degree of uniformity than nanotubes from industrially fabricated nanoparticles. However, the yield of such nanotubes was low.

The iron storage capacity of ferritin has been estimated to be 4500 iron per ferritin molecule<sup>5</sup>. This is calculated assuming the inner protein cavity to be 8 nm in diameter and the structure of the iron mineral core to be ferrihydrite. In practice a maximum of 3000 iron atoms can be taken up by bacterial ferritins and even less by mammalian ferritin<sup>6,7</sup>. This indicates that the ferritin's mineral core is a heterogeneous structure and its exact composition is not fully understood. Here we show that the heterogeneous structure of the mineral core, caused by phosphate, a natural substrate of ferritin, influences the nanotubes yield. A dramatic increase in carbon nanotubes was observed for in-house prepared apo ferritin comparing to a commercial apo ferritin sample by thorough removal of impurities and loading of iron in phosphate free conditions.

## **EXPERIMENTAL PROCEDURES**

### **Ferritin samples**

Horse spleen ferritin and horse spleen apo ferritin were purchased from Sigma. *P. furiosus* ferritin was recombinantly overproduced and purified as previously described<sup>8</sup>. All dilutions of protein samples were performed in Hepes buffer, 50 mM, pH 7.5 unless indicated otherwise.



- sample 1 - commercial apo horse spleen ferritin that in house was loaded with 2000 iron in Hepes buffer
- sample 2 –commercial apo horse spleen ferritin that in house was additionally treated to remove remaining iron and other possible impurities and then was loaded with 2000 iron in Hepes buffer
- sample 3 - commercial horse spleen ferritin
- sample 4 - same as sample 2 except that iron loading was performed in the presence of phosphate buffer, 50 mM, pH 7.5.

### **Apo ferritin preparation**

This procedure was applied to commercial apo horse spleen ferritin sample 1 for preparation of sample 2 and 4. In order to produce a homogeneous iron nanoparticle we removed the ferritin inner core, i.e. we prepared the apo ferritin, and then loaded the ferritin sample with iron only. The process begins by reducing the sample with sodium dithionite,  $\text{Na}_2\text{S}_2\text{O}_4$ : ferritin (up to 0.5  $\mu\text{mole}$  ferritin 24-mer) was washed over a YM-100 membrane in a 50 ml Amicon cell with anaerobic 50 mM sodium dithionite solution (200 ml) in 50 mM Hepes, pH 7.5. The resulting concentrate was collected anaerobically into a glass bottle sealed with a butyl-rubber stopper and an equal amount of a fresh sodium dithionite solution was added. After overnight incubation an anaerobic 10% (w/v) 2,2'-bipyridyl solution in ethanol was added to the sample to reach a final concentration of bipyridyl of 0.5% in order to complex the remaining Fe(II). The resulting 10 ml mix was extensively dialyzed against the 50 mM Hepes, pH 7.5 buffer in 12 ml dialysis Slide-A-Lyser cassettes (Pierce) and concentrated in an Amicon cell over YM-100.

### **Iron loading**

Iron loading of apo ferritin samples (1) and (2) was performed as follows. A water solution containing 0.1% HCl (v/v) that stabilizes the

Fe(II) against auto-oxidation was made anaerobic by flushing with argon. An appropriate amount of this solution was added anaerobically into a glass bottle sealed with a butyl-rubber stopper and containing solid iron sulfate salt in the amount necessary for the preparation of 10 mM iron sulfate solution. Iron sulfate solution was then added to the apo ferritin samples on air to obtain 2000 Fe/Ftn ratio.

### **Protein determination**

Protein concentration was determined with BCA reagent (<http://www.piercenet.com/>) according to the instructions of the manufacturer.

### **Nanotubes production**

Nanotubes were produced by the CVD method according to a procedure worked out in the Molecular Biophysics group, Kavli institute of Nanosciences, TU Delft.

100  $\mu$ l sample of 0.1 mg/ml iron-loaded ferritin was placed on SiO<sub>2</sub> chip of *circa* 1 cm<sup>2</sup>. After 3 minutes the chip was rinsed with MilliQ and blow-dried with N<sub>2</sub> gas.

Subsequently, the chip was transformed into an oxygen plasma oven for 3 minutes at 60 mTorr for burning the protein coat away and leaving the metal mineral core of the ferritin on the chip.

The sample was then placed in the quartz tube of the CVD furnace and the system was heated to 850°C under Ar (0.5 L/min) atmosphere. When the heating up was completed, a 10 minutes growth step was performed under an atmosphere of CH<sub>4</sub> (2 L/min), C<sub>2</sub>H<sub>4</sub> (0.04 L/min) and H<sub>2</sub> (0.7 L/min). After cooling to 400°C under Ar atmosphere the samples are ready for analysis.

### **Iron determination**

Iron was determined as described in <sup>8</sup> based on <sup>9,10</sup> using ferrene as iron chelator and the extinction coefficient of the iron-ferrene complex of 35500 M<sup>-1</sup>cm<sup>-1</sup> at 593 nm.

## RESULTS AND DISCUSSION

Commercial ferritin or commercial apo ferritin loaded with a desired amount of iron are the samples that are normally used for nanotubes production with CVD. However, the nanotubes yield from both samples is very low and unsatisfactory for industrial applications.

In order to understand the reason for this low production yield, we performed nanotubes growth from three ferritin samples:

- sample 1 - commercial apo horse spleen ferritin that in house was loaded with 2000 iron in Hepes buffer
- sample 2 - commercial apo horse spleen ferritin that in house was additionally treated to remove remaining iron and other possible impurities and then was loaded with 2000 iron in Hepes buffer
- sample 3 - commercial horse spleen ferritin

We observed that the yield of nanotubes in samples 1 and 3 is nearly zero. Sample 2 gives a dramatic increase in the number of nanotubes (Fig. 7.2).

This phenomenon could arise from the structure of the ferritin mineral core. Under physiological conditions ferritin takes up iron in the presence of phosphate. This results in an iron oxide–hydroxide–phosphate mineral particle. The ratio of iron to phosphate varies from 2 to 10 in bacterial and mammalian ferritins, respectively<sup>11</sup>. The presence of phosphate changes the structure of the mineral core to more heterogeneous, hence a more heterogeneous nucleation particle for nanotubes production. In order to investigate the influence of phosphate on the nanotube production yield we performed growth from a sample 4, which is the same as sample 2 except that iron loading was made in the presence of phosphate buffer. This resulted in a low nanotubes yield, similar to sample 1 (Fig. 7.2).

Iron determination on apo ferritin samples 1 and 2 prior to addition of 2000 iron resulted in 7 iron/Ftn and 1 Fe/Ftn, respectively,

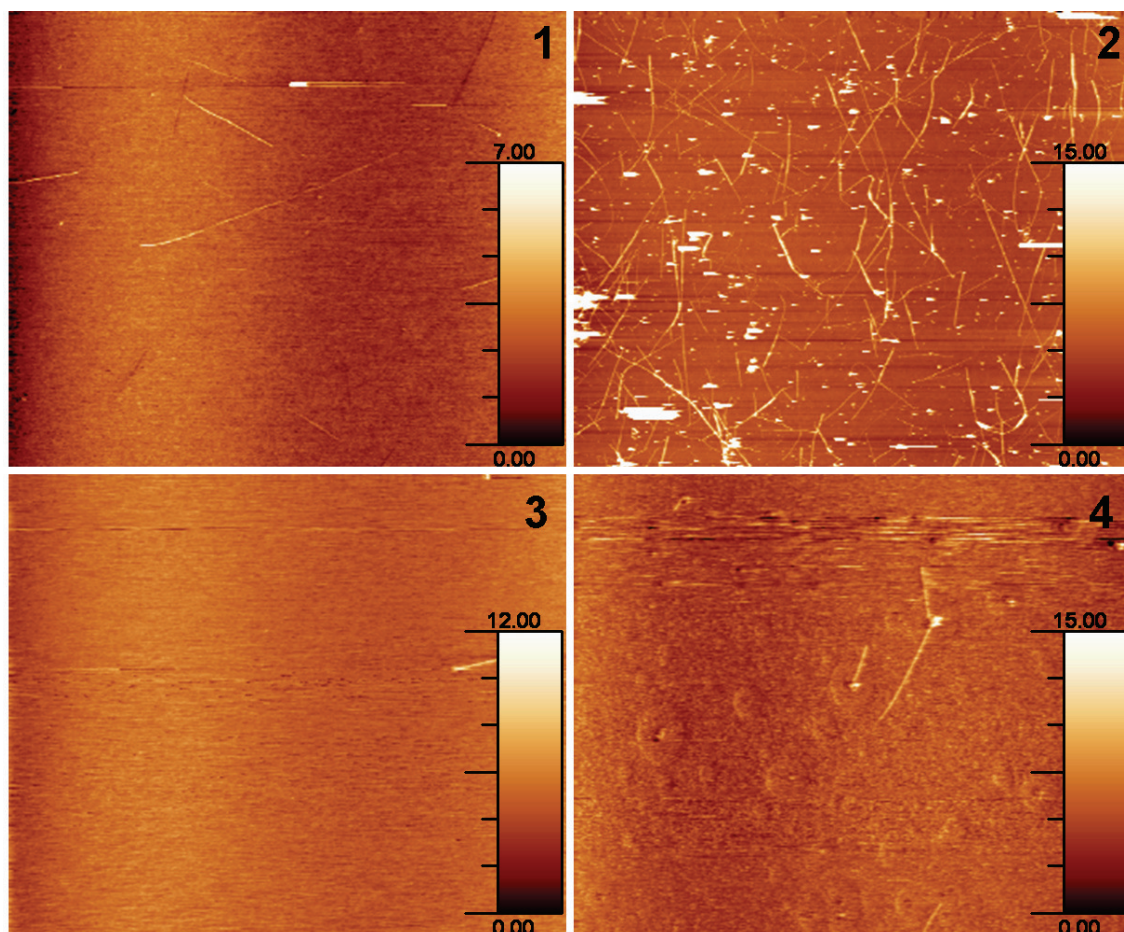


**Figure 7.2.** 10x8  $\mu\text{m}$  Atomic Force Microscopy images of CVD-grown carbon nanotubes. Tubes are imaged on  $\text{SiO}_2$  supports on which they were produced. Scale bars are in nm. Sample 1 – commercial apo horse spleen ferritin that in house was loaded with 2000 iron in HEPES buffer. Sample 2 - commercial apo horse spleen ferritin that in house was additionally treated to remove remaining iron and then was loaded with 2000 iron in HEPES buffer. Sample 3 – commercial iron containing horse spleen ferritin. Sample 4 – same as sample 2 except that iron loading was performed in phosphate buffer. The figure was prepared with WSxM 4.0<sup>12</sup>

indicating that in-house made sample is more pure than commercial apo preparation.

The same high production yield as obtained with sample 2 was achieved with *P. furiosus* ferritin. This protein has been overproduced in *E. coli* to a yield of  $\frac{1}{4}$  of total cell free extract protein with a cell yield of approximately 8 g/l. Because the protein originates from a hyperthermophilic organism living optimally at  $100^\circ\text{C}$ , we purified the protein in one heat step by incubating the cell free extract at  $100^\circ\text{C}$ . The high overproduction and ease of purification make this protein attractive for various industrial applications one of which is nanotubes production.

The results described in this study show that the presence of phosphate, in the mineral core of ferritin results in poor nanotubes yield. A thorough emptying of ferritin samples prior to iron loading is essential for high production yield. Although further research on statistics of the nanotubes production yield would be interesting, this method of ferritin preparation and nanotube production presents an advance towards producing the nanotubes in industrially substantial amounts. Taking into account the high overproduction of *P. furiosus* ferritin and the ease of purification, this recombinant protein is a good candidate for nanotubes production in industrially substantial amounts.

**Acknowledgments** Tillmann Pape (Imperial College London, UK) is greatly acknowledged for providing the electron microscopy image of ferritin

## REFERENCES

1. Wang, G. Carbon-nanotube based electrochemical biosensors: a review. *Electroanalysis* 17, 7-14 (2005).
2. Hummer, G., Rasaiah, J. C. & Noworyta, J. P. Water conduction through the hydrophobic channel of a carbon nanotube. *Nature* 414, 188-190 (2001).
3. Cai, D., Mataraza, J. M., Qin, Z. H., Huang, Z., Huang, J., Chiles, T. C., Carnahan, D., Kempa, K. & Ren, Z. Highly efficient molecular delivery into mammalian cells using carbon nanotube spearing. *Nature Methods* 2, 449-54 (2005).
4. Li, Y., Kim, W., Zhang, Y., Rolandi, M., Wang, D. & Dai, H. Growth of single-walled carbon nanotubes from discrete catalytic nanoparticles of various sizes. *J Phys Chem B* 105, 11424-11431 (2001).
5. Crichton, R. R. *Inorganic biochemistry of iron metabolism: from molecular mechanisms to clinical consequences* (John Wiley & Sons, Chichester, 2001).
6. Hudson, A. J., Andrews, S. C., Hawkins, C., Williams, J. M., Izuhara, M., Meldrum, F. C., Mann, S., Harrison, P. M. & Guest, J. R. Overproduction, purification and characterization of the *Escherichia coli* ferritin. *Eur. J. Biochem.* 218, 985-995 (1993).
7. Baaghil, S., Lewin, A., Moore, G. R. & Le Brun, N. E. Core formation in *Escherichia coli* bacterioferritin requires a functional ferroxidase center. *Biochemistry* 42, 14047-14056 (2003).

8. Tatur, J., Hagedoorn, P. L., Overeijnder, M. L. & Hagen, W. R. A highly thermostable ferritin from the hyperthermophilic archaeal anaerobe *Pyrococcus furiosus*. *Extremophiles* 10, 139-148 (2006).
9. Pierik, A. J., Wolbert, R. B., Mutsaers, P. H., Hagen, W. R. & Veeger, C. Purification and biochemical characterization of a putative [6Fe-6S] prismane-cluster-containing protein from *Desulfovibrio vulgaris* (Hildenborough). *Eur. J. Biochem.* 206, 697-704 (1992).
10. Hennessy, D. J., Reid, G. R., Smith, F. E. & Thompson, S. L. Ferrene - a new spectrophotometric reagent for iron. *Can. J. Chem.* 62, 721-724 (1984).
11. Lewin, A., Moore, G. R. & Le Brun, N. E. Formation of protein-coated iron minerals. *Dalton Trans.* 3597-3610 (2005).
12. Horcas, I., Fernández, R., Gómez-Rodríguez, J. M., Colchero, J., Gómez-Herrero, J. & Baro, A. M. WSXM: A software for scanning probe microscopy and a tool for nanotechnology. *Review of scientific instruments* 78, 013705 (2007).







## CHAPTER VIII. Conclusions and recommendations

Ferritin from *Pyrococcus furiosus* has been overproduced, purified and characterized via EPR, UV-Vis and X-ray studies. The importance of the current work originates from the fact that a limited number of archaeal ferritins have been studied, namely one ferritin and one DPS protein. Therefore, fundamental biochemical knowledge about the archaeal ferritins is so far limited. Furthermore, originating from an anaerobe, PfFtn is an interesting model to study the role of ferritin in anaerobic organisms and their physiological redox partners. This information is important to provide a basis for a fundamental biochemical understanding of ferritins as well as for designing therapies against iron related diseases.

The work described in this thesis was performed on recombinant protein overexpressed in *E. coli*. However, the expression of native ferritin by *P. furiosus* has also been shown. Interestingly, closely related species of *P. furiosus*, namely *P. abyssi* and *P. horikoshii*, do not possess a gene encoding for an H-chain ferritin like the one from *P. furiosus*. This could be because *P. furiosus* is an inhabitant of shallow waters and may be exposed to oxygen occasionally. This sets the necessity for a fast iron removal system such as the ferroxidase center of H-chain ferritins. For comparison, *P. horikoshii* and *P. abyssi* species live at 1.4 and 2 km below sea level while *P. furiosus* thrives in shallow marine waters.

The protein has been overproduced to  $\frac{1}{4}$  of total cell-free extract with a cell yield of approximately 8 g/l. The purification was achieved in one heat step by incubating the cell-free extract at 100 °C. The high overproduction and ease of purification make this protein attractive for various applications. An additional application favoring factor is the protein's hyperthermostability; the protein retains its iron incorporation activity after up to 12 h incubation at 100 °C or 1.5 h autoclaving at 120 °C. The iron incorporation rate increases dramatically with temperature. Consequently, hyperthermophilic enzymes such as PfFtn may be good

models for pre-steady state kinetics and quasi steady-state conditions at ambient laboratory temperatures. The  $K_{0.5}$  value of Pfftn is approximately 5 mM Fe(II).

Crystallization of ferritin was achieved with the hanging drop vapor diffusion method against 2 M ammonium sulfate. Pfftn crystals exhibited a pyramidal shape with an approximate size of 100-200  $\mu\text{m}$ . The best crystals of as-isolated ferritin and those soaked in Fe or Zn prior to data collection diffracted to 2.75 Å. The structure determination was carried out with the molecular replacement method using ferritin from *Thermatoga maritima* as the search model. The 24 Pfftn subunits assemble in the 432 symmetry also found in other ferritins. An exception to this rule is ferritin from the archaeon *A. fulgidus* (Afftn) that crystallized in 23 symmetry. Consequently, the four large pores present in the Afftn sphere do not occur in Pfftn. The 23 symmetry of Afftn remains an exception among ferritins, or at least does not occur in all archaeal ferritin, and more research is needed to explain such a conformation.

The thermostability of Pfftn was analyzed via comparison of its crystal structure with structures of ferritins from two thermophiles and two mesophiles. It appears that the high number of intrasubunit hydrogen bonds, therefore, the integrity of the monomer rather than the 24-mer, is responsible for the overall hyperthermostability of the protein. By implication, we expect ferritin from *T. maritima* ( $T_{\text{opt}} = 80\text{ }^{\circ}\text{C}$ ) to be more thermostable than Pfftn ( $T_{\text{opt}} = 100^{\circ}\text{C}$ ).

The as-crystallized Pfftn crystals revealed occupation of one metal center A in the ferroxidase center in each ferritin subunit. Upon soaking in Fe(II) or Zn(II) solutions all three metal centers, two of the ferroxidase center and a third site C, were occupied by metal. This observation is relevant for the ongoing discussion in the literature on whether the iron sites of the ferroxidase center form a stable cofactor or a transient center during the iron uptake reaction. In this thesis it is shown that the absence of iron sites B and C in the as-isolated Pfftn crystals is due to Fe complexation by a crystallizing agent and not

necessarily due to the translocation mechanism.

The Pfftn ferroxidase dinuclear iron center redox potentials of  $E=+210$  and  $+50$  mV are higher than the potentials of core reduction that for other ferritins have been reported to vary between  $-0.2$  and  $-0.5$  V. Therefore, provided that the Pfftn core reduction potential is in the order of those found for other ferritins, the core reduction cannot take place through the redox-catalytic action of the ferroxidase center unless the redox potential of the core iron would be modified by factors such as Fe(II) complexity.

The possible iron and oxoanions entry and exit routes in ferritins, the three- and four-fold channels, are often characterized by rule of thumb as being hydrophilic and hydrophobic, respectively. As it is more applicable to mammalian ferritins, the extent of this rule to other ferritins varies. Pfftn three- and four-fold channels appear similar to those from bacterial ferritins; the three-fold channel is less hydrophilic and the four-fold channel is more polar than those from mammalian ferritins.

Besides the structural ferritin gene, a cluster of genes was identified in *P. furiosus* encoding putative proteins similar to ferritin-like/DNA-binding-protecting helical proteins. These genes are PF1195, PF1190, PF1196 and PF1193. The latter is a DPS-like protein of *P. furiosus* that has been recently characterized by other researchers. Blast comparison against PF1195, PF1190 and PF1196 results in annotations such as BFRs, chromosome segregation proteins, and DNA break repair proteins. This gene cluster may play a role in *P. furiosus*' increased DNA protection that is necessary in a hyperthermophilic environment.

An iron loaded Pfftn was applied as a nucleation seed in experiments on nanotubes production via the method of chemical vapor deposition. Interestingly, a low nanotube yield resulted from as-isolated ferritin, loaded with iron. Contrarily, a high nanotube yield was observed when as-isolated protein would be first emptied and then loaded with iron. The reason of this lays probably in the structure of the physiological ferritin core. The as-isolated ferritin may contain several metals and oxoanions and therefore have rather amorphous core

structure compared to the pure dense iron core achieved via a thorough emptying and subsequent iron loading. This observation reminds of the studies where structures of ferritin iron mineral core from healthy individuals and patients with iron-associated degenerative disorders were compared. Ferritin mineral core from healthy tissues is of ferrihydrite  $5\text{Fe}_2^{\text{III}}\text{O}_3 \cdot 9(\text{H}_2\text{O})$  structure. The ferritin cores from patients with iron related degenerative disorders had wüstite  $\text{Fe}^{\text{II}}\text{O}$  and magnetite-like  $\text{Fe}^{\text{II}}\text{Fe}^{\text{III}}_2\text{O}_4$  structure. One of the differences between ferrihydrite and wüstite/magnetite is their density, which is lower in ferrihydrite. Research on the factors that lead to different ferritin minerals in the brain of patients with iron-associated degenerative disorders, such as pH, temperature, oxygenation and possibly more, may lead to a possibility for treatment.

Further research on *P. furiosus* ferritin may include pre-steady state kinetics that will be easy to follow because the protein is hyperthermophilic and its kinetics is slow at room temperature. Time resolved crystallography will provide more information on the mechanism of iron incorporation. Study of the genes PF1195, PF1190 and PF1196 may give insight into the defense mechanism of *P. furiosus* from hyperthermal environment and extend our knowledge about the ferritin family proteins.





## Abbreviations

AfFtn	<i>Archaeoglobus fulgidus</i> ferritin
AFM	Atomic force microscopy
BbrevDPS	<i>Bacillus brevis</i> DPS
BFR	Bacterioferritin
CjFtn	<i>Campylobacter jejuni</i> ferritin
CNT	Carbon nanotubes
CVD	Chemical vapor deposition
DPS	DNA protecting protein during starvation
DPSL	DPS-like protein
EcBFR	<i>Escherichia coli</i> bacterioferritin
EcFtn (EcFtnA)	<i>Escherichia coli</i> ferritin
EPR	Electron paramagnetic resonance
EXAFS	Extended X-ray absorption fine structure spectroscopy
FC	Ferroxidase center
HuHF	Human H chain ferritin
MAD	Multiwavelength anomalous dispersion
MR	Molecular replacement
MRI	Magnetic resonance imaging
NCS	Noncrystallographic symmetry
PDB	Protein data bank
PfFtn	<i>Pyrococcus furiosus</i> ferritin
SAD	Single-wavelength anomalous dispersion
SSM	Secondary structure matching
SsolfDPSL	<i>Sulfolobus solfataricus</i> DPSL protein
TLS	Translation–libration–screw
TmFtn	<i>Thermotoga maritima</i>
XANES	X-ray Absorption near edge structure spectroscopy

## Curriculum vitae

Jana Tatur was born on the 5<sup>th</sup> of April 1975 in Kramatorsk, Ukraine. She began her university education at the Department of Ecology and Chemical Technology, Technical University of Donetsk, Ukraine. After her first year of study Jana moved to Moscow, Russia to continue her education at the Academy of Fine Chemical Technology where she received her BSc degree in 1999. In 2000, aspired to top education in biotechnology and passionate to experience diverse cultural backgrounds Jana enrolled in the International Master of Science Program in Chemical Engineering with a specialization in Biotechnology from Delft University of Technology (TU Delft), The Netherlands. In August 2001 she did an internship at the Genetics Laboratory of DSM Delft. During 2002 simultaneously with her MSc program Jana worked as a research assistant in the section Enzymology, Department of Biotechnology, TU Delft. In 2002 Jana obtained her MSc degree in Biotechnology. Her MSc research project “Denitrification in the hyperthermophilic *Pyrobaculum aerophilum*: Nitrite reductase” was carried out in the section Enzymology, Department of Biotechnology, TU Delft under the supervision of Prof. S. de Vries. In 2002 Jana began her PhD research in the same research section under the supervision of Prof. W.R. Hagen on the project presented in this thesis. During her PhD program, Jana attended international courses (Protein Crystallography – Denmark; the European Course on Biotechnology Ethics – Italy; Membrane Proteins, Bioinformatics and Proteomics and Protein Folding and Structure – Greece) and she presented the results of her work at international scientific conferences (USA, Denmark, Greece) and in international scientific journals. In 2004 she was awarded a second shared prize from the TU Delft university fund “Marina van Damme grant” for talented women in science. In 2007 she was granted a “Rubicon” post-doctoral scholarship for her research proposal by the Dutch Council for Scientific Research (NWO) to do research in the Membrane Protein Crystallography group of Prof. S. Iwata at the Imperial College London, UK, where she is currently working.



## **Acknowledgements**

A feeling of immense gratitude is overwhelming me to people I met since I came to Delft for my MSc study and up to the end of my PhD program. It would be impossible for me to express my emotion in a concise form required by a thesis. It would be insufficient just to list your names. Yet...

I would like to acknowledge my promoter, the splendid biochemist and talented teacher Fred Hagen. Thank you for giving me the opportunity to do the PhD research in your group. I was lucky to be able to learn from your proficiency in EPR and electrochemistry and get a broad biochemical training under your supervision. Thank you for being a coauthor of our publications, and for all your support. Peter-Leon Hagedoorn is greatly acknowledged for the useful and interesting discussions. Without his suggestion to work on the ferritin project this thesis would not have been written. I am deeply grateful to Simon de Vries, an outstanding scientist and great person. His supervision of my MSc diploma work, as well as the discussions during my PhD research, extended from the projects issues to the examination of a wide area of biosciences. His fascinating scientific discussions, advises and support are always encouraging and stimulating to me. I am very thankful to Marc Strampraad who was so kind to teach me enzymology in the very beginning of my work in this group. Thank you very much to Jaap Jongejan, a superb chemist and wonderful and modest person, who was my mentor during my MSc program and a group member during my PhD work. I would like to express a special gratitude to Dirk Heering for our collaborative work on intriguing ferritin electrochemistry and for many interesting and useful discussions.

I greatly acknowledge Ann O'Brien, the coordinator of my MSc program, Margot Weijnen, the professor from TU Delft, Marco van den Berg, my supervisor from DSM Delft, Maria Armenia Carrondo, the professor of the protein crystallography group from Portugal, Leila Lo Leggio, my tutor during the crystallography course in Denmark, Pedro

Matias, my collaborator in crystallography from Portugal and many more people.

I would like to express my gratefulness to members of the Biotechnology Department: Han, Gijs, Peter, Ank, Lies, Lesley, Frieda, Marlene, Jennifer, Arno, Sjaak, Herman, Robert, Joop, Jan, Astrid, Ginie, Jos, Apilena, Hans, Marcel, Bob, Gerard, Dmitriy, Marjana, and the list goes on.

Thank you, my fellow students from the MSc programs 2000-2002, BODL and TWAIO. The two years of our study and life in Delft were one of the most precious periods in my life.

I am very grateful to Dini, Tony, Boudewijn, Xiaonan, Inga, Jonas, Arminster, Slava, Christian, Alex, Tania, and Nikolai for their unlimited support and companionship. Thank you to Kristina from the Biocatalysis and Organic Chemistry group and Vasili from the EM group for your help. Thank you to colleagues from the Enzymology group: Rosario, Ksenia, Peter, Marieke, Loesje, Esengül, Barbara, Laura, Sandra, Ana, Nahid, Emile, Alexei, Elena, Ram, Harti, and from the Molecular Biophysics group: Cees, Christine, Alexei, and people that I did not mention here, for our discussions and the possibility to learn from each other. I will be happy to continue our relations in the future.

In short, I am greatly and sincerely acknowledging my supervisors, colleagues, friends, fellow students, program coordinators, lecturers, collaborators, sponsors, and my family who contributed in the work presented in this thesis and in my study, research, and life in Delft.

